UNIVERSITÀ DEGLI STUDI DI TRIESTE

e

UNIVERSITÀ CA' FOSCARI DI VENEZIA

XXXIII CICLO DEL DOTTORATO DI RICERCA IN CHIMICA

CONFINEMENT OF ENDO-β1,4-GLUCANASE AND PETASE ON SILICA SYSTEMS

Settore scientifico-disciplinare: **CHIM02**

DOTTORANDO
VINCENZO LOMBARDI

COORDINATORE
PROF.ENZO ALESSIO

SUPERVISORE DELLA TESI
PROF.ALVISE BENEDETTI

“Quelli che s'innamorano di pratica senza scienza
son come il nocchiere, che entra in naviglio senza timone o bussola,
che mai ha certezza dove si vada”

Leonardo da Vinci

SUMMARY

CHAPTER 1 6

INTRODUCTION 6

1.1 AIM OF THE THESIS 6

1.1.1 Background 6

1.1.1 Project overview 8

1.2 ENZYMATIC CONFINEMENT AND SUPPORT MATERIALS STATE OF ART 14

1.2.1 Non-covalent confinement 16

1.2.1.1 Adsorption method 18

1.2.1.2 Ion interaction method 20

1.2.1.3. Entrapment method 21

1.2.2 Covalent confinement 24

1.2.2.1 Covalent bond on support 25

1.2.2.2 Cross-linking reaction 26

1.2.3 Enzymatic kinetics in the confinement systems 28

1.3 NON-POROUS AND MESOPOROUS MATERIAL SUPPORTS: STATE OF THE ART 36

1.3.1 Silica Materials: Sol gel mechanism and particles formation 37

1.3.2 Mesoporous Materials 41

1.3.3 The bioinspired method: A eco-friendly synthesis to produce silica material 44

1.3.4 Chemical functionalization of the supports for the confinement enzyme 46

1.4 IMMOBILIZATION OF ENDOGLUCANASE AND PETASE 48

1.4.1 Endo-β-1,4-glucanase 48

1.4.2 PETases 50

CHAPTER 2 52

EXPERIMENTAL PART 52

2.1 SYNTHESIS OF DIFFERENT SILICA SUPPORTS 52

2.1.1 Synthesis of the non-porous silica particles via Stöber method 52
2.1.1.1 Materials 52
2.1.1.2 Synthesis of non-porous silica via Stöber method 52
2.1.1.3 Synthesis of non-porous silica via modified Stöber method 53
2.1.2 Synthesis of mesoporous silica via soft and hard methods 54
2.1.2.1 Materials 54
2.1.2.2 Synthesis of MSN with soft template method (series MC) 54
2.1.2.3 Synthesis of MSN with hard template (series MS). 55
2.1.2.4 Synthesis of DFNPs (KCC1 series). 55
2.1.3 Synthesis of silica support via bioinspired method 56
2.1.3.1 Materials 56
2.1.3.2 Bioinspired method 56
2.1.4 Characterization 57
2.2 CHEMICAL FUNCTIONALIZATION OF DIFFERENT SILICA SUPPORTS 58
2.2.1 Materials 58
2.2.2 Silica support functionalization via 3-Aminopropyltriethoxysilane (APTES). 59
2.2.2.1 Functionalization via acid silylation (method A) 59
2.2.2.2 Functionalization via grafting in organic solvent (method B) 59
2.2.2.3Functionalization via acid silylation using a controlled dripping (method C) 59
2.2.2.4 Direct Functionalization via Co-condensation synthesis (method D) 60
2.2.3 Silica support functionalization via (3-mercaptopropyl)trimethoxysilane (MPTMS). 60
2.2.4 Silica support functionalization via (3-Glycidyloxypropyl) trimethoxysilane (GPTMS). 60
2.2.4.1 Functionalization with polyethyleneimine 60
2.2.5 Silica support functionalization via N-[(3-trimethoxysilyl)propyl] ethylenediaminetriacetic acid (TMS-EDTA). 61
2.2.6 Silica support functionalization via 3-Chloropropyltrimethoxysilane (CPTMS) and sodium azide 61
2.2.7 Silica support biotinylated via CuAAC (Cu(I)-catalyzed azide/alkyne cycloaddition) click reaction. 61

2.2.8 Characterization 62
2.2.8.1 Ninhydrin assay for the detection α-amines 63
2.3 PROTEIN EXSPRESSION AND PURIFICATION 64
2.3.1 Materials 64
2.3.2 PETase exspression 64
2.3.3 Characterization and protein purification 65
2.4 COVALENT AND NON-COVALENT CONFINEMENT SYSTEMS 67
2.4.1 Materials 67
2.4.2 Covalent confinement 68
2.4.2.1 Cross linking method with glutaraldehyde as cross-linking agent 68
2.4.3 Non-covalent confinement 69
2.4.3.1 Protein adsorption 69
2.4.3.2 Proteins entrapment using the Bioinspired method 69
2.4.3.3 Adsorption streptavidin-Alexa fluor 647 A on Silica support biotinylated 69
2.4.4 Characterization 69
2.4.4.1 Protein quantification 70
2.4.4.2 Endoglucanase assay 71
2.4.4.3 PETase assay 72
CHAPTER 3 73
RESULTS AND DISCUSSIONS 73
3.1 NON-POROUS SILICA PARTICLES. 73
3.2 MESOPOROUS SILICA PARTICLES VIA SOFT AND HARD TEMPLATING 78
3.3 SILICA SUPPORTS PREPARED BY BIOINSPIRED METHOD 84
3.4 CHEMICAL FUNTIONALIZATION OF THE NON-POROUS AND MESOPOROUS SILICA SUPPORT 89
3.4.1 APTES and CPTMS cases on different non-porous supports. 90
3.4.1.1 Biotinylation of the azide silica by CuAAC Click reaction 94
3.4.1.2 Analysis with fluorescent streptavidin of the binding efficiency of biotinylated silica support 95
3.4.2 Functionalization of Mesoporous silica supports. 97
3.5 PROTEIN EXSPRESSION AND PURIFICATION 100

3.5.1 PETase 100
3.5.2 Purification of Endo-β-1,4-glucanase (Cell_EG) 101
3.6 COVALENT CONFINEMENT 102
3.6.1 Cross-linking reaction 102
3.6.1.1 Protein cross-linking 102
3.6.1.2 Protein cross-linking on functionalized silica particles 106
3.7 THE NON-COVALENT CONFINEMENT 110
3.7.1 Protein adsorption 110
3.7.1.1 Adsorption on non-porous silica support 110
3.7.1.2 Adsorption on functionalized non porous silica supports 114
3.7.1.3 Adsorption on functionalized mesoporous supports 116
3.7.1.4 Adsorption on silica bioinspired with different polyamine additives. 118
3.7.2 Protein entrapment. 121
3.8 CATALYTIC ACTIVITY ON DIFFERENT CONFINMENT SYSTEMS OF THE Cell_EG PROTEIN 125
3.9 ENTRAPMENT CONFINEMENT OF PETase PROTEIN 129
CHAPTER 4 132
CONCLUSIONS 132
4.1 FINAL REMARKS AND FURTHER PERSPECTIVES 132
ACKNOWLEDGEMENTS 139
BIBLIOGRAPHY 140

CHAPTER 1

INTRODUCTION

1.1 AIM OF THE THESIS

1.1.1 Background

The aim of the project is the production of different enzymes confinement systems on different silica particles of different sizes.
In general, enzymes are macromolecules, whose main function is to catalyze a specific chemical reaction. An enzyme[1] is a biocatalyst that interacts with one or a group of substances, called substrate, to catalyze a specific reaction. This reaction forms an intermediate complex -"transition state"- that requires less energy to proceed. The intermediate complex is unstable and quickly breaks down to form reaction products and the unchanged enzyme is free to react with another substrates. The affinity of the enzyme to recognize the substrate is called molecular specificity [1]. Even though the enzymes can be used in several reactions, their commercial use is limited by the costs and their low reusability factor [2].
In light of these evidence, the scientific and industrial interests are focused on finding a better strategy to reuse enzymes and, at the same time, to improve their performances. A method to recovery the enzymes is based on their confinement on a support matrix. The type of the support and the adaption of the enzyme on the surface could improve its catalytic performance. Thereby, the enzyme confinement strategy become an interesting tool to increase efficiency and enzyme lifetime. All together these characteristics of the enzymes, after their confinement, are much appreciated in many fields such as engineering, chemical catalysis, industry, pharmacology and biotechnology (**Fig. 1**) [3]. Nowadays, immobilized enzymes are preferred, over their free counterpart, due to their prolonged availability and avoid redundant extraction and purification processes.

[1] The enzyme is a protein with catalytic proprieties.

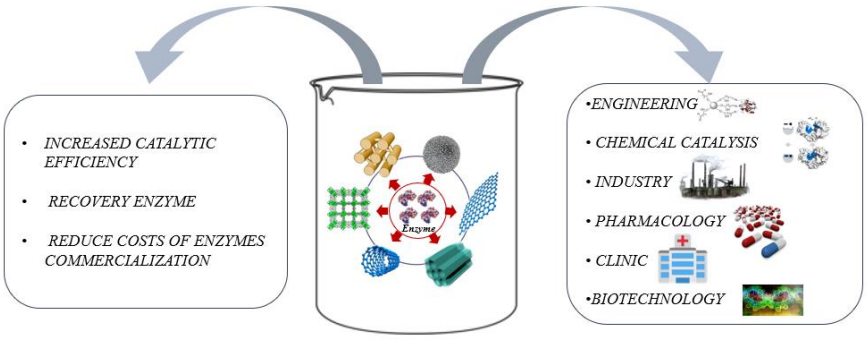

Fig. 1 The principal properties and fields use of confinement enzyme system.

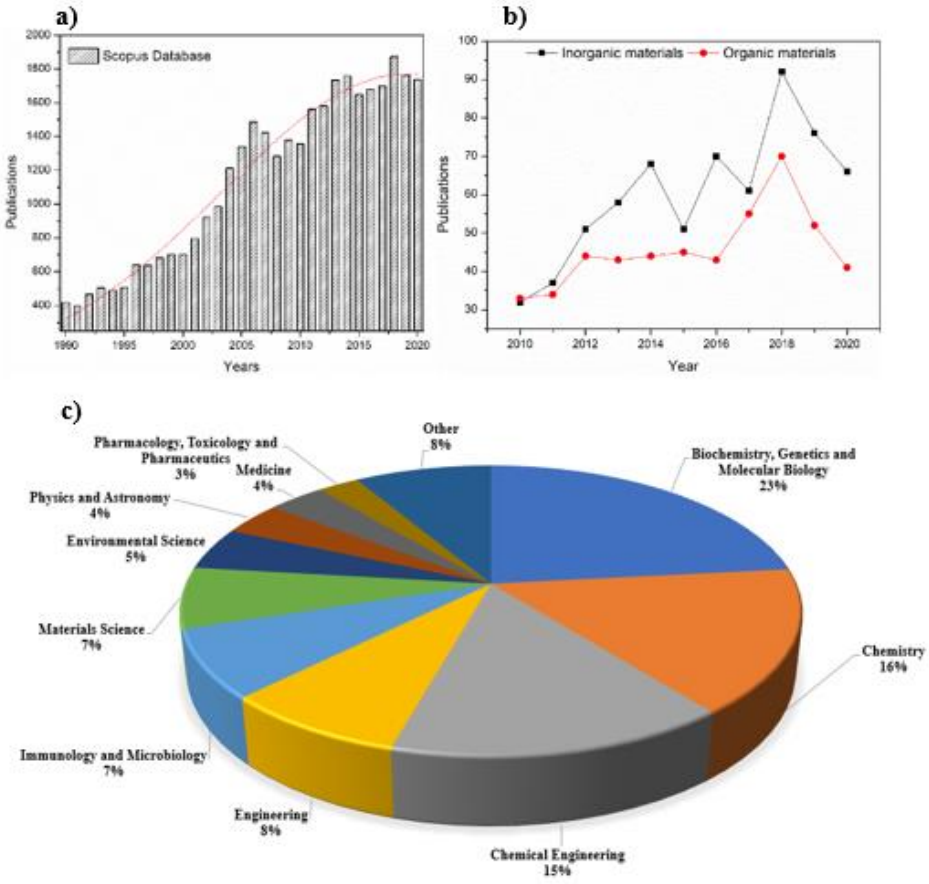

Fig. 2 a) Publications of enzyme immobilization by Scopus databases, **b)** Publications on different organic and inorganic materials used as confinement supports, **c)** Publications by subject area.

Fig. 2a-b report the publications, per year, on enzyme confinement and on the principal research of organic and inorganic materials used as confinement supports

(Scopus database). In addition, in the **Fig. 2 c** shows the main subject areas related to the immobilization of enzymes [4], [5].

1.1.1 Project overview

The project of the thesis is focused on the synthesis and functionalization of different silica supports and the immobilization of the Bovine Serum Albumin (BSA), Cellulase-endo-β 1,4-glucanase from *Aspergillus niger* (Cell-EG), PETase from *Ideonella sakaiensis* and streptavidin (STREP) proteins. The research is divided into three parts. A general view of the project is reported in **Fig. 3**.

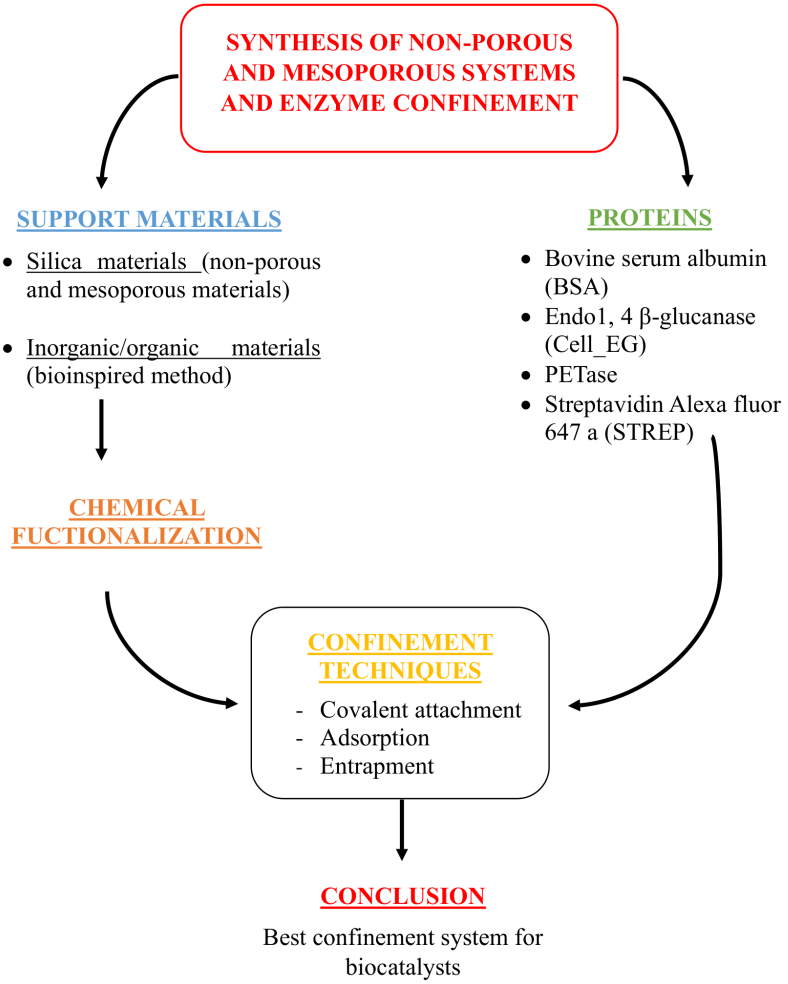

Fig. 3 Outline of the aim of the thesis.

The first part of the project concerns the syntheses of different non-porous and mesoporous silica systems **(Fig. 4)** by different preparation methods.

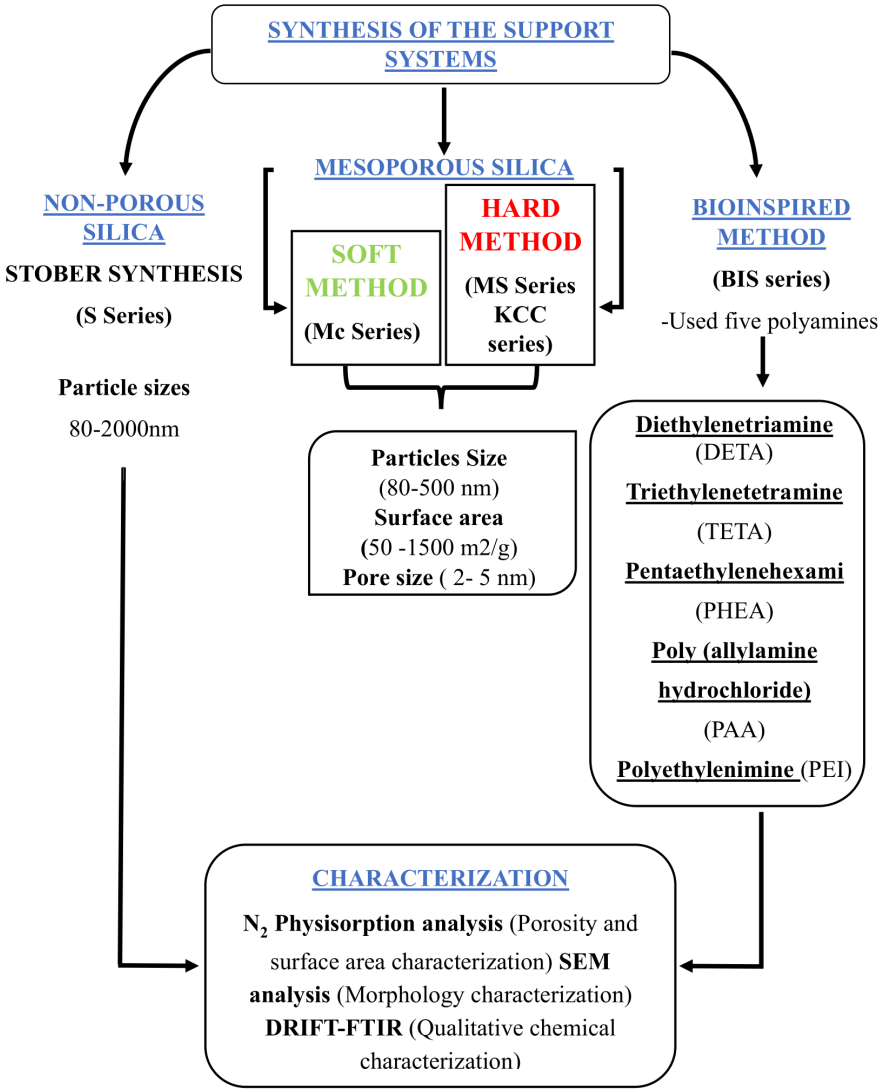

Fig. 4 Experimental outline for synthesis of different non-porous and mesoporous silica systems.

First, the synthesis of non-porous silica following the classical Stöber method and its optimization was investigated. According to the reaction conditions and to the tetraethyl orthosilicate (TEOS) and ammonia concentration, silica particles with different sizes (diameter in the range of 80 - 250 nm) could be obtained. Furthermore, the control of some other parameters of the synthesis such as the

dripping speed of the alkoxysilane precursor (TEOS) and the addition of an electrolytic compound (KCl) was used to synthesize particles with larger diameters up to 1 -2 μm.

The mesoporous silica systems were synthesized using soft and hard template methods. With the soft method, some surfactants, such as cetyltrimethylammonium bromide (CTABr), triblock-polymeric (Pluronic 157), and methylcellulose, were used as templates to develop the porosity of the structure. The obtained silica nanoparticles showed a large surface area (> 1000 m^2/g), with pore diameters of about 2 nm.

The hard method, instead, was used to synthesize silica systems with different pore sizes using swelling agents such as n-hexane, cyclohexane, methylbenzene, and ethylene glycol. A range of 2 - 5nm pore sizes was obtained with a corresponding very large surface area (500-1100m2/g).

Finally, silica particles were synthetized through a bio-inspired synthesis. The reaction proceeds at room temperature, at pH=7, in presence of Na_2SiO_3 and a polyamine such as diethylenetriamine (DETA), triethylenetetramine (TETA), pentaethylenehexamine (PEHA), polyallylamine (PAA), and polyethyleneimine (PEI). An organic/inorganic hybrid matrix was obtained with tunable surface features, based on the reaction conditions.

The morphology of the synthesized systems was analyzed by Scanning Electron Microscopy (SEM), while the surface areas and the pore diameters were investigated by nitrogen physisorption analysis. Infrared Fourier transform spectroscopy (IR-DRIFT) was used to characterize the surface groups of the silica systems.

The second part of the thesis focuses on the functionalization of the supports with organosilane precursors, such as 3-aminopropyl-trietoxysilane (APTES), 3-mercaptopropyl-triethoxysilane (MPTMS), 3-glycidyloxypropyl-trimethoxysilane (GPTMS), N-(trimethoxysilylpropyl)-ethylenediamine triacetate trisodium salt (EDTATMS), 3-chloropropyl-triethoxysilane (CPTMS) (see **Fig. 5**). APTES was used as elective organosilane. In order to increase the grafted groups on the surface of the silica particles, four different methods (called A, B, C, D) were tested to set the best functionalization protocol.

The first method (A) is a coating method that involves an acid-catalyzed reaction. The second one (B) is a grafting method in an organic solvent, performed without a catalyst. The third method (C) is similar to the first one, but in this case, the organosilane precursor was dropped with a piston pump (Prostar varian 210) at a fixed flow and time. The fourth one (D) is a co-condensation method, in which the

particles were synthesized using an accurate molar ratio between TEOS and APTES. With this last one-pot method, the nanoparticles are already functionalized after the synthesis. The nonporous silica particles were functionalized with APTES using all the previously described methods. The chemical grafting on mesoporous systems was accomplished with the methods A and B, using all the organosilane precursors listed above. On the other hand, the classic silanization was not used for the silica bioinspired materials but the supports were already functionalized after synthesis.

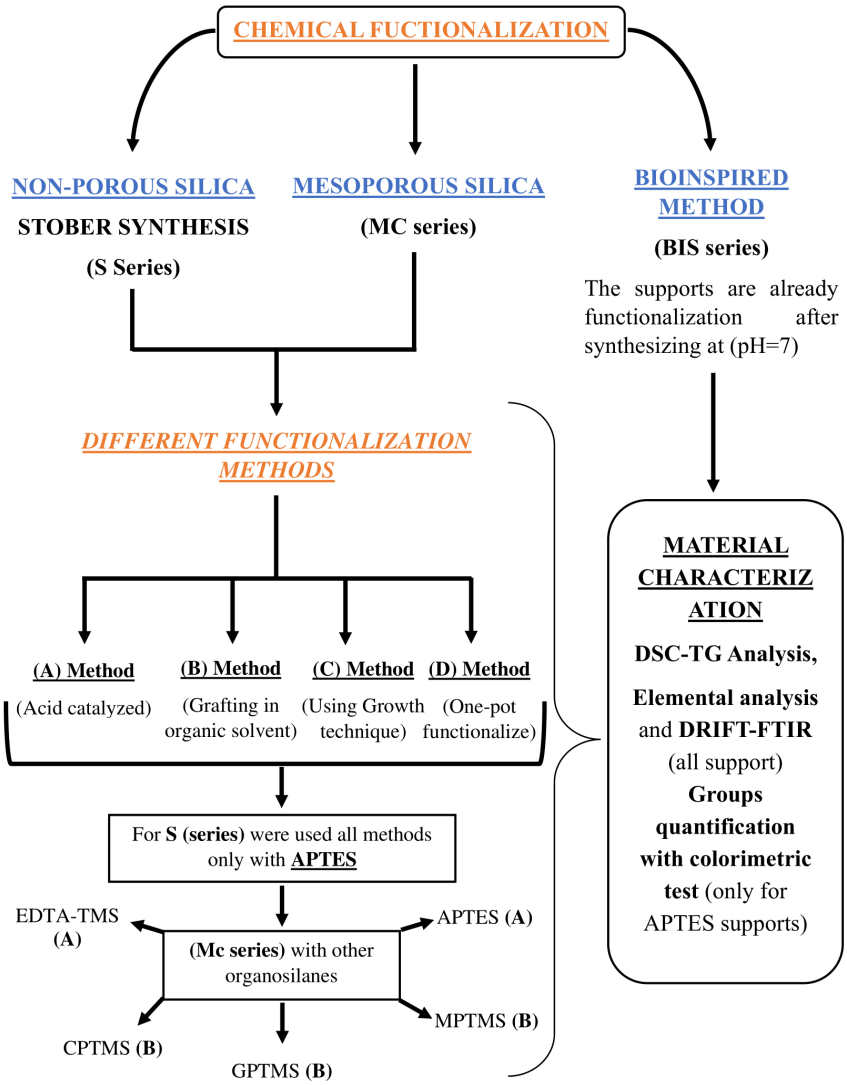

Fig. 5 Experimental outline of the materials functionalization.

The functionalized samples were analyzed by Diffuse Reflectance Fourier Transform Infrared Spectroscopy (DRIFT-IR), Thermogravimetric Analysis (TGA) and the Differential Scanning Calorimetry (DSC) elemental analysis CHNS, Uv-Visible and characterized by Scanning Electron Microscopy (SEM).
Finally, in the last part of the project different enzymes confinement strategies (i.e., **covalent bonds, adsorption,** and **entrapment**) on different silica supports are investigated (see **Fig. 6**).

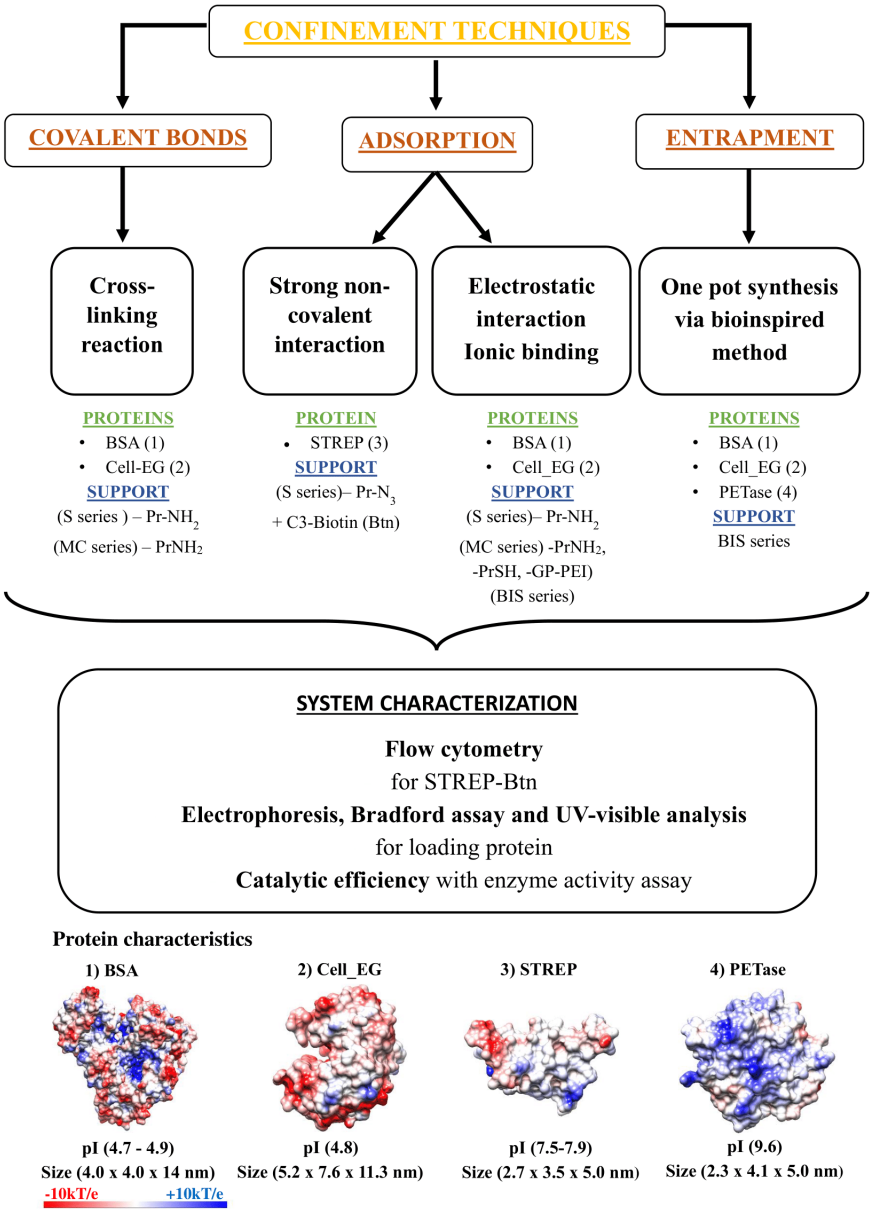

Fig. 6 Experimental outline of the confinement techniques.

The covalent bonds strategy was used to block the Cell_EG and BSA proteins. The second and third strategies were performed for the BSA, Cell-EG and Strep proteins. In the case of the STREP proteins, firstly, a covalent interaction was used to block the biotin (Btn) on the silica surface. Secondly, the streptavidin was bound to the biotin through a non-covalent interaction. Finally, after the analysis of the different strategies, the one with the best activity was identified and then used for the confinement of the PETase protein.

For the covalent bond strategy, the cross-linking method was chosen, in which the bond is formed between the amine groups of the protein and the carbonyl groups of a cross-linking agent (glutaraldehyde).

For the non-covalent confinement, the adsorption and entrapment strategies represent easy methods to confine the protein on the support without any chemical bond between them (see § 2.4 for the detailed description of the methods). The adsorption method is used after the functionalization of the supports in a buffer solution at fixed values of pH, adsorbed time, and buffer concentration. The adsorption of the streptavidin[2] was performed on the silica supports functionalized with biotin. The latter was performed by Cu-catalyzed azide-alkyne cycloaddition (CuAAC) reaction between the azide groups present on the surface of the particles and the alkyne added to the biotin structure to form a 1,2,3 triazole heterocyclic compound.

On the other hand, the entrapment method takes place during the synthesis of the supports. In this case, the proteins are entrapped into the support matrix using mild conditions, such as room temperature, pH 7, and water solvent. The interaction support-protein in both adsorption and entrapment systems concerns the electrostatic and ionic binding interactions between the positive charge of the amine or polyamine groups of the support surface and the negative charge of the proteins at neutral pH.

The immobilization systems were analyzed with sodium dodecyl sulphate - polyacrylamide gel electrophoresis (SDS-PAGE) and UV-visible analysis to measure the amount of the proteins loaded on the different supports. The confinement of STREP-Btn was analyzed with flow cytometry. In addition, the enzymatic assays were used to analyze the enzyme stability and its catalytic activity before and after immobilization. Consequently, the thermostability, pH resistance, and recycling of the biocatalyst confined was evaluated.

[2] See § 2.4.3.3

1.2 ENZYMATIC CONFINEMENT AND SUPPORT MATERIALS STATE OF ART

The confinement techniques are relevant to produce the best stability interaction between the support and the enzyme. The final interaction is also related to the adaptation of the enzyme onto the support surface; its structure is stabilized and does not generate many unfolding processes [6]. For each enzyme, the structural stability on the support surface is very important to not modify its catalytic activity and, in some cases, to improve it.

In general, the confinement techniques can be classified in two macro-areas (see **Fig. 7**). In the first one, the protein guest does not interact covalently with the support by intermolecular forces [7]. In the second one, the protein is bound to the support by strong covalent bonds and orientates itself in a certain direction [8]. The orientation for an enzyme is important because allows to directly expose the active site to the substrate consequently improving its catalytic activity.

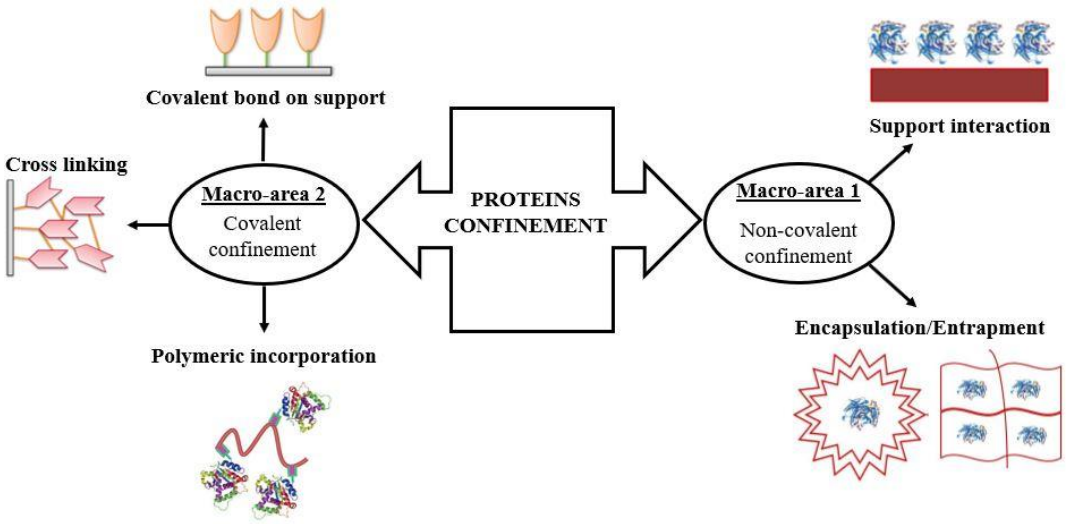

Fig. 7. General scheme of confinement techniques.

The macro-area relative to the non-covalent interactions can be further divided in: support interactions (adsorption [9], ionic interaction [10], interaction with chelate metal[11]), non-covalent entrapment [12] and encapsulation [13]. The support interactions comprise all the non-covalent bonds between the support surface and the protein. Entrapment and encapsulation methods are based on the caging of the

protein within the support by non-covalent bonds that allow the substrate and the products to pass but retaining the enzyme into the matrix. The caging of the protein is obtained during the synthesis of the support. In general, in both entrapment and encapsulation methods, the support is an organic/inorganic polymer network.

The macro-area related to the covalent interaction is divided into covalent attachment [14], cross-linking [15], polymeric interaction [16]. These techniques use a covalent bond to irreversibly block proteins on the support. **Table 1** summarizes the principal developmental phases of confinement enzymes.

Table 1 [17]

Developmental Phases of confinement enzymes

Phase	Years	Development
Early Phase	1916-40	Glass, Alumina, Hydrophobic compound coated glass.
Underdeveloped Phase	1950	Nonspecific physical adsorption of enzymes on solid carriers
Developing Phase	1960	Entrapment of whole cells in synthetic gel, Encapsulation in artificial cell, Adsorption-cross-linking, Active site titration, Cross-linked enzyme (CLE), cross-linked enzyme crystals (CLEC), Immobilization or post-treatment by denaturant.
Development Phase	1970	Many new method subgroups, for example affinity binding and coordination binding and many novel variations have been developed. Increased enzyme loading in order to enhance the activity.
Post Developed Phase	1980	Engagement (double engagement), covalent multilayer immobilized enzymes, organo-soluble lipid-coated enzyme, introduction of genetically engineered tags
Rational Design Phase	1990- till now	Stability and activity in organic solvents, high enzyme loading and less diffusion limitation, project to new material for enzyme more stabilize the enzyme on the support

1.2.1 Non-covalent confinement

The non-covalent confinement of the protein on the surface of the support is very complex since there are many interactions to consider. A scheme of the principal non-covalent confinement techniques is reported in **Fig. 8**.

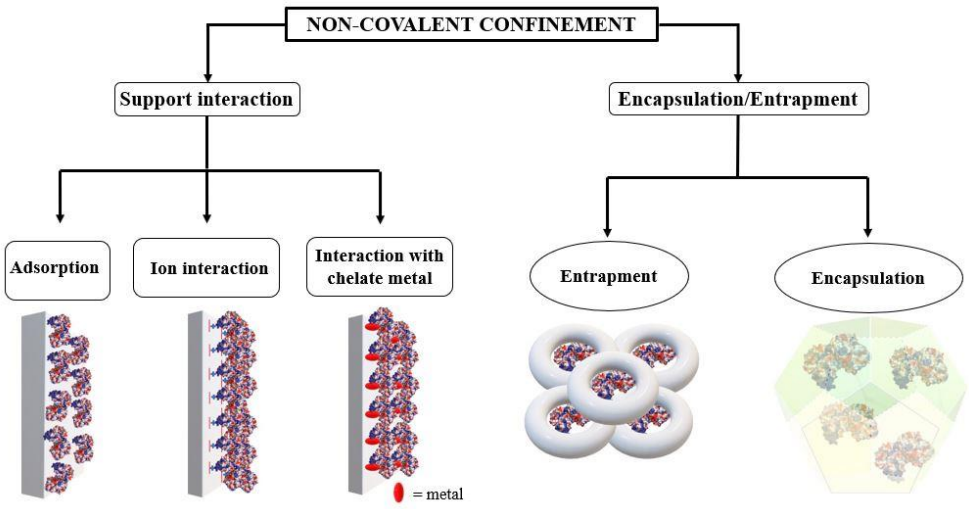

Fig. 8 Scheme of the principal non-covalent confinement techniques.

In general, the driving forces are electrostatic interactions [18] (ion- instant dipole interaction), π- π stacking [19] and Van Der Waals dispersion forces [20] (two permanent dipoles, a permanent and an induced dipole, and two induced dipoles).
The electrostatic interaction occurs between the protein charge and the support charge at a certain distance (r). The π- π stacking is more stable interaction among the non-covalent ones and is generated between the aromatic compounds of the protein and the support through the overlapping of the π-system of the two aromatic rings [21].
The Van der Waals dispersion forces (which are attractive in nature- Dispersion forces derive their name from the close connection between their origin and the cause of optical dispersion) are the sum of the interactions among atoms or molecules of the protein-support system. The total energy related to the dispersion forces is negative, indicating attraction, and it becomes zero with increasing distance **r** according to $\mathbf{1/r^6}$ [22].

Another factor that makes the definition of these forces challenging derives from the conformational flexibility of the protein molecules. Indeed, since the folded conformation of the proteins is only marginally stable (standard Gibbs energies of unfolding are in the range of about 20–60 $kJmol^{-1}$), any change of the protein environment can perturb this conformation. This critical stability could give to the protein a conformational change induced by the surface of the support that can lead to an optimized and more stable contact between the protein and the surface. This structural adaption of the protein, over time, generally causes an apparent macroscopic irreversibility of the protein confinement process [18]. In general, the degree of protein confinement on a solid surface depends on both the structure of the protein (e.g., the small proteins, are rigid, have a low trend to structural alterations) and the chemical and physical properties of the solid surface.

The non-covalent confinement process is influenced by other factors such as temperature, pH, ionic force, and the composition of the buffer solution [23]. The temperature influences both the equilibrium state and the kinetic of the confinement. In general, an increase of the temperature provides more energy to the system, resulting in an increase in the amount of confined protein. The pH determines the electrostatic state of the protein. When the pH is equal to isoelectric point (pI) of the protein the total charge on its surface is neutral. When the pH is less than the protein isoelectric point, the surface charge is negative, while when the pH is higher than the isoelectric point, the surface charge is positive.[24]–[26] Several papers report a high loading of the protein onto the support surface when the pH is equal to the isoelectric point of the protein.

The ions concentration in the buffer solution is another factor that controls the confinement typology related to the ionic forces (Debye forces) present in the system. The ionic strength determines the Debye length, that is the distance related to a significant charge separation in an electrolyte [26]. Thus, when the ionic strength is higher, shorter is the distance of the electrostatic interactions between charged electrolytes. As a result, the adsorption is hampered when the ionic strength between the protein and the electrolyte is higher than the ionic strength between the protein and the support. In this case, the protein interacts more easily with the electrolyte in the solution than with the support. When the ionic strength between the electrolyte and the protein is lower than the protein-support strength, the adsorption on the support is favored. These electrostatic effects can modify the confinement kinetics of the protein and the ions concentration depend on the buffer composition, which is used to maintain the pH of the solution stable. From the composition of the buffer (e.g., phosphate buffer is formed by sodium monobasic

phosphate and sodium dibasic phosphate) is possible to select the ion types and their concentration [27]. In the following sections, the methods of adsorption, ionic interaction and entrapment are described more in deep.

1.2.1.1 Adsorption method

The adsorption is a non-covalent confinement method extensively studied both from a theoretical (modeling) and an experimental point of view. In general, the protein adsorption on the support is schematized in **Fig. 9**.

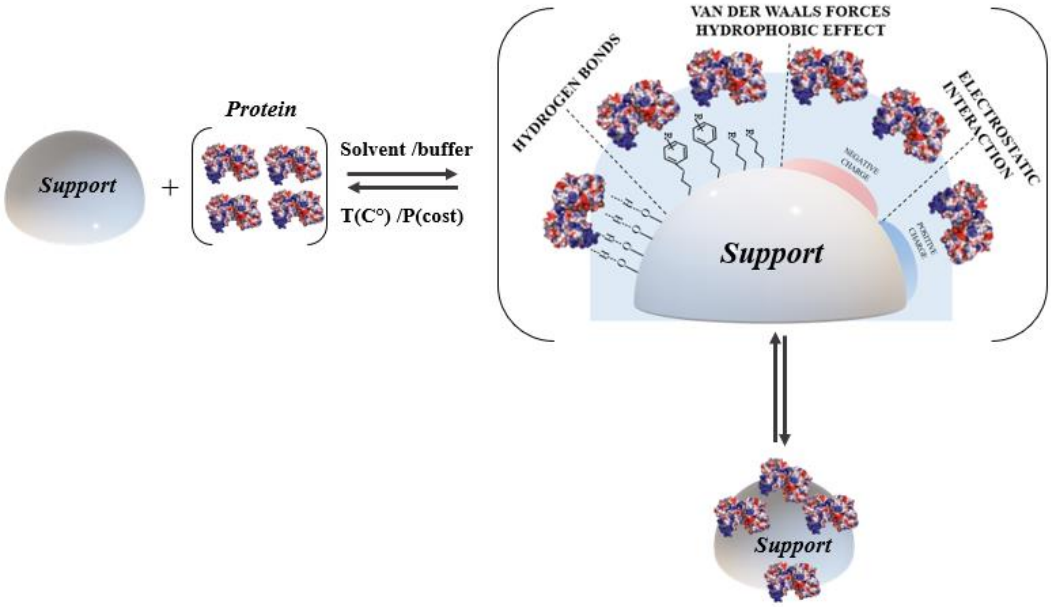

Fig. 9. Scheme of the adsorption process.

The interaction starts when the protein interacts with the support surface through weak forces at certain distance (r) to generate a complex protein-support. The principal driving forces of the adsorption mechanism are electrostatic and Van Der Waals interactions and hydrophobic effects. All these forces contribute to the adsorption process and they depend on the protein and on the physico-chemical properties of the support. However, some other parameters such as temperature, pH and substrate addition may weaken the bond. Furthermore, the adsorbed enzymes or other proteins are usually resistant to proteolysis and aggregation thanks to their hydrophobic interaction with the support surface [28], [29]. This interaction is due to an energy compensation between the conformational entropy of the protein and

the enthalpic energy of the adsorption process that stabilize the protein structure on the interfaces [30], [31].

In general, the adsorption process depends from kinetic and energetic factors. Literature data report that several approaches deal with mathematical models (based on kinetic or thermodynamic methods) in order to understand the absorption mechanism. From one side, the kinetic models [24], [32], [33], describe the events and phenomena during the process of adsorption, starting from an empty solid surface until the surface saturation is reached. From the other side, the thermodynamic models consider the energetic aspects involved in the protein adsorption and predict the final equilibrium state of adsorption based on some parameters such as pH, ionic strength, temperature, surface chemistry, protein composition, etc. [34]. A key element of the equilibrium models is a suitable expression of the Gibbs free energy of a given system, that includes enthalpic contributions from protein–protein and protein–surface interactions as well as the entropic contributions from the respective protein adsorption state and the surrounding solvation shell.

The knowledge of the Gibbs free energy minimum of the systems can give information on adsorption kinetic or about cooperative and surface clustering effects of the proteins [24], [35], [36].

1.2.1.2 Ion interaction method

The ionic interaction approach is based on the attraction between opposite charge groups present both on the protein and the support surface as shown in **Fig. 10**.
In a water environment, at a specific pH value, these surfaces are surrounded also by their counterions generating an electrical double layer [31].

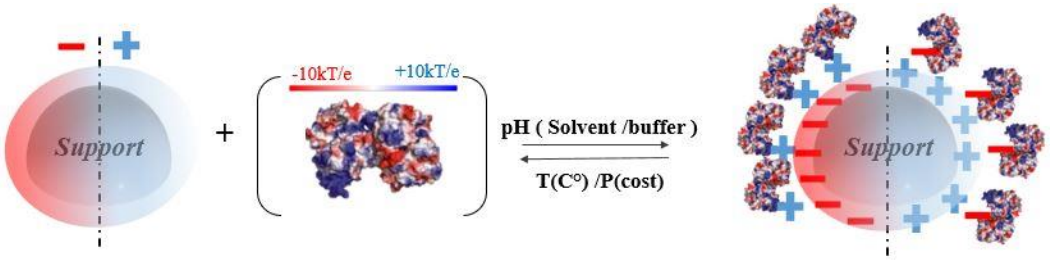

Fig. 10 Scheme of the ionic interaction process.

When the electrical double layers overlap, an ions redistribution is obtained. If one of the layers of protein or support carries a great excess of charge it would result in a considerable net amount of charge in the contact region between the protein layer and the sorbent surface. The excess of charge is compensated by ions with low molecular weight that pass from the solution to the absorbent layer and regulate the amount of charge at the interface [22], [37]–[39]. This interaction is reversible and depends on the modulation of the ionic strength of the solution, pH, and temperature. For example, the increase of the ionic strength or pH can cause a release of the protein from the interface of the support to the solution.
In their works, B. da Silva et al. [40] and the K. Chen et al. [41], observed that the protein-support complex, obtained from ionic interaction, depends on the intensity of the different interactions (coulomb interaction, charge regulation and ion-dipole) that can be generated during the process. The authors reported that an ionic interaction can be controlled by the ions quantity in the buffer solution and the pH values.
Seyrek et al. [42] established the consequences of concomitant repulsions and attractions of electrostatic origin in protein/polyelectrolyte association in a buffer solution. They showed that the anisotropy of electrostatic domains around a protein plays a dominant role in determining the ionic strength dependence of the binding to a polyelectrolyte. As a result, the affinity of the protein to the polyelectrolyte was

regulated by both the charge present on the surface of the protein (inhomogeneity of the Coulomb potential) and the short and long-range interactions with the polyelectrolyte typical of an adsorption process. Once, the ionic interactions can occur simultaneously in an adsorption process in a buffer environment.
The use of this method is very convenient since the binding of the protein with the support is much simpler and the conditions used are milder than in the covalent bond. Moreover, for an enzyme, the ionic binding causes slight modifications in the conformation of the active site, leading to a high enzyme activity. However, enzyme desorption may occur when an electrolyte solution (e.g., buffer solution hypertonic) of high ionic strength or with different pH was used. This is due to a weak bond between the proteins and the support molecules. In the case of an ionic bond, the interactions between the enzyme and the support are much stronger than the physical adsorption.

1.2.1.3. Entrapment method

In the entrapment method (see the scheme in **Fig. 11**), the proteins are occluded in synthetic or natural polymeric networks that retain the enzyme but allow the substrates and the products to pass.

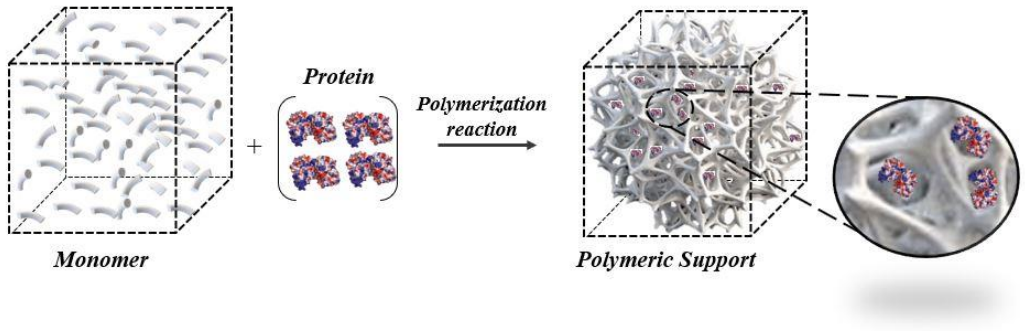

Fig. 11 Scheme of the encapsulation approach.

The driving forces are the same of the adsorption and ionic interaction. The protein entrapment can be an alternative way to keep separate the biological catalyst from the solution reagents phase, but the polymeric network can also be considered as an active support that can influence the enzyme structure and conformations, its dynamics, and the local environment, with a direct effect on its catalytic activity [43].

In general, this non-covalent confinement is divided in “hard” and “soft” entrapment [44]. In hard entrapment, the protein is confined into a fixed matrix, in which the protein structure must adapt to the rigid matrix walls. In this case, silica [45], zirconia [46], titanium oxides [47], graphene derivatives and metal-organic frameworks (MOF) [48] can be used as principal hard matrix. According to the experimental conditions selected, the structural architecture of these materials can be modulated varying the pores size and shape and also, the surface area.

In the soft entrapment the protein is confined in a flexible matrix where the protein can move more freely. In this case, the flexible matrix fits protein as a glove. As a result, the protein does not undergo much conformational changes. These soft materials such as membrane, natural polymeric (chitosan), cellulose and saccharide matrices (oligo or disaccharides) can possibly mimic the biological environment [49].

Soft and hard entrapments, can be obtained using different techniques: fiber entrapping [50], gel entrapping [51], encapsulation [52], etc.

The first methods, developed by Snamprogetti, consists in the physical entrapment of enzymes inside the microcavities of porous fibers [53] (nanofibers or pristine materials) [54].

The gels entrapment process concerns the enzymes confinement in sol-gel matrices. D. Avnir and co-workers reported [55], in a pioneering study, the immobilization of different enzymes by sol-gel process by hydrolytic polymerization of tetraethoxysilane. The morphology of the final silica sol-gels structure depended on the method of drying [56], [57]. In addition, T. Reetz and co-workers [58] found that, when lipases were entrapped in sol-gels produced by $Si(OEt)_4$, the resulting systems exhibited disappointingly low activities in the esterification of lauric acid by 1-octanol. Since this result could be due to the too hydrophilic microenvironment, they entrapped the lipase in a sol-gel prepared from a mixture of $Si(OMe)_4$ and $R\text{-}Si(OMe)_3$ containing non-hydrolysable alkyl moieties. In this case the matrix, more hydrophobic, would have facilitated interfacial activation of the lipase. Intriguingly, they observed rate enhancements of 2–8-fold compared with the traditional lyophilized lipase powders. This method has been widely used for the immobilization of enzymes [59]. Additives such as polyethylene glycol (PEG), polyvinyl alcohol and albumin, can have a stabilizing effect on sol-gel entrapped enzymes. Indeed, Zanin and co-workers [60] compared three different methods – physical binding, covalent attachment, and gel entrapment, in the presence and absence of PEG 1450 – for the immobilization of Candida rugosa lipase. Their activities were determined in the hydrolysis of olive oil.

Immobilization yields varied from 3 to 32%. The most active biocatalyst resulted by the encapsulation in the presence of PEG.

N. Ganonyan and co-works [61] reported a bio-friendly procedure for the entrapment of enzymes such as glucose oxidase, acid phosphatase and xylanase in silica aerogel, retaining both the enzymatic activity and the structure of the aerogel. All the steps of the aerogel synthesis were modified and optimized for reducing the risk of enzyme denaturation and for preserving the typical aerogel structure of the composite. The Michaelis-Menten kinetics (which represents the trend of the reaction rate catalyzed by enzymes) was observed for the entrapped enzymes, indicating that the enzymes are highly accessible and diffusional limitations of the substrate are negligible. Furthermore, S. Betigeri & H. Neau [62] observed that, when the lipase enzyme was entrapped in chitosan, it showed an enhanced enzyme activity and entrapment efficiency preventing its friability and leaching. The support matrix is biocompatible and nontoxic and it is receptive to chemical modifications due to its hydrophilic nature and high affinity toward proteins.

X. Wu et.al [63] reported the first example of multiple enzymes entrapped in MOF, which can be readily prepared via a co-precipitation procedure in an aqueous solution at environmental conditions. In this case, glucose oxidase (GOx) and horseradish peroxidase (HRP) were chosen for the cascade system[3] and used to prepare the multiple enzyme-embedded zeolitic imidazolate framework (ZIF-8). The GOx&HRP/ZIF-8 nanocomposite displayed high catalytic efficiency, high selectivity, and enhanced stability due to the protecting effect of the framework.

In another recent work, B. Heater et al. [64] have entrapped lipase into crystal protein (Cry3Aa). The Cry3Aa crystal-mediated entrapment, provides multiple benefits to the lipase, including a high enzyme loading, a significantly improved thermostability, an increased proteolytic resistance and the ability to be utilized as a recyclable biodiesel catalyst.

These different examples evidence that the entrapment system may be a good and quick strategy, sometimes done in one-pot step, to block the enzyme into the matrix preserving its catalytic activity.

[3] The model of the cascade enzymes represents a model formed by more enzyme that acts together on the substrate.

1.2.2 Covalent confinement

The covalent confinement is based on the chemical interactions between the protein and the support. These interactions generate strong covalent bonds. The chemical bond involves the sharing of electron pairs between atoms. Usually, the covalent bonds formed between the enzyme and the support are σ-bonding or π-bonding [65], [66]. The sigma bonds (σ bonds) are the strongest covalent chemical bonds.
In the covalent confinement, the protein uses the reactivity of lateral groups (amine, carboxyl, thiol, and aromatic ring) of the amino acids to generate a covalent interaction with the support. In general, as reported in **Fig. 12** the covalent confinement methods are divided in: Covalent bond on support, Cross-linking and Polymeric incorporation. In the following sections, the methods of the covalent bond on support and the cross-linking will be analyzed in detail[4].

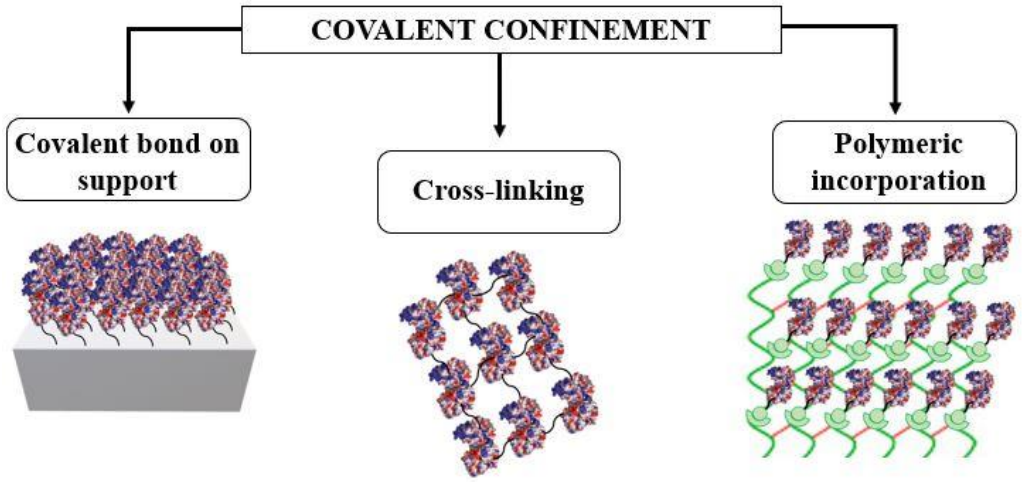

Fig. 12 Scheme of the covalent techniques.

[4] The polymeric incorporation is not deep because it is not used in this project.

1.2.2.1 Covalent bond on support

The covalent bond on support mainly depends on the formation of a covalent bond between the enzyme and the support material (see the scheme in **Fig. 13**). The problems related to this method concern the support morphology, hydrophilicity, numbers of reactivity groups, choice of molecular spacer arms, types of the activating agents to generate a covalent bond on the support.

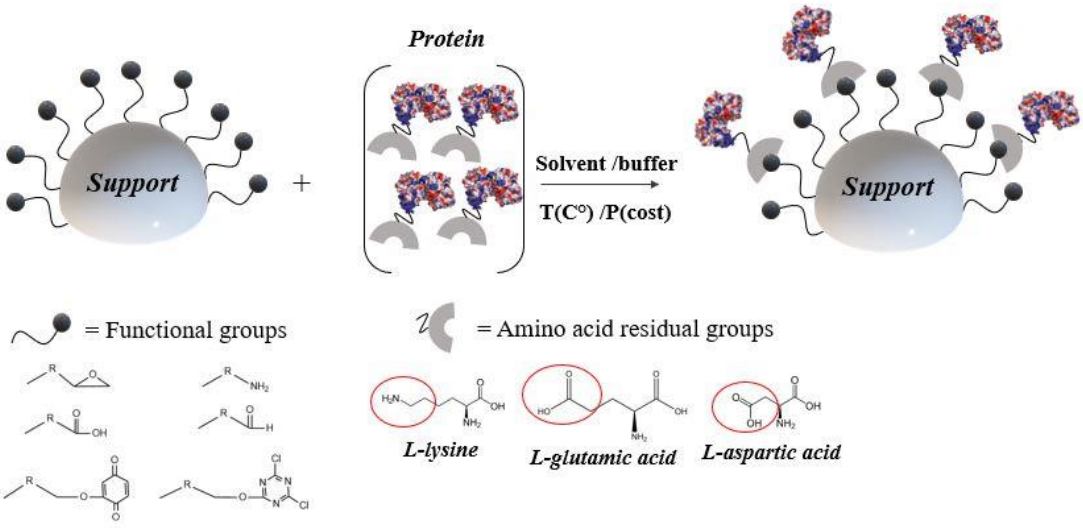

Fig. 13 Scheme of the covalent bond formation between the support and the protein.

The covalent linkage is strong and stable, and depends on the support material including polyacrylamide, porous glass, agarose, and porous silica [67], [68]. The reactivity, between the enzyme and the support, depends on the different functional groups present on the surface of the support such as carboxyl group, amino group, indole group, phenolic group, sulfhydryl group, thiol group, imidazole group, and hydroxyl group. Enzyme activities can be unaffected by the confinement, preventing the modification of the amino acids presents in the active site. The covalent binding of the enzyme with the support involves two main steps: the activation of the support by the addition of the reactive compound and the further modification of the surface matrix [68]. The activation step produces the electrophilic group on the surface of the support, so that it reacts with the strong nucleophiles groups of the proteins [4]. Moreover, higher specific activity and

stability, with controlled protein orientation, can be achieved when peptide-modified surfaces are used for enzyme linkages. For example, the enzyme shows high thermal stability when it is covalently linked to cyanogen bromide (CNBr)-agarose and CNBr-Sepharose. In this case, carbohydrate moiety and glutaraldehyde can act as spacer arm [69]. Moreover, covalent binding of enzymes in modified silica gel carriers (by removing unreacted aldehyde groups with SBA-15 supports) has shown enhanced enzyme stability and acts as hyperactive biocatalysts. Covalent binding of enzymes with mesoporous silica and chitosan can increase the half-life and thermal stability of the enzymes [70].

1.2.2.2 Cross-linking reaction

The cross-linking is another irreversible method for enzyme immobilization that does not necessarily require the presence of a support to prevent enzyme loss dispersion into the solution (see **Fig. 14 a**) [71], [72].

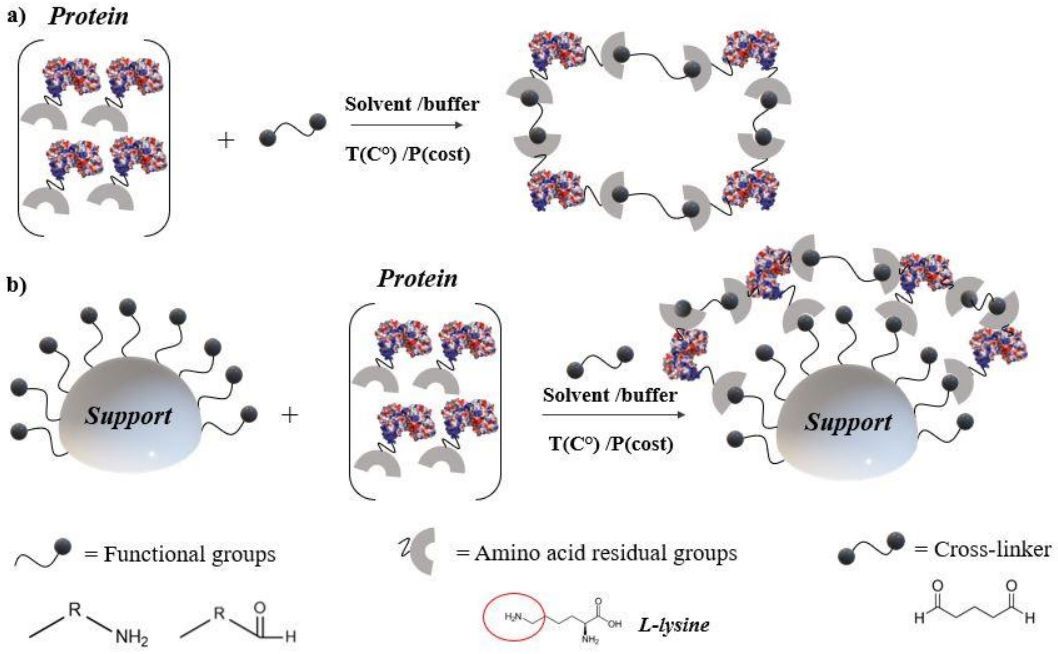

Fig. 14 a) Scheme of the Cross-linked enzyme aggregate (CLEA) **b)** cross-linking reaction between the protein and the support

The cross-linking is another irreversible method for enzyme immobilization that does not necessarily require the presence of a support to prevent enzyme loss dispersion into the solution (see **Fig. 14 a**) [71], [72]. This method can also be used to generate a covalently bonded protein-protein complex, but also among proteins and the surface of the solid support as shown in **Fig. 14 b**.

Cross-linking is obtained by the formation of intermolecular cross-linkages between the enzyme molecules by means of bi- or multifunctional reagents. In general, this technique is called CLEA (Cross-Linked Enzyme Aggregate) and glutaraldehyde is the most used cross-linking reagent due to its low cost and high availability (see **Fig. 14 a**) [73], [74]. For decades, this method used the aggregation and the reaction of the free α-amino groups of lysine residues, on the surface of neighboring enzyme molecules, with oligomers or polymers of glutaraldehyde resulting from inter- and intramolecular aldol condensations. Cross-linking reactions entail both Schiff's base formation and Michael-type 1,4 addition to α, β-unsaturated aldehyde moieties. The exact cross-linking mode is pH-dependent [75]. This method promotes high loading levels of the proteins and it manages to maintain the activity of the enzyme after the cross-linking process.

Another disadvantage is the formation of protein oligomers bound to the support surface, invalidating the results of the analysis revealing the quantity of bound protein. The activity of CLEA depends on several factors such as precipitant agent, additive, cross-linker, cross-linking time, enzyme concentration, temperature, pH and agitation [76].

1.2.3 Enzymatic kinetics in the confinement systems

The activity of the enzyme is the crucial aspect that should be analyzed in the immobilization systems. This parameter shows if the confined enzyme has a lower or a higher activity compared with the free enzyme.
In particular, the study of the rate of reaction catalyzed by the enzymes is called enzymatic kinetics [77], [78]. The general reaction (R.1.1),

(R.1.1) $$[S] \rightarrow [P]$$

where [S] is the substrate and [P] is the product of the reaction, is irreversible and with a low reaction rate.
When an enzyme is involved in the reaction R.1.1, the reaction rate increases since the enzyme acts as a catalyst (**Fig. 15**).

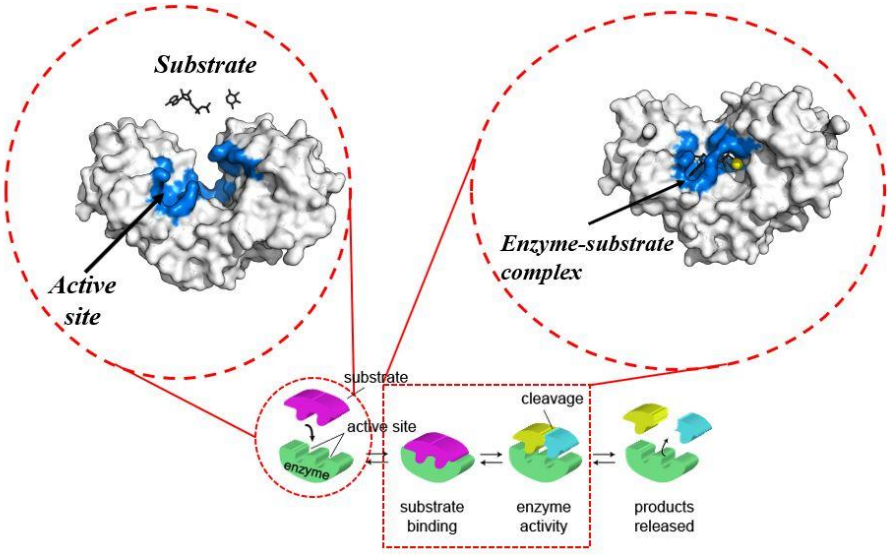

Fig. 15 Graphical representation of the interaction between the substrate and the enzyme during the catalysis reaction.

Due to the presence of the enzyme, R.1.1 becomes R.1.2.

(R 1.2) $$E + S \underset{k_{-1}}{\overset{k_1}{\rightleftarrows}} ES \underset{k_{-2}}{\overset{k_2}{\rightleftarrows}} EP \underset{k_{-3}}{\overset{k_3}{\rightleftarrows}} P + E$$

The first part of the equation (E+S↔ES) represents the initial interaction between the enzyme and the substrate, and the ES term describes the formation of the complex enzyme-substrate, which is the intermediate of the reaction. The second part (EP↔E+P) shows the EP complex, which in turn decays rapidly to product and enzyme (E+P). The ES ↔ EP terms describe the structural rearrangement of the complex (ES). In particular, the transformation of the substrate into the product remains tied for a short time to the enzyme to form the enzyme-product complex (EP). **Fig. 16** shows the plot of the free energy involved in the enzymatic catalysis reaction vs the reaction coordinate [79].

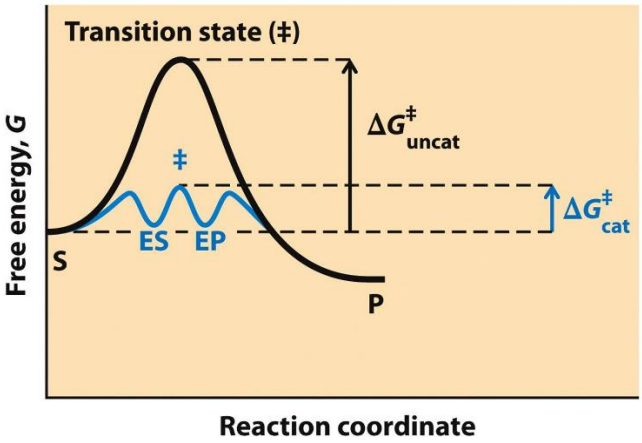

Fig. 16 Plot of the free energy of the enzymatic reaction [79].

The reaction velocity is described from the Michaelis -Menten equation (Eq. 1) [80].

(Eq. 1) $$v = \frac{V_{max}\,[S]}{K_M + [S]} \quad \text{where} \quad V_{max} = K_2[E_0]$$

where **v** is the velocity of the enzyme reaction, V_{max} is the maximal velocity for a specific enzyme concentration (this value depends on experimental condition: pH, temperature, reaction medium composition ect.), [***S***] is the substrate concentration and K_M is the Michaelis-Menten constant that represents the affinity of the enzyme to the substrate. If the K_M value is low the affinity is strong. For high K_M values, the affinity is low. The K_M and V_{max} values represent the kinetic parameters of the enzyme.

However, when the enzyme is confined on a solid surface it may behave differently from a free enzyme[E_0] in solution. The final behavior of the enzyme confined [E_s] on a solid may be affected by several factors: the different conformation of the enzyme after immobilization, the presence of different environments in the reaction solution, a different partitioning of the substrate between the solution and the support and the diffusional effects. **Fig. 17** shows the values of **v** for three enzyme-substrate systems[81], [82].

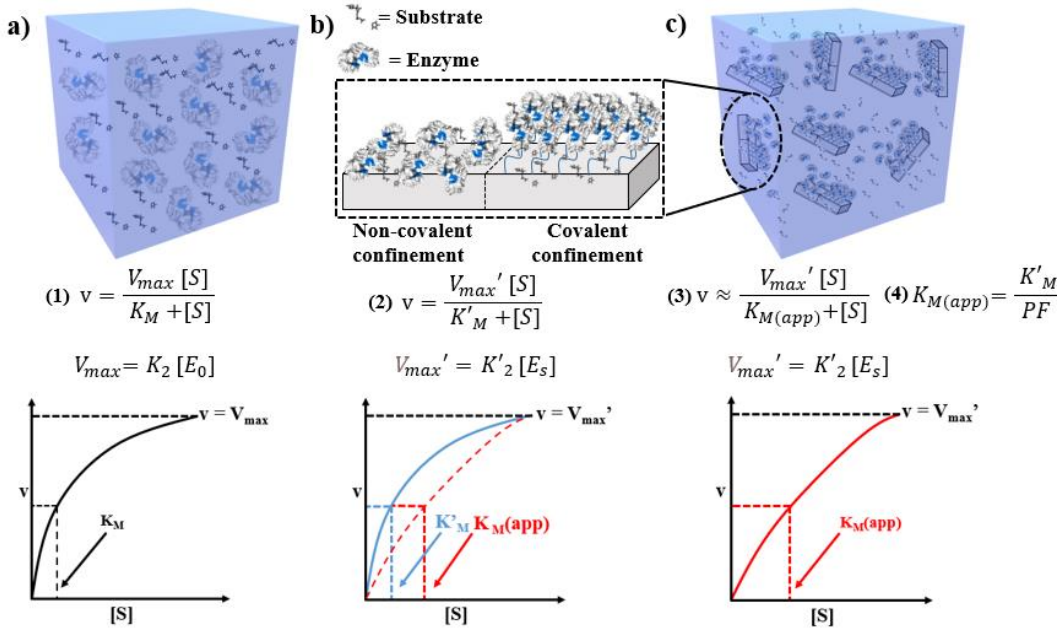

Fig. 17 a) Classical case of an enzyme and substrate in solution **b)** Enzyme confined on the support with the substrate diffusion **c)** Enzyme confined system in presence of the substrate in the solution [81].

In the first case, the enzyme and the substrate are in solution (**Fig. 17a**) and the reaction rate is controlled by the classical Michaelis -Menten equation (Eq. 1).

In the second case (**Fig. 17b**), both the enzyme and the substrate interact with the solid support. They may exist in different conformations and, consequently, the rate constants may be altered. In addition, the reaction can proceed in different environments. As a result of these effects, the Michaelis parameters, K_2 and K_M, may be different from those of the free solution. So, we consider K'_2 and K'_M as new parameters and equation (Eq. 1) becomes:

(Eq. 2) $$v = \frac{V_{max}[S]}{K'_M + [S]} \quad \text{where} \quad V_{max} = K'_2[E_s]$$

However, there is also the possibility that, diffusion effects of the substrate could be present in the solid support, leading to a change in the reaction rate of the confined enzyme (see graph in **Fig. 18a-b**).
The limiting rate, $K'_2[E_s]$, can have the same value both in the absence or presence of diffusion effects since this term corresponds to the complete saturation of the enzyme by the substrate. On the contrary, at low substrate concentrations, the diffusion has a significant effect on the reaction rate. In some cases, the rate can be lowered increasing K_M. This may be due to a low substrate availability for the enzyme. The change of the K'_M value is indicated with an apparent Michaelis constant, $K_{M(app)}$ which can assume values greater than K'_M. In this case, the diffusion effect causes a decrease of the reaction rate of the enzyme.

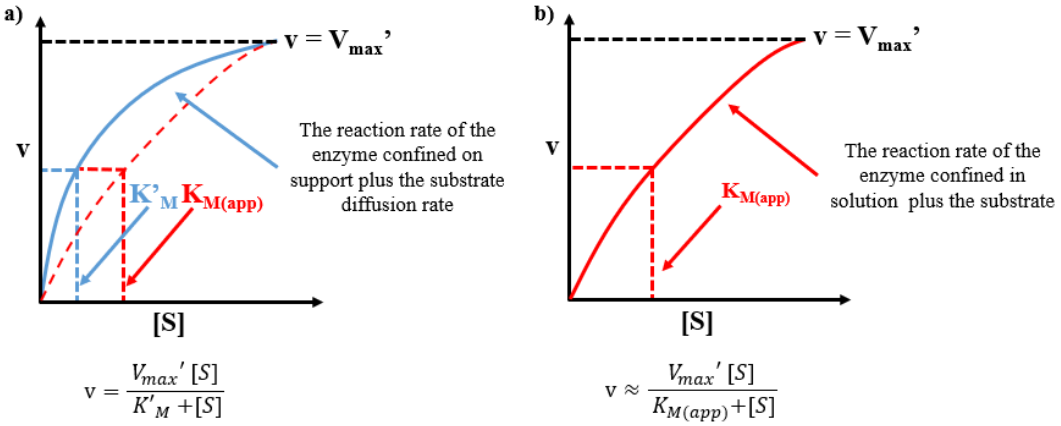

Fig. 18 Comparison between **a)** the enzyme confined in the presence of the substrate diffusion and **b)** the rate enzyme confined rate in the solution with the substrate.

In the third system (**Fig. 17c**), the enzyme is confined on the support and the substrate is present in solution. In order to interact with the enzyme, the substrate

has to diffuse into the solid. Therefore, as in the previous case, the diffusion is important. However, there is an additional factor to consider: the partition coefficient (P) related to the amount of the substrate in solution and on the support. This factor may increase the rates when greater than unity. In this case, the rate equation can be written as (Eq. 3)

(Eq. 3) $$v \approx \frac{V_{max}'[S]}{K_{M\,(app)}+[S]} \quad \text{where} \quad V_{max}' = K'_2[E_s]$$

The apparent Michaelis constant $\boldsymbol{K_{M\ (app)}}$ is related to the $\boldsymbol{K'_M}$ value for the immobilized enzyme by equation (Eq. 4):

(Eq. 4) $$K_{M\,(app)} = \frac{K'_M}{PF}$$

where P is a partition coefficient and F is a Thiele function (Eq. 5) to be taken into account when diffusion is involved in catalytic problems. This function depends on the support thickness ***l***, the enzyme concentration [$\boldsymbol{E_s}$]and the diffusion coefficient ***D*** for the substrate in the support.

(Eq. 5) $$F = \frac{\tan \gamma l}{\gamma l} \quad \text{where} \quad \gamma = \frac{1}{2}\sqrt{\frac{V_{max}'}{DK'_M}}$$

In the case of enzyme confinement on spherical support as shown **Fig. 19**. that follows the Michaelis-Menten kinetics, Himberg and coworkers [83] proposed (Eq. 6):

(Eq. 6) $$D\frac{1}{r^2}\frac{d}{dr}\left(r^2\frac{dS(r)}{dr}\right) = \frac{V_{max}'S(r)}{K'_M+S(r)}$$

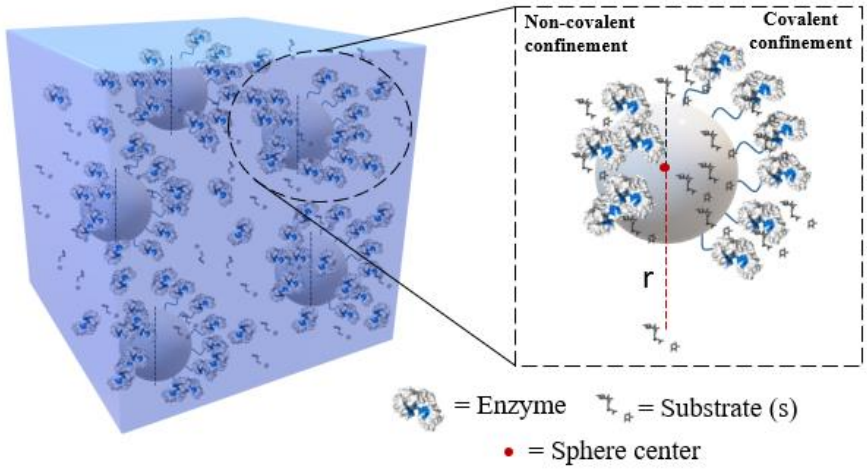

Fig. 19 Enzyme confinement on spherical support.

that describes the stationary distribution of the substrate. ***D*** is the diffusion coefficient of the substrate within the spherical support, ***S(r***) is the concentration of the substrate at a distance ***r*** from the center of the support particle, K'_2 and K'_M are the true catalytic and the Michaelis constants, respectively, for the reaction within the support. Due to conformational and environmental effects they can differ from the kinetic parameters of the free enzyme, K_2 and K_M

The kinetic parameters of the confinement enzymes can also depend on other factors such as temperature and pH. Temperature plays a particular role in enzyme confinement and substrate transformation. At higher temperatures, the enzyme converts more rapidly the substrate to the product which is accumulated in the solution. In the case of free enzyme in solution, the increase of product concentration and temperature may cause a structural instability of the enzyme leading to a loss of activity. For a confined enzyme, the interaction with the support can increase the structural stability at higher temperature, even though, also in this case, an accumulation of the product on the support can decrease the catalytic activity (see **Fig. 20 a**).

The pH variation in the solution may generate a different partitioning of hydrogen ions or hydronium between the solution and the confined enzyme. The pH effect can influence the reaction rate resulting in a shift of the pK values of the confined enzyme with respect to the free enzyme values. This effect can be due to accumulated hydroxyl ions or hydronium ions on both the confined enzyme and the

charged support. As a result, the optimum pH values change for the confined enzyme with respect to the free enzyme values (see **Fig. 20 b**).

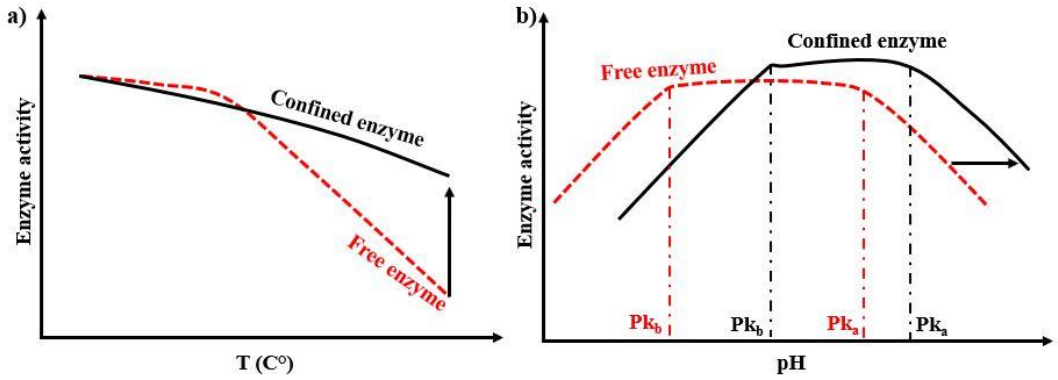

Fig. 20 a) Temperature effect and **b)** pH effect on free enzyme and confined enzyme [81][84].

C. Rodrigues and coworkers [85], [86] evidenced that some other variables such as the aggregation effect, the diminished enzyme inhibition, the presence of pores (when the support is a porous matrix), the enzyme rigidification, etc. can improve the activity, the specificity and the selectivity (real or apparent) of the immobilized enzyme. The aggregation is much lower for the free enzyme but depends on the concentration in the solution. Some cases evidenced an improved activity of immobilized enzymes with respect to the aggregated free enzymes even though, the improved activity could be an artifact. In this case, the increase of the catalytic effect may be due to a greater amount of enzyme on the support and not to an increased stability of the enzyme. Concerning the enzyme inhibition, free enzymes in solution may be inhibited by high concentrations of the substrate or by some of the products, decreasing the observed activity. In some cases, when these enzymes are confined on a support, the inhibition effect diminishes and an increased enzyme activity after immobilization may be expected. This effect on the improved activity can be the result of a higher affinity between the substrate and the active site, reducing some allosteric inhibitions.

Therefore, the higher enzymes activity, after immobilization, can be due to a decrease of the enzyme inhibition, and not to a more active conformation of the enzyme. In addition, when the enzyme is confined into a pore structure, the presence of pores can have several protective effects on the enzyme structure such as an apparent increase in the enzyme activity and stability. Another variable that strongly determines the enzyme activity is the so-called enzyme rigidification. A strong enzyme structure rigidification is obtained when the enzyme is bound to the surface

of the support by multipoint covalent bonds. The rigidification prevents enzyme conformational changes and it increases the enzyme activity, solvent resistance and thermal stability. The rigidification can also stabilize a more active conformation of the enzyme. Some enzymes, such as the lipase classes, can exist in different conformational states: the open and closed forms. In the close form, the active site is protected by a hydrophobic pocket. When the substrate interacts with the pocket (interfacial activation) via hydrophobic interaction, the lid is open exposing the active site to the medium. Other classes of enzymes can be hyperactivated by a conformational change induced by an activator or some specific medium [87], [88]. In addition, other factors such as effect of medium partition, diffusional limitations, production of a new more active conformation can also influence the enzyme activity [89].

Y. Zhang and coworkers [90] studied the electrostatic stabilization, the enhanced capture of substrates and the effect of metal ions that may enhance the activity of confined enzymes. The electrostatic stabilization between the enzyme and the support can affect the apparent activity of the confined enzymes and the presence of polyelectrolytes can also enhance of 15-fold the kinetic parameters. An activity change is also observed when specific metal ions are incorporated into the support. Finally, properly designed systems, used in the immobilization, can capture the substrates through hydrophobic or electrostatic interactions. The adsorption and desorption of substrates on supports are dynamically balanced, leading to a higher substrate concentration in the vicinity of the enzyme. This enrichment of substrate, which is also known as the positive partition effect, apparently reduces the Michaelis constant, $\mathbf{K_{M\ (app)}}$, giving an increased apparent enzymatic activity.

All these factors can enhance the activity of the confined enzyme, but the final result strongly depends on the type of the support, from the enzyme characteristics, and its interaction with the support.

1.3 NON-POROUS AND MESOPOROUS MATERIAL SUPPORTS: STATE OF THE ART

The bond between the supports and the enzymes is crucial to determine the success of the enzyme immobilization. The bond depends not only on the protein characteristics, but also on the nature and characteristics of the support matrix. Based on their chemical composition, the support matrices are classified into two main classes: inorganic and organic. The first one includes glass, silica gel, alumina, metal oxides, zirconia, and many other silica-based materials. These systems are widely used for their thermal and mechanical resistance, their rigidity and their suitable porosity.

The class of organic support represents a wide group of compounds divided in: natural supports and synthetic supports.

The natural supports usually are from natural origin and are water-insoluble. This class includes collagen, chitosan, carrageenan, alginate, cellulose, starch, agarose, etc.. Due to their chemical structure, the distinctive features of these natural polymers are their ability to form inert gels which can be easily activated. They can bind to proteins or enzymes in a reversible and irreversible way. They are available in large quantities, inexpensive, and they show high thermal and mechanical resistance.

The synthetic supports are ion-exchange resins, which have a porous surface and are insoluble in nature. This class includes polystyrene, polyvinyl chloride (PVC), polyacrylate, polyamide, polypropylene, diethylamino-ethyl cellulose (DEAE cellulose), UV-activated polyethylene glycerol, etc..

In general, the choice of the support depends on economic advantages, inertness, stability, structural strength, ability to enhance enzyme specificity/ activity, easy recovery, ability to reduce product inhibition, and ability to prevent nonspecific adsorption and bacterial contamination.

The next sections reports in detail the non-porous and mesoporous silica based systems used as supports in the thesis [17], [43], [91].

1.3.1 Silica Materials: Sol gel mechanism and particles formation

The sol-gel process is widely applied to produce inorganic materials due to its ability to form pure and homogenous products at mild conditions. This technique, classified as *Soft chemistry* is widely used for tailored materials and nanoparticles production [92]. The process includes a two steps reaction: metal alkoxides [M (OR) n with R = ring-alkyl or aryl] hydrolysis and hydroxyl groups condensation.
The hydrolysis reaction is influenced by steric and inductive effects and can be acid and base catalyzed. The reaction proceeds by bimolecular nucleophilic displacement reactions (S_N2-Si) involving pentacoordinate intermediates or transition states [93], [94].

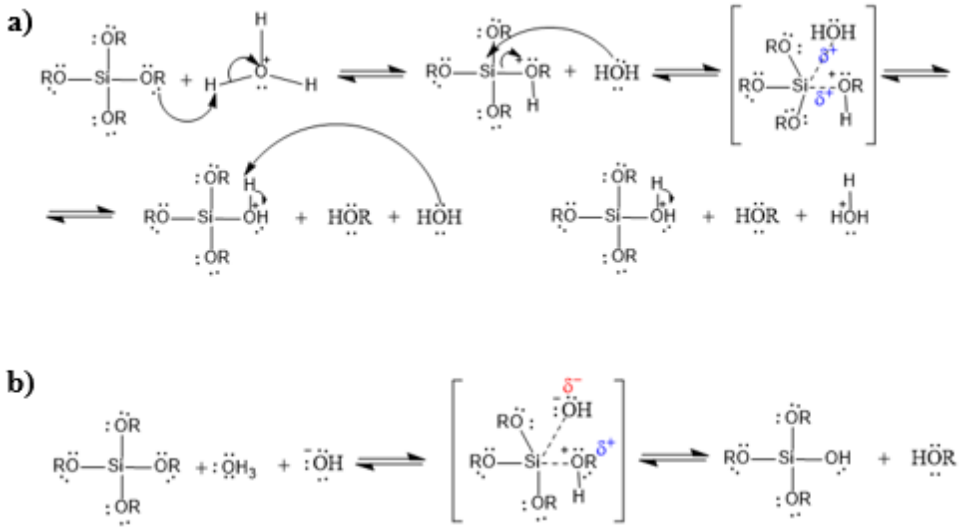

R. 2 a) Mechanism of the acid-catalyzed hydrolysis **b)** Mechanism of the base-catalyzed hydrolysis.

Under acid conditions, an alkoxide group is protonated in a rapid first step. Electron density is withdrawn from silicon, making it more electrophilic and thus more susceptible to be attacked by water (**R. 2a)**. Under basic conditions, the water dissociates to produce a nucleophilic hydroxide anion during a rapid first step; after that, the anion attacks the silicon center (**R. 2b)**. The hydrolysis reaction may follow the reverse process, in which the alkoxide group displaces a hydroxyl group to produce an alkoxide ligand plus water as a by-product.

This reverse process, re-esterification, always occurs via mechanisms S_N2 (**R. 3)** [92]. During the hydrolysis, also transesterification could take place, in which alcohol displaces an alkoxide group to procedure an alcohol molecule. This reaction often occurs when alkoxides are hydrolyzed in alcohols containing different alkyl groups [95].

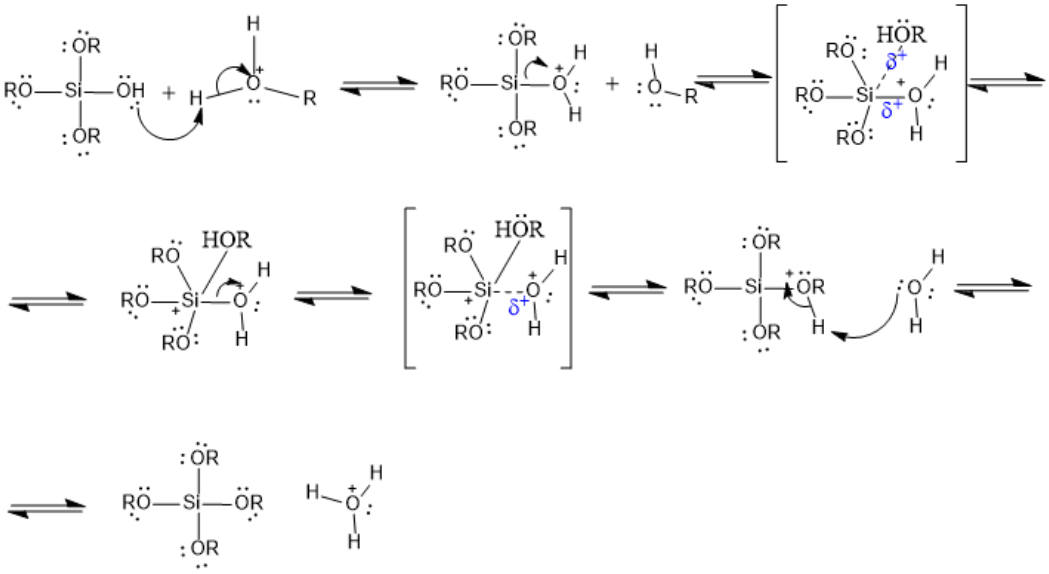

R. 3 Re-esterification reaction by bimolecular nucleophilic substitution reactions.

The condensation reactions occur by either a de-alcoholization or dehydration process with the formation of an alcohol or water molecule. As the hydrolysis reaction, also the condensation reaction depends on the pH of the solution. Under acidic conditions (**R. 4a**), the condensation mechanisms occur through a protonated silanol species. Protonation of the silanol makes the silicon more electrophilic and thus more susceptible to the nucleophilic attack. At basic conditions (**R. 4b**), the reaction involves the attack of a nucleophilic deprotonated silanol on neutral silicate species [92] [95].

As a result, the final reaction produces a sol-phase of inorganic polymers network that can condense into particles that remain stably suspended or can aggregate in a particular gel or can grow so much that they settle out of suspension.

The continuous collisions and the aggregations between primary particles, formed in the sol-phase, can led to the growth of the particle clusters linked together into a gel phase.

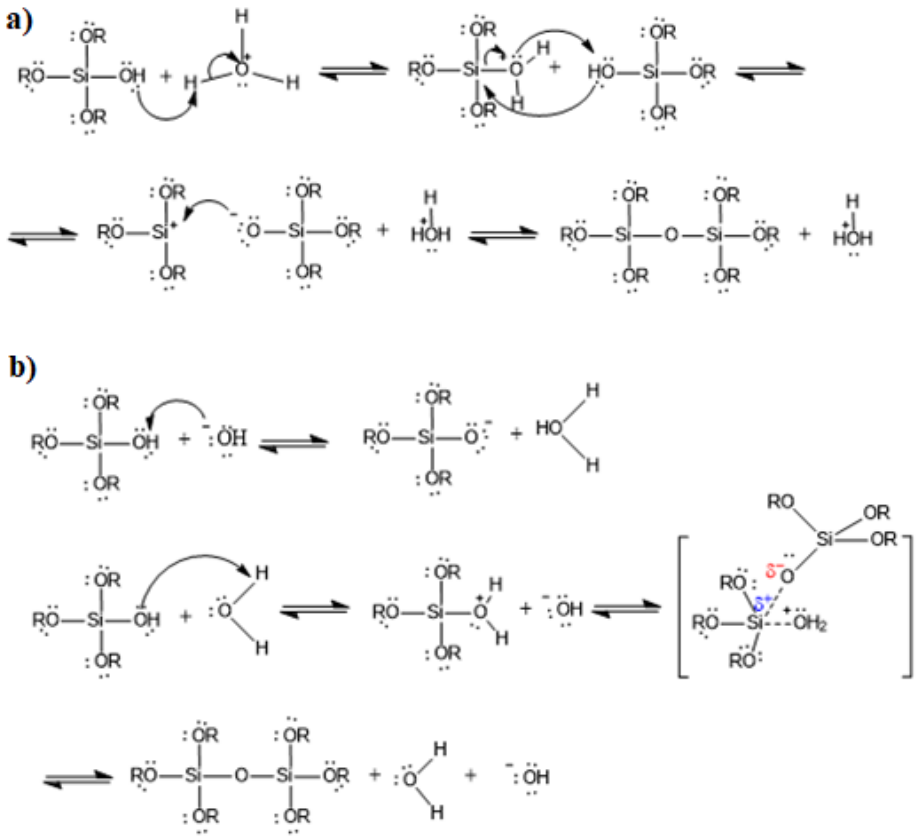

R. 4 a) Mechanism of the acid-catalyzed condensation **b)** Mechanism of the base- catalyzed condensation.

Since a shorter time of nucleation decreases the final total number of nuclei and increases the final particle size of the synthetic silica colloids, the rates of the hydrolysis intermediates formation and of the condensation mechanisms is crucial. This fact confirms that the relative rate of the two reaction mechanisms can be decisive for the final quality of the product.

The most famous method to produce monodisperse non-porous silica particles was developed by Stöber, Fink, and Bohn (SFB) [96]. The process involves the hydrolysis of tetraethyl-orthosilicate (TEOS) in a basic solution of water and alcohol. During the reaction, the particles grow up to a critical size of about 350nm [97].

Silica particles larger than 1 μm can be commonly prepared by a seeded-growth technique known as the multistage SFB method (see **Fig. 21**). This technique involves a first step where seed particles are formed. In this step, the diameter of the particles may reach a critical size as predict by the classical reaction described

above (**R. 2-4**). The next steps, defined as growth steps of the silica particles, are obtained by the slow addition of the TEOS precursor. As a result, the increased TEOS concentration facilitates the formation of new particles that aggregate on the particles previously formed. The aggregation increases the diameter of the particles. It is possible to obtain different particle sizes as a function of the temperature, the concentration of the reagents (NH_3, H_2O, presence of a polyelectrolyte such as KCl, and TEOS) and by setting the drop rate of TEOS [98], [99].

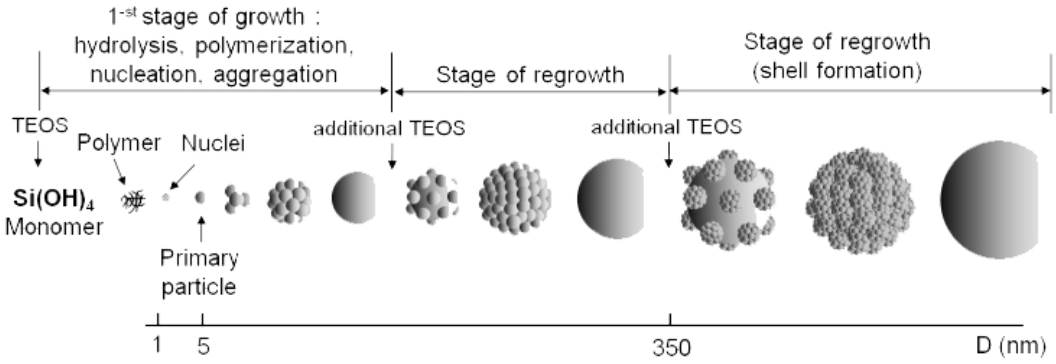

Fig. 21 Modified Stöber method (Seeded–growth technique) [97].

1.3.2 Mesoporous Materials

The mesoporous materials are widely used as carriers in the enzyme confinement systems. An advantage of these materials is the possibility to change their surface morphology changing the synthesis conditions. In particular, the mesoporous materials prepared via the sol gel-method are produced by two different approaches: Soft-templating and hard-templating.

In the soft method, organic molecules such as surfactants block copolymers, and silane coupling agents are used as structural directing agents. Several theoretical models have been developed for describing the formation mechanism of the mesoporous systems via the soft method. **Fig. 22** reports the principal mechanisms: liquid-crystal templating mechanism (LCT) and cooperative formation mechanism (CFM) [100].

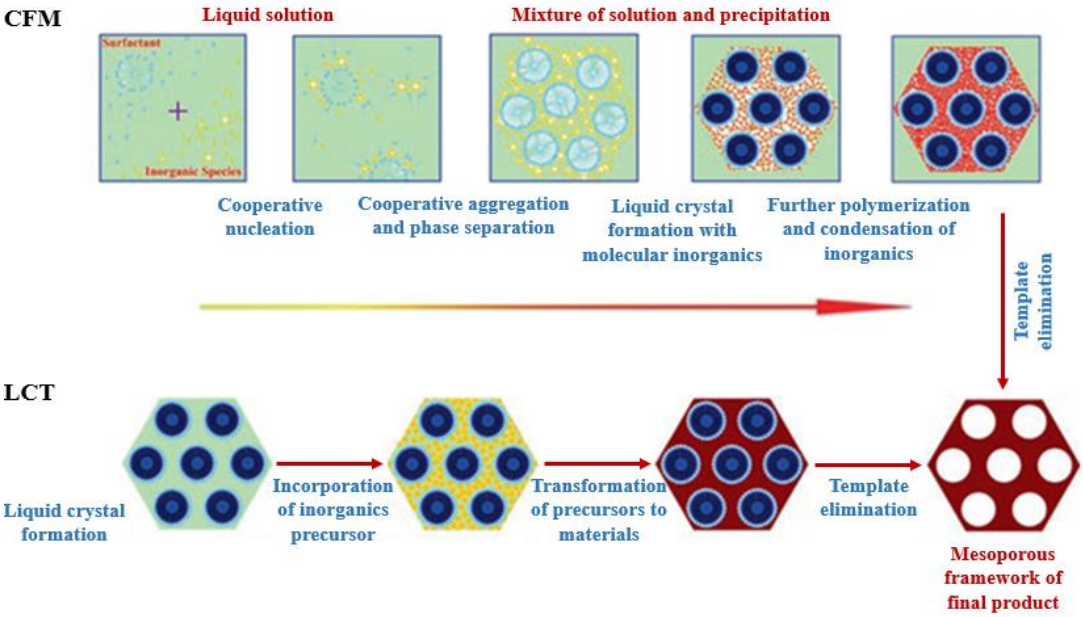

Fig. 22 Principal mechanisms for the synthesis of mesoporous material: cooperative formation mechanism (CFM) and liquid-crystal templating mechanism (LCT) [100].

The hard-templating method (**Fig. 23**) uses a guest material (swelling agent) to generate a pore structure modification in the matrix support. The process can be divided in three steps: 1) the precursor infiltration inside meso-channels of the silica template; 2) the conversion of the precursor in the nanochannels; 3) the removal of the mesoporous silica template.

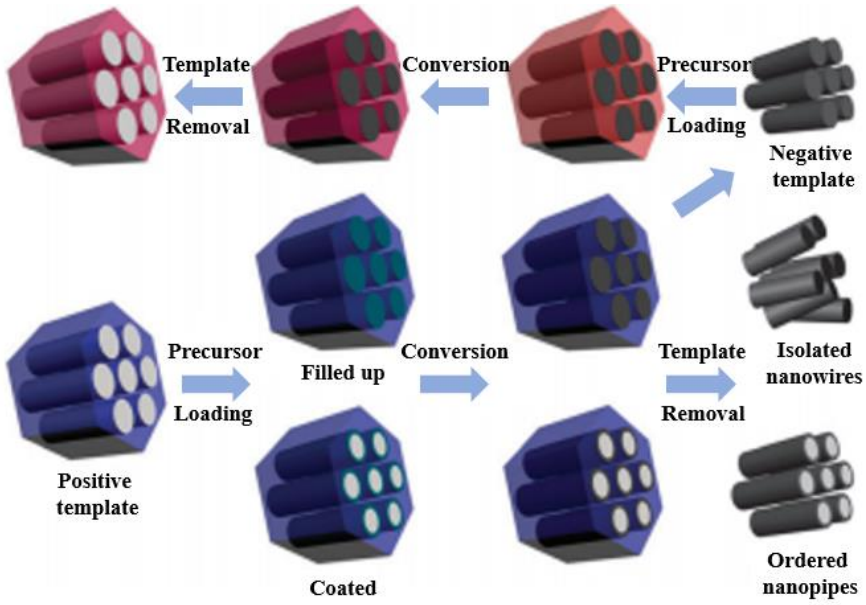

Fig. 23 Hard template process [101].

Those methods are used to prepare different mesoporous materials (see **Fig. 24**) such as MCM [9, 10], SBA [104], FDU [105], MSU[106], HOM[107], KIT[108] series.

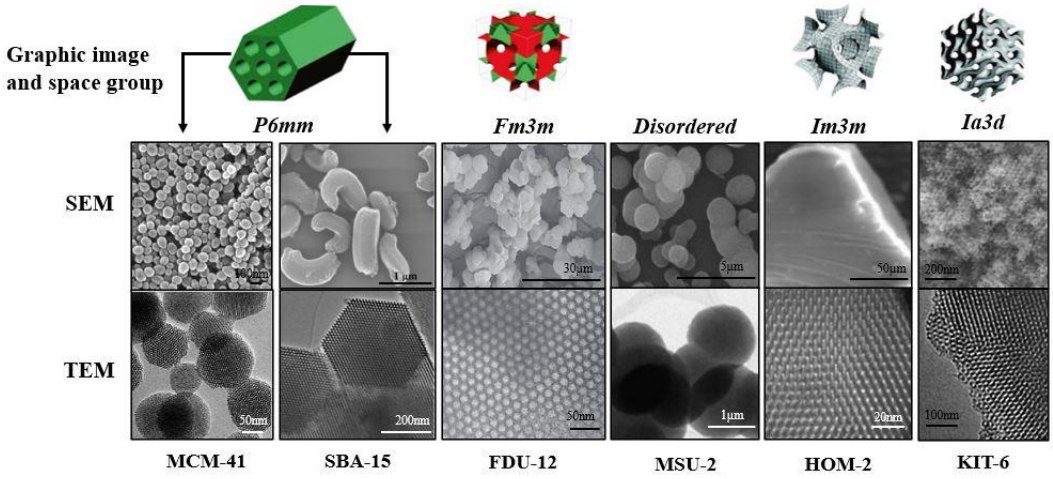

Fig. 24 SEM and TEM images of different mesoporous silica materials [100], [107], [109]–[113].

Thanks to their morphology and to the easy synthesis, the MCM and SBA structures are widely used as supports for enzyme confinement. However, also dendritic fibrous systems such as KCC1or DFNPs are widely used as supports [114]. Unlike

MCM and SBA structures, DFNPs (**Fig. 25**), obtained via hard templating, have a disordered structure and derive from a cooperative assemble between the micelles and the silicates formed in the solution to generate a dendritic pore structure.

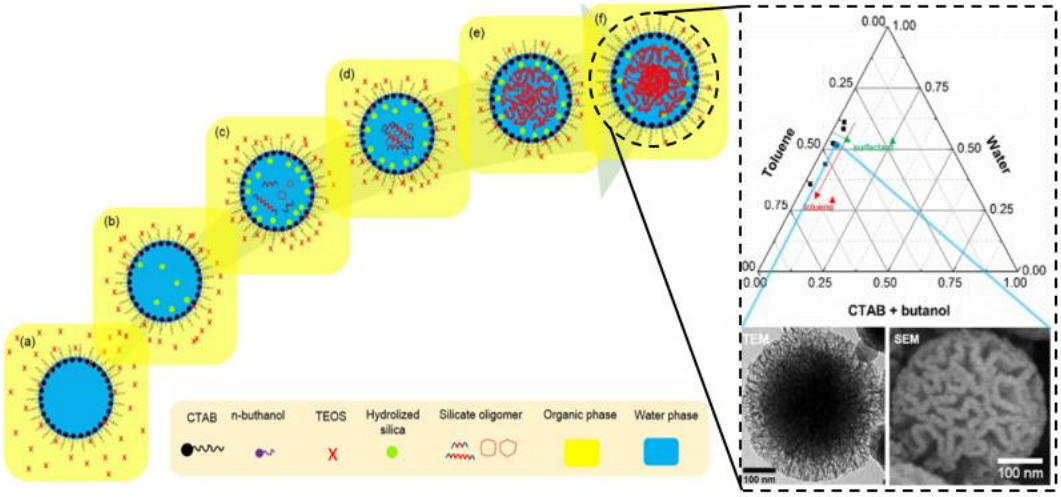

Fig. 25 Formation mechanism of dendritic fibrous silica particles (DFNPs) [115].

1.3.3 The bioinspired method: A eco-friendly synthesis to produce silica material

Bioinspired methods use soft strategies to produce inorganic mesoporous structures; **Fig. 26** shows an example for silica. In general, the bioinspired process is designed on the chemical principles underpinning the biological processes. An example is the bioinspired silicification method inspired by the natural bio-silicification. Indeed, in nature exist different organisms such as diatoms, sponges, and grasses that are able to form a variety of complex and hierarchical biogenic silica structures under mild physiological conditions [116].

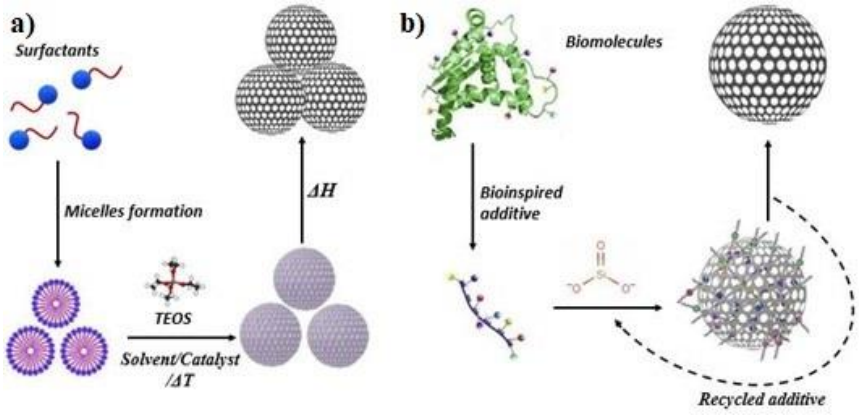

Fig. 26 a) Typical synthesis of the mesoporous silica particles (MSN), **b)** Development of bio-inspired silica synthesis [117].

The bio-silica produced in the organisms is used as mechanical structural support, as protection against predators and as sensors. In the bio-silicification, the silicic acid, a non-toxic compound and soluble in aqueous environments, is the starting precursor [118]. Probably the formation of the bio-silica polymer is due to specific proteins (Silicatein-α [119]), peptides, and amines, which catalyze the condensation reaction of the silicic acid to form a silica polymeric network. However, this mechanism is not yet fully understood. On the other hand, biosynthesis generates an ornate and hieratical silica structure at mild pH (near-neutral), at room temperatures (<40°C) in a friendly aqueous ('green') environment [120].
In a typical silica bio-inspired process, the polymerization reaction occurs in water using mild conditions and with Na_2SiO_4 as a precursor. The reaction is activated by additives used as catalysts and templates. At the end of the reaction, they are

removed. The mild conditions of the bioinspired method might be relevant for generating the silica platforms for the enzyme confinement [116], [121].

A principal advantage of this method is that the materials properties (e.g., surface area, particle size, porosity, etc.) can be fine-tuned through the use of appropriate processing parameters, additives and silica precursors, the preparation time is short, it requires mild conditions and it is flexible.

The R5 peptide was the first molecule used as catalyst for the bioinspired method and it was able to maintain a high activity and stability of some confined enzymes (catalase, horseradish peroxidase and β-Galactosidase). However, R5 peptide is very expensive, and thus alternative additives have been considered [12], [122], [123].

For instance, C. Forsyth [124] and co-works used different amines such as pentaethylenehexamine (PEHA), tetraethylenepentamine (TEPA), triethylenetetramine (TETA), and diethylenetriamine (DETA) for the entrapment of the lipase enzyme into the bioinspired silica support. The authors obtained high immobilization efficiency close to 100% and high levels of activity and stability.

Polyethyleneimine (PEI) was also successfully used for enzyme entrapment, even though poor results were obtained for lipase and carboxylesterase immobilization [125], [126]. Although many works report a significant loss of activity for the confined enzyme, the PEI additive appears efficient for horseradish peroxidase immobilization [127]. In addition, also additives like polyallylamine (PAH), polyamidoamine dendrimers (PAMAM), and poly-L-lysine (PLL) can successfully immobilize enzymes such as D-amino acid oxidase, glucose oxidase, horseradish peroxidase, adenosine deaminase [128] . However, the comparison between different immobilization systems is not straightforward due to the limitations caused by the diffusion effects of the substrate and product formed after reaction. The success of the system depends very much on the size of the substrate used in activity tests the confinement systems.

1.3.4 Chemical functionalization of the supports for the confinement enzyme

The surface interaction between the enzymes and the supports is a crucial step to generate the final confined systems. In general, the chemical and physical proprieties of the surface of the support can be improved or modified by a suitable surface functionalization [100], [129], [130]. The functionalization can influence the catalytic efficiency and the dispersion ability of the enzyme and the interactions between the enzyme interfaces. In addition, the surface modification is used to provide biocompatibility, steadiness, and functionality to the supports for their further applications [131]. During the enzyme immobilization, the presence of the functionalized group can control the electrostatic interaction and reduce the diameter of the channels to facilitate the enzyme entrapment in the nanochannels of the support carrier. The surface functionalization can occur through direct or post-synthetic functionalization (grafting) [129], [132]. The direct functionalization method is performed during the synthesis of the support. This strategy has several advantages such as homogeneous surface coverage in one-pot synthesis, a better control over the amount of incorporating ligand on the surface, and the possibility to use a wide range of functional groups. The grafting method is used to link functional groups after the support synthesis

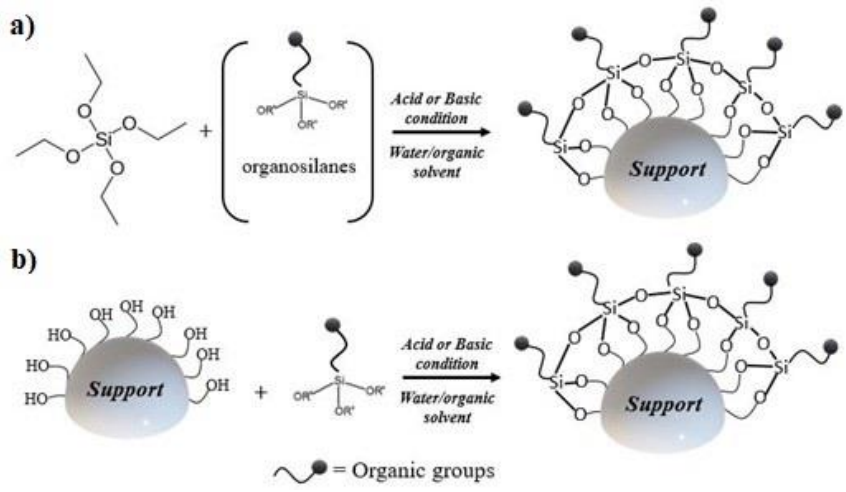

Fig. 27 a) Direct functionalization method, **b)** post-synthesis grafting method.

In the case of the silica support, the direct functionalization method (see **Fig. 27 a**) is performed using a precursor (TEOS) together with different organosilanes such as (3-Aminopropyl) triethoxysilane (APTES), (3-mercaptoopropyl) trimethoxysilane (MPTMS) or (3-Glycidyloxypropyl) trimethoxysilane (GPTMS), which actively participate to the synthesis. In the grafting method (see **Fig. 27 b**), the silica support is functionalized by a silylation process, which can graft the desired functional groups. In this case, the silanol groups can be replaced by a target organic ligand through a single-phase or multistep attachment. The clustering of the functional groups and the formation of an isolated cluster are the main disadvantages of this procedure.

1.4 IMMOBILIZATION OF ENDOGLUCANASE AND PETASE

In all industrial activities, the production of natural and synthetic waste is inevitable and, consequently, it is one of the most important issues to be addressed in the near future. Among the strategies and methods to transform waste in resource, now, recycling is one of the most used. However, physical and chemical methods of recycling can have some adverse effects mainly related to the environmental impacts that they could cause. In the last years, among the recycling processes, the use of enzymes has been receiving growing attention. In particular, the cellulase families are used for recycling biomass waste to produce bioethanol, and the PETase families for recycling PET bottles. Nevertheless, the main disadvantages of a strategy involving enzymes are always strongly related to the recovery and the production of the biocatalyst. For this reason, the immobilization or confinement of the enzymes may be a valid solution to some of the problems related to the use of enzymes in industrial processes.

1.4.1 Endo-β-1,4-glucanase

In the last decades, biomass has been widely used as a sustainable resource for the production of biofuels (e.g. bioethanol, biohydrogen, and biodiesel) [133]. In particular, the Endo-β 1,4-glucanase is part of a wide family, called glucanase, that catalyzed the hydrolysis of the cellulose in the biomass to produce reducing oligosaccharides (see **Fig. 28**) [134], [135]. Endo-β-1,4-glucanase is the main for cellulose degradation, it is produced by *Aspergillus Niger* and it belongs to the glycosyl hydrolase family 12. It is known to catalyze glycosidic bond cleavage with net retention of anomeric configuration. In general, the structure of the cellulases is divided into two main parts: a carbohydrate-binding domain (CBD) and a catalytic domain (CD). The (CBD) domain facilitates the interaction between the enzyme catalytic domain (CD) and the cellulose network. The (CD) domain is the principal site where the catalytic hydrolysis occurs [136]. The hydrolysis mechanism is catalyzed in an acid or basic environment, where the catalytic reaction stepwise passes through a glycosyl-enzyme intermediate to letting the substrate be hydrolyzed via oxocarbenium- ion transition states [137]–[139]. Moreover, considering the cellulosic ethanol production, cellulase costs about 40% of the total

cost and, in general, is used in the soluble form, which presents several drawbacks such as low stability, poor reusability, and limitations when used in continuous reactors [140], [141].

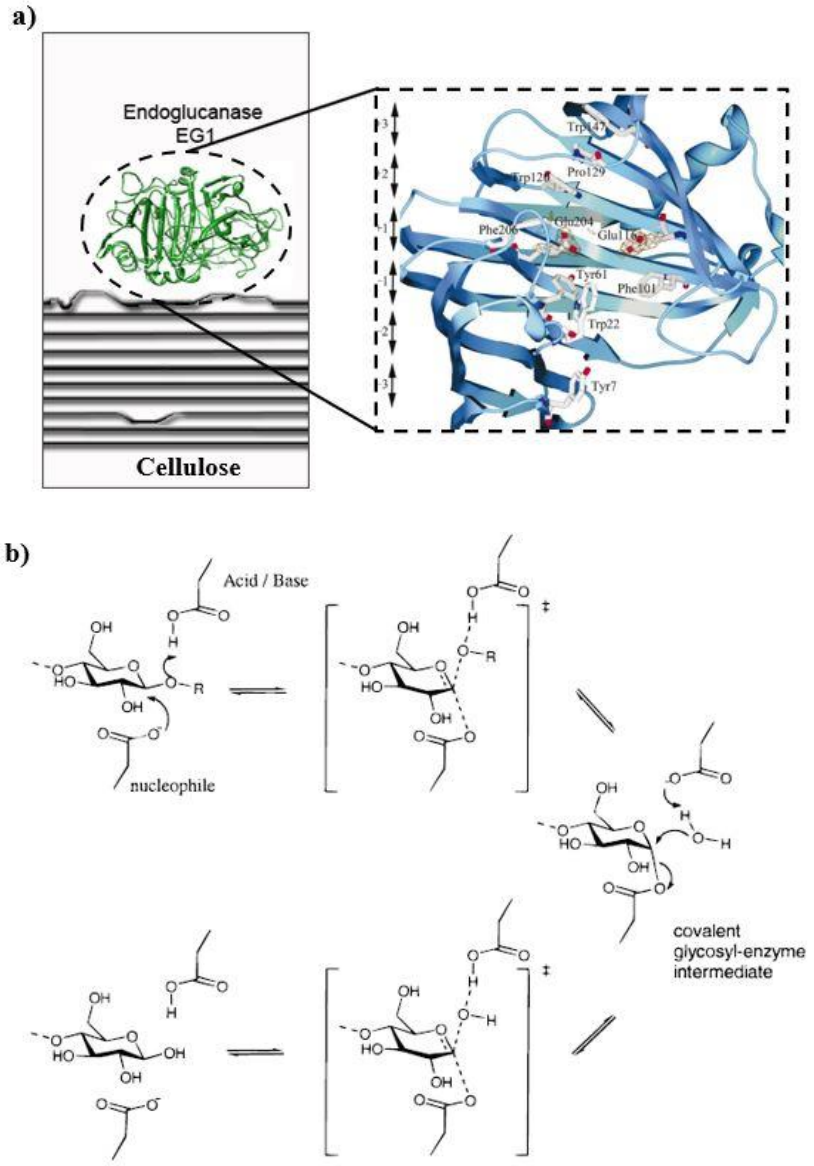

Fig. 28 a) Endo-β-1,4-glucanase structure and catalytic site, **b)** reaction catalysis [138].

1.4.2 PETases

The Polyethylene terephthalate (PET) is one of the most used plastics, in addition to polyethylene, polypropylene, polystyrene, polyvinyl chloride, and polyurethane, and its worldwide production amounted to 56 million tons in 2013 [142]. PET has various applications and it can be used for the production of manufacturing bottles, fibers, films, and containers [143]. The PET waste is dumped on land and in oceans and, eventually, it is deteriorated into microplastics threatening the marine ecosystem. In general, the degradation of PET is obtained by chemical techniques based on the polymerization of the powder produced, that transform the polymer into the initial raw material. These chemical techniques can be very expensive and not eco-friendly [144].

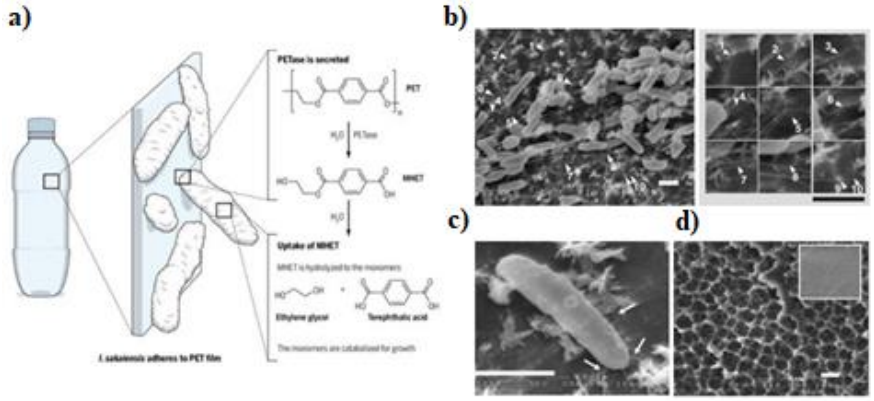

Fig. 29 a) Scheme of the degradation a PET bottle, **b)** SEM images of a bacterium that degrades and assimilates PET, **c)** SEM images of *I. sakaiensis* cells grown on a PET film for 60 hours, **d)** SEM image of a degraded PET film surface [142], [144].

As an improved approach, the work of S. Yoshida and co-workers[144] showed that some microbes such *Ideonella sakaiensis*, (see **Fig. 29**) adapted properly and evolved to partially degrade man-made plastics into carbon and energy sources. In particular, the authors showed that the microbes species degrade the plastic by using enzymes (PETase and METase) efficiently converting PET into its two monomers, terephthalic acid, and ethylene glycol.

On comparative analysis with esterase enzymes such as lipases and cutinases, PETase was found to have more effective activity at low temperature, in degrading PET films. The work of X. Han and coworkers [145] presents the structure of the PETase from the PET-consuming microbe *Ideonella sakaiensis*. The authors

explained that the PETase adopts the canonical α/β- hydrolase fold, in which the strictly is conserved catalytic triad Serine (S 131)-Histidine (H 208)-Aspartic acid (D 177). Several unique features are present near the catalytic center such as two intra- molecular disulfide bridges (DS1 and DS2) and Tryptophan (W156) adjacent to the catalytic center displays variable conformations in the crystal structures.
Tryptophan (W156) is found in every PET-hydrolyzing enzyme. **Fig. 30a** shows the PETase structure with the catalytic sites evidenced in **Fig. 30b-c.** The authors reported a three-steps reaction mechanism for PET hydrolysis. The first step concerns the substrate-binding formation where different conformations of Tryptophan (W156) are possible (**Fig. 30d)**. During the second step, PET enters the substrate-binding cleft. The carbonyl group placed in the active site is ready to be hydrolyzed by the nucleophilic attack of Serine (S131). As last step, the resulting benzoic acid group of the hydrolytic compound becomes more planar, and it is induced by W156 to turn and form a face-to-face stacking interaction. As a result, the enzyme hydrolysis reaction may cause an initial dissolution of the polymer [146]–[148].

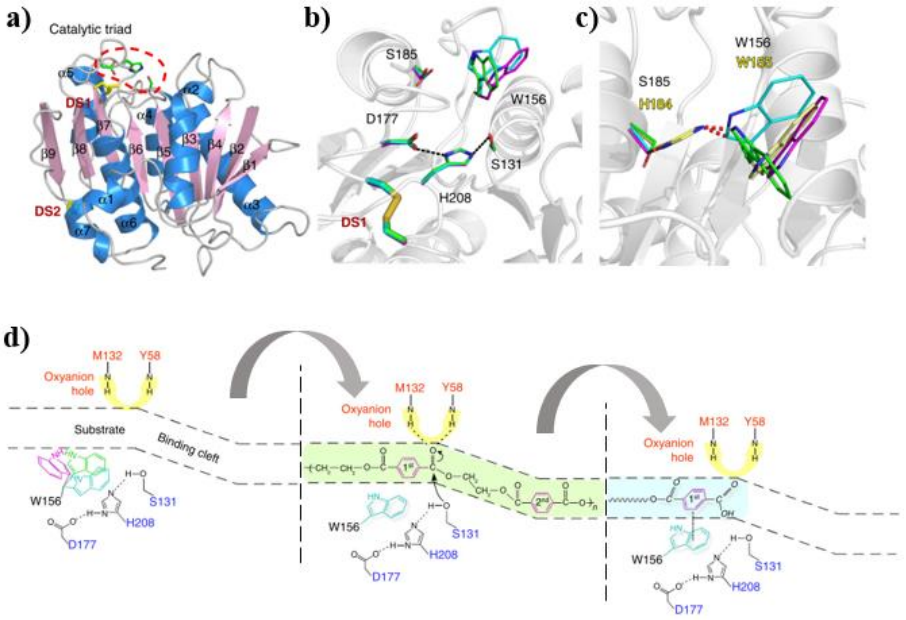

Fig. 30 a) Graphic model of the PETase enzyme structure, **b), c)** Catalytic site, **d)** Hydrolysis mechanism reaction of the PETase [149].

CHAPTER 2

EXPERIMENTAL PART

2.1 SYNTHESIS OF DIFFERENT SILICA SUPPORTS

2.1.1 Synthesis of the non-porous silica particles via Stöber method

2.1.1.1 Materials

Table 2 reports a list of reagents used for the samples preparation. They were used without further purification.

Table 2

Reagents	Abbreviation	PM (uma)	Purity	Density (g cm^{-3})	Supplier
Ethanol	EtOH	46.07	99.8%	0.79	Aldrich
ammonia solution	NH_3	35.05	28wt%	0.90	Fluka
tetraethyl orthosilicate	TEOS	208.33	98%	0.93	Aldrich
potassium chloride	KCl	74.55	99%	1.98	Fluka

2.1.1.2 Synthesis of non-porous silica via Stöber method

Silica particles, obtained via Stöber method [96], were prepared by hydrolysis and condensation of tetraethyl orthosilicate (TEOS) in ethanol and in presence of ammonia as catalyst. In a jacketed beaker (250 ml) with thermostatic bath a first solution with a preferred concentration of ethanol (14.6 M), ammonia (1.6 M) and millQ water (4.9 M) was added. The solution was stirred for 5 min to ensure a complete mixing. A second solution of TEOS (0.1 M) was added slowly (dripping) into the first solution at 30 °C overnight. After the addition of TEOS, the clear solution gradually turned opaque due to the formation of a white silica suspension, and it was continuously stirred for 24 h. The final colloidal solution was separated by centrifugation from the suspension at 9000 rpm and washed with water and ethanol for three times, and then they were dried in an oven at 60 °C overnight.

2.1.1.3 Synthesis of non-porous silica via modified Stöber method

The Silica particles with larger size were obtained using the method of Yu et al. and performed with a piston pump (Prostar varian 210) [150].
The synthesis of silica particles was conducted in a 250 mL jacketed glass where an ethanol solution (4.92 M) of TEOS (0.08 M) (solution I) was continuously supplied with a piston pump to the reaction mixture (solution II) of water (3.2 M), ethanol (4.92 M), ammonia (2.41 M) and KCl electrolyte (0.002 M). The solution (I) was dropped into the solution (II) with the supply rate of 0.2 mL min^{-1}. The reaction temperature was 30 °C and the stirring speed was 300 rpm. After supply of solution I, the obtained particles were purified by centrifugation at 9000 rpm and washed with ethanol three times. Finally, the SiO_2 particles were dried in stove at 60 °C.

2.1.2 Synthesis of mesoporous silica via soft and hard methods

2.1.2.1 Materials

Table 3 reports a list of reagents used for the samples preparation. They were used without further purification.

Table 3					
Reagents	Abbreviation	PM (uma)	Purity	Density (g cm^{-3})	Supplier
Ethanol	EtOH	46.07	99.8%	0.79	Aldrich
ammonia solution	NH_3	35.05	28wt%	0.90	Fluka
tetraethyl orthosilicate	TEOS	208.33	98%	0.93	Aldrich
hexadecyltrimethylammonium bromide	CTABr	364.45	98%	1.11	Aldrich
sodium hydroxide	NaOH	40	98%	2.13	Aldrich
n-hexane	NHEX	86.18	95%	0.66	Aldrich
Toluene	TOL	92.14	99%	0.87	Aldrich
Urea	UREA	60.06	99%	1.34	Aldrich
Acetone	ACE	58.08	99%	0.80	Aldrich
sodium stearate	Na-STE	306.46	99%	1.02	Aldrich
TYLOSE MH300 (Methyl 2-hydroxyethyl cellulose)	MHEC	n/a	n/a	1.30	Aldrich
Methanol	MeOH	32.04	99%	0.80	Aldrich
n-butanol	n-BuOH	74.12	99%	0.81	Aldrich

2.1.2.2 Synthesis of MSN with soft template method (series MC)

The MSN synthesis was performed following the method of Chen et.al starting from TEOS as precursor, hexadecyltrimethylammonium bromide (CTABr) as template and ammonia as catalyst [100]. In a jacketed beaker of 250 ml an amount of CTABr (0.08 M) was dissolved in a solution of deionized water (40 M) ethanol (4.10 M) and ammonia (0.34 M). An amount of the TEOS was slowly dropped into the solution and mixed for 2 h at 30 °C. The final colloidal solution was filtered and washed with deionized water and ethanol. The product was dried and calcined for 5 h at 550 °C, to remove the organic part. The synthesis was performed with different surfactants such as sodium stearate and methyl 2-hydroxyethyl cellulose (Tylose).

2.1.2.3 Synthesis of MSN with hard template (series MS).

A new series of MSN was performed using an organic co-solvent as swelling agent to increase the micelle size and obtaining a mesoporous system with larger pore size. In this case, TEOS hydrolysis and condensation were catalysed by sodium hydroxide (NaOH). In a jacketed beaker of 250 ml CTABr (0.001 M) and NaOH (0.003 M) were dissolved in water (53 M) and mixed for 10 min at 30 °C. An amount of n-hexane (0.23 M) was added under vigorous stirring (500 rpm) for 15 min to form an emulsion. After the emulsion formation the stirring was stopped waiting for the separation of the two phases. At this point, a TEOS solution (0.01 M) was added and mixed for 5 h. The final product was filtered and washed with deionized water and methanol (MeOH). The product was dried and calcined in air at two temperature and rates: 90°C at 1 °C/min and 550 °C at 5 °C/min for 5 h.

2.1.2.4 Synthesis of DFNPs (KCC1 series).

The KCC1 synthesis was prepared following the work of Febriyanti et al. [151]. In typical synthesis, n-butanol (0.21 M) was dissolved in toluene (4.40 M) followed by adding TEOS (0.18 M). Subsequently, a solution of CTABr (0.04 M), urea (0.16 M) in deionized water (26 M) was quickly added into the above solution. After vigorous stirring for 30 min, the mixture that turned into emulsion was transferred to a 50 mL Teflon lined autoclave and heated at 120 °C for 4 h. The resulting product was isolated by centrifugation, washed with deionized water and acetone and dried in air for 24 h. Finally, the as-synthesized product was calcined at 550 °C for 6 h in air.

2.1.3 Synthesis of silica support via bioinspired method

2.1.3.1 Materials

In **Table 4** are listed all the reagents used for the samples preparation. They were used without further purification.

Table 4

Reagents	Abbreviation	PM (uma)	Purity	Density (g cm^{-3})	Supplier
sodium metasilicate pentahydrate	Na_2SiO_3 x $5H_2O$	212.14	95%	2.61	Aldrich
hydrochloric acid	HCl	36.46	37%	1.3	Aldrich
diethylenetriamine	DETA	103.17	99%	0.95	Aldrich
triethylenetetramine	TETA	146.23	97%	0.98	Aldrich
pentaethylenehexamine	PEHA	232.37	99%	0.95	Aldrich
polyethyleneimine	PEI	~25000	99%	n/a	Aldrich
polyallylamine hydrochloride	PAA	~50000	99%	n/a	Aldrich

2.1.3.2 Bioinspired method

The typically bio-inspired synthesis [116] was performed preparing, into a 150 ml tube, the first solution of Na_2SiO_3 x $5H_2O$ (0.03 M) and 70 ml of deionized water. In a second tube the additive was weighed out in a molar ratio [Si]:[N]=1 and was dissolved in 20 ml deionized water. The reaction mixture was neutralized adding a pre-determined amount of 1 M HCl while stirring to reach the final pH of 7 ± 0.05 after 5 min. For post-synthetic treatment, in a second step, to the supports synthesized at pH 7, further pre-determined amount of 1 M HCl was added to reach the desired pH value (pH 5 or pH 2) [29]. After the reaction, the suspension was centrifuged at 5000 rpm for 15 min and washed 3 times in deionized water. After washes, the product has been dried in a vacuum oven for 5 h. The synthesis was performed using other additives (DETA, TETA, PAA, PEI).

2.1.4 Characterization

The porosity of the samples was analyzed by nitrogen physisorption measurements collected at liquid nitrogen temperature (−196 °C) using a Micromeritics ASAP 2010 volumetric adsorption analyzer. The Brunauer Emmett Teller (BET) equation was used to calculate the specific surface area, the pore size distributions by the Barrett Joyner Halenda (BJH) model. The study of the morphology was performed by Zeiss Sigma VP FE-SEM c/o the Centro di Microscopia "Giovanni Stevanato" in Venezia-Mestre (VE, Italy). The particle size distribution was calculated by the ImageJ software. The degree of BIS samples purification was analyzed by the Diffuse Reflectance Fourier Transform Infrared Spectroscopy (DRIFT-IR) with a NEXUS-FT-IR instrument implementing a Nicolet AVATAR Diffuse Reflectance accessory.

2.2 CHEMICAL FUNCTIONALIZATION OF DIFFERENT SILICA SUPPORTS

2.2.1 Materials

In **Table 5** are listed all the reagents used in the samples preparation. They were used without further purification.

Table 5

Reagents	Abbreviation	PM (uma)	Purity	Density (g cm^{-3})	Supplier
Ethanol	EtOH	46.07	99.8%	0.79	Aldrich
ammonia solution	NH_3	35.05	28wt%	0.90	Fluka
tetraethyl orthosilicate	TEOS	208.33	98%	0.93	Aldrich
(3-Aminopropyl) triethoxysilane	APTES	221.37	99%	0.94	Aldrich
(3-Mercaptopropyl) trimethoxysilane	MPTMS	196.34	95%	1.05	Aldrich
(3-Glycidyloxypropyl) trimethoxysilane	GPTMS	236.34	98%	1.07	Aldrich
N-[(3-trimethoxysilyl)propyl] ethylenediaminetriacetic acid	EDTA-TMS	462.21	45%	1.26	ATK Chemical
(3-Chloropropyl) trimethoxysilane	CPTMS	198.72	97%	1.09	Aldrich
toluene	TOL	92.14	99%	0.87	Aldrich
sodium acetate anhydrous	NaOAc	82.03	99%	1.53	Aldrich
acetic acid	AcOH	60.05	99%	1.05	Aldrich
cyclohexane	Cy	84.16	99%	0.78	Aldrich
n-propylamine	PrA	59.11	98%	0.72	Aldrich
Triethylamine	TEA	101.19	99%	0.73	Aldrich
Tetrahydrofuran	THF	72.11	99%	0.89	Aldrich
Methanol	MeOH	32.04	99%	0.80	Aldrich
Dimethylformamide	DMF	73.09	99%	0.94	Aldrich
Sodium azide	NaN_3	65.01	99%	1.85	Fluka
Copper (II) sulfate	Cu SO_4	159.61	99%	3.603	Aldrich
Biotin alkyne	B-Alkyne	281.37	98%	n/a	Lumiprobe
(+)-Sodium L-ascorbate	SA	198.11	98%	1.66	Aldrich
polyethyleneimine	PEI	~25000	99%	n/a	Aldrich

2.2.2 Silica support functionalization via 3-Aminopropyltriethoxysilane (APTES).

The functionalization with APTES was performed using four different method.

2.2.2.1 Functionalization via acid silylation (method A)

In a beaker, 0.3 g of silica particles were dispersed in water (1.40 M) and ethanol (8.14 M) under stirring. In another vial, under stirring, a solution of water (1.40 M) and ethanol (8.14 M) was prepared. Glacial acetic acid was added to adjust the pH to 5.0 and then APTES (0.13 M) was added. This solution was then dropped to the first one, the final solution was left under stirring for 3 h. The resulting silica particles were collected by centrifugation at 9000 rpm for 30 min and washed in water and ethanol. The obtained product was dried overnight at room temperature.

2.2.2.2 Functionalization via grafting in organic solvent (method B)

In a glass flask, 0.4 g of silica particles were dispersed in toluene (8.85 M) under stirring at 50 °C for 30 min. APTES (0.03 M) to the solution was added under reflux at 110 °C and mixed for 24h. The final product was centrifuged at 9000 rpm for 10 min, washed three times with ethanol solution and dried at room temperature overnight.

2.2.2.3Functionalization via acid silylation using a controlled dripping (method C)

In a glass flask, 0.3 g of silica particles were dispersed an acetate buffer solution (0.01 M at pH 5) and ethanol (8.20 M) under stirring at room temperature. In another vial, a solution of ethanol (8 M) and APTES (0.13 M) was prepared. This solution was then dropped to the first one by a piston pump with a supply rate of 0.2 mL min-1. After dropping, the final solution was left under stirring for 3 h. The resulting silica particles were collected by centrifugation at 9000 rpm for 30 min, washed three times with water and ethanol. The final product was dried at room temperature overnight.

2.2.2.4 Direct Functionalization via Co-condensation synthesis (method D)

In a glass flask, a solution of water (2.70 M), ethanol (14.64 M), and ammonia (4 M) was prepared. In another vial, a quantity of TEOS (0.08 M) and of APTES (0.03 M) were dissolved in ethanol (14 M) under stirring at room temperature for 10 min. This solution was then dropped to the first one, the resulting solution was mixed for 24 h at room temperature. The resulted colloidal solution was centrifuged at 9000 rpm for 30 min, washed three times with water and ethanol. The final product was dried at 70 °C.

2.2.3 Silica support functionalization via (3-mercaptopropyl)trimethoxysilane (MPTMS).

In a glass flask, 0.3 g of silica particles were dispersed in cyclohexane (4.50 M) under stirring at room temperature. In a second glass flask the second solution of cyclohexane (4.50 M), n-propylamine(0.12 M), and MPTMS (0.05 M) was prepared. This solution was added to the first one and mixed for 1 h at room temperature. The resulting silica particles were collected by centrifugation at 9000 rpm for 30 min, washed three times with water and ethanol. The product was dried at room temperature.

2.2.4 Silica support functionalization via (3-Glycidyloxypropyl) trimethoxysilane (GPTMS).

Surface modification of silica supports with GPTMS was performed according to methods already present in literature [22]. 1 g of dry silica particles were dispersed in dry toluene (9 M) and then GPTMS (0.01 M) and triethylamine (0.02 M) were added. The resulting mixture was refluxed under nitrogen atmosphere at 110 °C and mixed for 4 h. The resulting silica particles were collected by filtration and washed with THF. Finally, product was dried at 120 °C for 8 h.

2.2.4.1 Functionalization with polyethyleneimine

After GPTMS functionalization further modification was carried out using a polyamine (PEI). In this case, 0.15 g of the silica functionalized with GPTMS were dissolved in 10 ml of methanol. 0.23 g of PEI were added to the solution and mixed

for 3 h under reflux at 60 °C. The resulting silica particles were collected by filtration and washed several times with methanol. Product was then dried at 60 °C for 3 h.

2.2.5 Silica support functionalization via N-[(3-trimethoxysilyl)propyl] ethylenediaminetriacetic acid (TMS-EDTA).

In a glass flask, 0.08 g of silica particles were dispersed in water (23 M) under stirring at room temperature. A second solution comprising EDTA-TMS (0.20 M) and water (18.50 M) was added to the first one. Glacial acetic acid (1.5 M) was added to resulting solution and the suspension was mixed under mechanical stirring and under reflux at 90 °C for 24 h. The final product was centrifuged at 9000 rpm for 30 min and washed three times with water and ethanol. At the end, product was dried at 70 °C.

2.2.6 Silica support functionalization via 3-Chloropropyltrimethoxysilane (CPTMS) and sodium azide

The Silica supports functionalized with CPTMS were prepared similarly to APTES method B described previously. Then the grafted support was functionalized with sodium azide following the method of Mader et al. [152].
In a glass flask, 0.1 g of silica particles functionalized with CPTMS were dispersed in 5 mL of a saturated solution of sodium azide and DMF. The resulting mixture was mixed at 90 °C for 3 h. The silica particles were collected by centrifugation at 9000 rpm and washed under stirring in a water solution for 3 h in order to remove the remaining DMF. After the first wash in water, the product was centrifuged again at 9000 rpm and washed three times with water and ethanol. The product was dried at 60 °C for 12 h.

2.2.7 Silica support biotinylated via CuAAC (Cu(I)-catalyzed azide/alkyne cycloaddition) click reaction.

The click reaction was performed using silica functionalized with azide group and Biotin containing an alkyne group. The reaction was catalyzed with Cu (I).

In a tube a solution of $CuSO_4$ (0.2 mM), biotin (3.2 mM) was prepared and mixed at room temperature for 1 min. 0.05 mM of sodium ascorbate were added to the solution and mixed for 15 min. The resulting silica particles were collected by centrifugation and washed three times with water.

2.2.8 Characterization

The functionalized samples were characterized by Diffuse Reflectance Fourier Transform Infrared Spectroscopy (DRIFT-IR) with a NEXUS-FT-IR instrument implementing a Nicolet AVATAR Diffuse Reflectance accessory. The Thermogravimetric Analysis (TGA) and the Differential Scanning Calorimetry (DSC) were performed, by the Netzsch STA 409 C instrument, in air from 30 °C to 900 °C with a heating rate of 10 °C/min. The total nitrogen, carbon, and sulfur amounts were determined using a CHNS analyzer (Unicube by Elementer). For the CHNS analysis, the powder samples were dried and weighed (5-10 mg) in a tin capsule, which was then combusted in a reactor at 1000 °C. The analysis of the elements (N_2, CO_2, and SO_2) was performed by direct Temperature Programmed Desorption (direct TPD). The dimensions and the change morphologies of the samples were studied by scanning electron microscopy using a Zeiss Sigma VP FE-SEM c/o the Centro di Microscopia "Giovanni Stevanato" in Venezia-Mestre (VE, Italy). The UV-Vis analysis was carried out with an Agilent 8453 UV-visible spectrophotometer.

2.2.8.1 Ninhydrin assay for the detection α-amines

The reaction with ninhydrin (2,2-Dihydroxyindane-1,3-dione) was used to detect primary amines in the amino-modified samples. The result of this specific reaction was a purple color solution known as Ruhemann's purple. The reagent was prepared in a falcon tube by dissolving 0.1 g of ninhydrin in 30 ml of ethanol solution and mixed for 10 min. 0.03 g of the solid was added in 800 µL of ethanol and 200 µL of ninhydrin solution and mixed for 5 min. The reaction mixture was heated in thermo block at 95 °C for 5 min. After cooling at room temperature, the samples were collected by centrifugation at 10000 rpm. The supernatant was collected, and the color yield of the solution was measured at 570 nm by a UV–vis spectrophotometer. The reaction of glycine (2-amino acetic acid) with ninhydrin was used to define the calibration curve [153] as shown in **Fig. 31**. The groups density was calculated by equation (Eq. 7):

(Eq. 7) $$\textbf{Density NH}_2 = \frac{Gly\left(\frac{mg}{ml}\right) x\, Na\, x\, V(L)}{C(g)\, x\, S\left(\frac{m^2}{g}\right)}$$

Where Gly is a glycine concentration, Na is Avogadro's number, V is a volume solution, C is a sample in gram and S is the sample surface area (m^2/g).

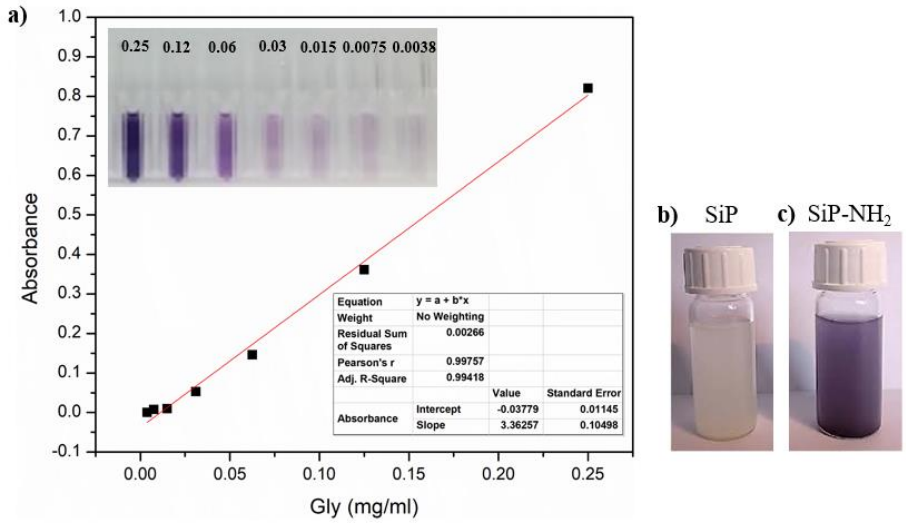

Fig. 31 a) calibration curve with glycine at different concentration, **b)** sample without functionalization, **c)** sample functionalization with APTES.

2.3 PROTEIN EXSPRESSION AND PURIFICATION

2.3.1 Materials

Table 6 reports the reagents used for the samples preparation. They were used without further purification.

Table 6					
Reagents	Abbreviation	PM (uma)	Purity	Density (g cm^{-3})	Supplier
pET21b(+)-Is-PETase-W159H-S238F plasmid	PETase	n/a	n/a	n/a	Addgene
OverExpress C41(DE3)	C41(DE3)	n/a	n/a	n/a	Aldrich
Rosetta (DE3)	R(DE3)	n/a	n/a	n/a	Aldrich
SHuffle® T7	T7	n/a	n/a	n/a	Aldrich
2xTY Microbial Medium	2xTY	n/a	n/a	n/a	Aldrich
Isopropyl β- D -1-thiogalactopyranoside	IPTG	238.31	98%	n/a	Aldrich
Acrylamide	AM	71.08	99%	1.13	Aldrich
2-Amino-2-(hydroxymethyl)-1,3-propanediol,	Trizma	121.14	99%	1.32	Aldrich
β-mercaptoethanol	βME	78.13	99%	1.11	Aldrich
bromophenol blue	BPB	670	99%	2.2	Aldrich
Glycerol	Gly	92.09	99%	1.25	Aldrich
hydrochloric acid	HCl	36.46	37%	1.3	Aldrich
sodium dodecyl sulfate	SDS	288.37	99%	1.01	Aldrich
ammonium persulfate	$(NH_4)_2S_2O_8$	228.18	99%	1.98	Aldrich
N,N,N′,N′-tetramethyl ethylenediamine	TEMED	116.24	99%	0.78	Aldrich
sodium hydroxide	NaOH	40	98%	2.13	Aldrich
Endo-β-1,4-glucanase	Cell_EG	n/a	n/a	n/a	Aldrich

2.3.2 PETase exspression

The PETase expression was refined by Austin et al. [154]. The protein was expressed in *E. coli* C41(DE3) in 2xTY media and induced by the addition of 1 mM final concentration IPTG. The cells were harvested by centrifugation at 2000 rpm for 10 min at 4 °C, disrupted by sonication, and the cell debris removed by centrifugation at 9000 rpm for 30 min. The protein was purified by Ni-affinity

chromatography followed by gel filtration on a Superdex 75 HR column. The expression was performed with other three different cell strains (Lemo21 (DE3), Rosetta, SHuffle® T7) and the process was scaled up to obtain a final protein concentration of 0.77 mg/ml.
After the first small-scale test expression, the protein was purified from 1 L of TB medium, using the Lemo 21 (DE3) induced with 0.4 mM IPTG and grown at 16°C for 20 hours.
The culture was centrifuged at 9000 rpm and the pellet was resuspended in sonication buffer (300mM NaCl, 50mM Sodium Phosphate, 3% Glycerol, 1% Triton X-100) and centrifuged at 9000 rpm to remove the cells debris. The sonicated sample was incubated with Ni-NTA resin. To the sample was added 30 mM imidazole to prevent unspecific binding to the resin. The resin has been transferred to a gravity-flow column and washed with 50 mM sodium phosphate pH 8, 300 mM NaCl, 30 mM imidazole and eluted with 50 mM sodium phosphate pH 8, 300 mM NaCl, 500 mM imidazole.

2.3.3 Characterization and protein purification

The proteins PETase and Endo-β-1,4-glucanase ware purified and analyzed with Size exclusion chromatography (SEC) performed with ÄKTA pure 25 M system (GE Healthcare).
The PETase protein was resuspended in a buffer (PBS 1X pH 7.2) and was loaded on a Superdex® Increase 75 column and equilibrated with buffer[5]. The fractions containing the pure protein were pooled and further concentrated by using 10000 NMWL. Amicon Ultra-15 ultrafiltration devices (Merck Life Science) at 2000 rpm and 4 °C on a Heraeus Multifuge X1R centrifuge (Thermo Fisher Scientific).
For the Endo-β-1,4-glucanase (Cell_EG) enzyme, the purification was performed with HiLoad 16/600 Superdex 200 prep grade column) in buffer Tris/HCl pH7.4 at 50 mM.
The molecular weight of the proteins was characterized with Sodium Dodecyl Sulphate Polyacrylamide Gel Electrophoresis analysis (SDS–PAGE). The gels were done with 12 % polyacrylamide both resolving gel and stacking gel. The protein samples were prepared by boiling for 10 min in the presence of denaturation

[5] **Equilibration buffer** (50 mM sodium phosphate, 300 mM NaCl, pH 8.0), **elution buffer 1 (**30 mM Imidazole, 50 mM sodium phosphate, 300 mM NaCl, 30 mM imidazole, pH 8.0) **elution buffer 2** (500 mM Imidazole, 50 mM sodium phosphate, 300 mM NaCl, 30 mM imidazole, pH 8.0)

buffer (Tris/HCl 0.5M at pH 6.8, 10 % SDS, 1 % β-mercaptoethanol, Bromophenol blue solution at 0.12 % and 0.6 g of Glycerol). After denaturation, the protein samples were loaded on the polyacrylamide gel (see **Fig. 32**) applying a voltage of 80 V and an intensity of electric current of 100 mA for 2 h. After migration, the gel was stained with Coomassie blue. Finally, the gel was analyzed with GeneTools from Syngene software to calculate the molecular weight of the proteins. The Broad Range Standards (Bio-Rad) marker was used to characterize the molecular weight of the protein sample.

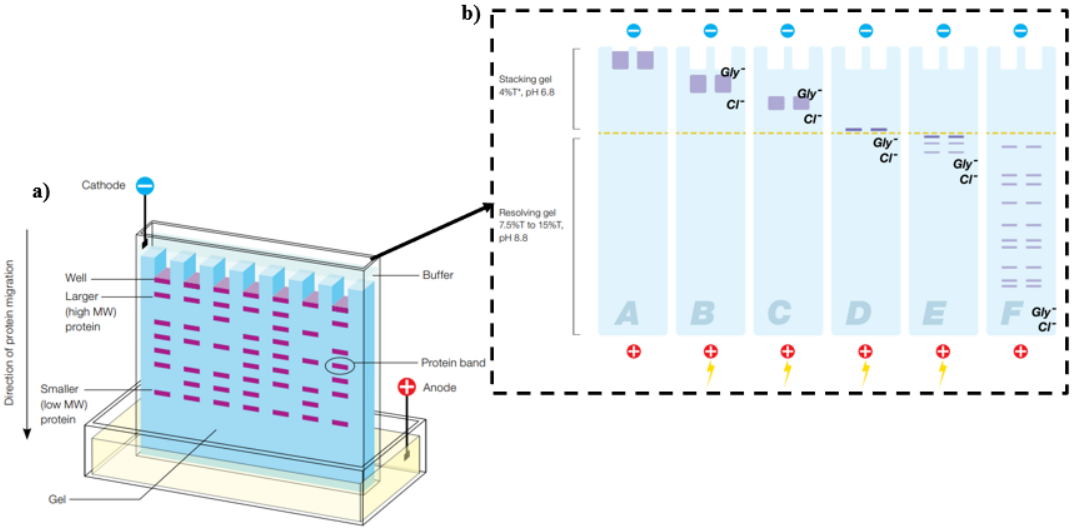

Fig. 32 a) Schematic of electrophoretic protein separation in a polyacrylamide gel. MW, molecular weight, **b)** Migration of the proteins and buffer ions in a denaturing discontinous PAGE system: (A) Denaturated sample proteins loaded into the wells. (B) Voltage is applied and the protein samples move into the gel. The chloride ions already present in the gel (leading ions) run faster than the SDS-bound proteins and form an ion front. The glycine ions, (trailing ions) flow in form the running buffer and form a front behind the proteins. (C) A voltage gradient is created between the chloride and glycinate ions, which sandwich the proteins in between them. (D) The proteins are stacked between the chloride and glycinate ion fronts. At the interface between the stacking and the resolving gels, the percentage of acrylamide increases and the pore size decreases. Movement of the proteins into the resolving gel is met with increased resistance. (E) The smoller pore size resolving gel begins to separate the proteins based on molecular weight only, since the charge to mass ratio is equal in all the proteins of the sample. (F) the individual proteins are separated into band patterns ordered according to their molecular weights [155].

2.4 COVALENT AND NON-COVALENT CONFINEMENT SYSTEMS

2.4.1 Materials

Table 7 reports a list of reagents used for the samples preparation. They were used without further purification. Except for Endo-β-1,4-glucanase protein, which was purified with SEC analysis as describe in § 2.6.3.

Table 7

Reagents	Abbreviation	PM (uma)	Purity	Density (g cm^{-3})	Supplier
Bovine serum albumin	BSA	60KDa	98	n/a	Aldrich
Endo-β-1,4-glucanase	Cell_EG	n/a	n/a	n/a	Aldrich
Streptavidin Alexa Fluor 647	STREP-AF-647	n/a	n/a	n/a	Thermo fisher
Sodium phosphate dibasic	Na_2HPO_4	141.96	99%	1.7	Aldrich
Sodium phosphate monobasic dihydrate	$NaHPO_4$ x 2H2O	156.01	99%	1.91	Aldrich
sodium hydroxide	NaOH	40	98%	2.13	Aldrich
Hydrochloric acid	HCl	36.46	37%	1.3	Aldrich
Sodium cyanoborohydride	$NaBH_3CN$	62.84	95%	1.2	Aldrich
Bradford reagent	BCA	n/a	n/a	n/a	Aldrich
3,5-Dinitrosalicylic acid	DNS	228.12	98%	1.8	Aldrich
Potassium sodium tartrate tetrahydrate	KNaT	282.22	99%	1.77	Aldrich
Phenol	PHEN	94.11	99.5%	1.07	Aldrich
Sodium metabisulfite	$NaSO_2$	190.11	99%	1.48	Aldrich
sodium metasilicate pentahydrate	Na_2SiO_3 x $5H_2O$	212.14	95%	2.61	Aldrich
hydrochloric acid	HCl	36.46	37%	1.3	Aldrich
diethylenetriamine	DETA	103.17	99%	0.95	Aldrich
triethylenetetramine	TETA	146.23	97%	0.98	Aldrich
pentaethylenehexamine	PEHA	232.37	99%	0.95	Aldrich
polyethyleneimine	PEI	~25000	99%	n/a	Aldrich
polyallylamine hydrochloride	PAA	~50000	99%	n/a	Aldrich
glutaraldehyde	GLU	100.2	50%wt in H_2O	1.06	Aldrich

2.4.2 Covalent confinement

2.4.2.1 Cross linking method with glutaraldehyde as cross-linking agent

2.4.2.1.1 Protein-protein cross linking

The cross-linking reaction was performed using only a protein solution with glutaraldehyde, to form protein-protein bonds.
In a tube, a protein solution (2 mg/ml in phosphate buffer solution (PBS) 50 mM at pH 7.4) and glutaraldehyde(0.42 mM) were prepared and mixed for 2 h at room temperature. After, $NaBH_4$ (10 mM) was added to the solution and mixed for 1 h. At the end, the resulting product was collected by centrifugation at 5000 rpm for 5 min and washed three times with water.

2.4.2.1.2 Cross linking between α-amine silica particles and protein.

The cross-linking method with amine silica support and proteins was divided in two steps. In first one, in a tube 10 mg of functionalized silica support were washed three times with phosphate buffer solution (PBS 0.05 M) at pH 7.4. After the final wash, the silica support was suspended in 0.5 ml of the PBS (0.05 M) containing 10% of glutaraldehyde (GLU) and mixed well for 1 h at room temperature. The resulting silica support was collected by centrifugation and washed with PBS several times to remove excess of glutaraldehyde. The silica support was resuspended in 0.5 ml of buffer PBS. In the second step, the protein was coupled to the silica support suspension, with a final concentration of 1 mg/ml and mixed for 4 h at room temperature. Then, in the suspension $NaBH_3CN$ (10 mM) was added and mixed for 1 h. The final product was centrifugated at 5000 rpm and washed three time with PBS. The supernatants were collected and analyzed for protein quantification (see § 2.4.4.1).

2.4.3 Non-covalent confinement

2.4.3.1 Protein adsorption

In a first tube, a protein stock solution was prepared at 10 mg/ml in distilled water or in PBS (0.05M) at pH 7.4. In a second tube, 10 mg silica samples were suspended in 1 ml of distilled water. These two solutions were mixed to a final volume of 2 ml and the final concentration of the support was 5 mg/ml and the protein concentration was 1 mg/ml. The samples were incubated for 2 h under stirring in a water bath at 30 °C at 200 rpm. The samples were then centrifuged at 5000 rpm for 15 min and washed three times with water. In each washing step, 1 ml of the supernatant was replaced with distilled water.

2.4.3.2 Proteins entrapment using the Bioinspired method

For the entrapment of proteins, during BIS synthesis as described in § 2.1.3.2, 1 mg/ml concentration of proteins was added immediately after neutralization with 1 M HCl, and the resulting solution was gently mixed, left unstirred for 5 min and centrifuged at 5000 rpm, washed, and dried as above. The supernatants were stored after each round in order to quantify free proteins remaining.

2.4.3.3 Adsorption streptavidin-Alexa fluor 647 A on Silica support biotinylated

The bioconjugation was performed preparing a water solution of 10 mg of the biotinylated silica and 0.01 M of the streptavidin-Alexa Fluor 647a. The solution was mixed at room temperature for 15 min. The final solution with silica particles and streptavidin was analyzed by cytometer analysis.

2.4.4 Characterization

The Bradford assay (see § 2.4.4.1) and enzyme assays(see § 2.4.4.2) were performed using an Agilent 8453 UV-visible spectrophotometer. The confinement systems were analyzed with SDS-PAGE analysis (see § 2.3.4) and Diffuse Reflectance Fourier Transform Infrared Spectroscopy (DRIFT-IR) with a NEXUS-FT-IR instrument implementing a Nicolet AVATAR Diffuse Reflectance

accessory. The cytometer analysis has been performed with Attune NxT Flow cytometer. 10000 events were collected and analyzed with a low flow rate of 25 uL min^{-1} for each sample. The instrument was set up with the following voltage parameters: forward side scattering (FSC) at 1 V, Side scattering (SSC) at 220 V and red laser for the detection of Alexa Fluor 647 fluorophore at 320 V.

2.4.4.1 Protein quantification

The quantification of protein loading was carried out by analyzing the supernatants recovered after the reaction and were analyzed by the Bradford assay [33]. The assay was performed by adding a predetermined amount of Bradford reagent to either the supernatant samples or calibration samples in cuvettes. The calibration curve was prepared using the BSA in a range 0.1–1.2 mg/ml. The final solution was mixed three times and the color was left to develop for 15 min. The samples absorbance was recorded at 595 nm using distilled water as blank. As the protein-dye complex is stable up to 60 min, the absorbance was recorded before 60 min and after 15 min of the Bradford reagent addition. For each calibration, averages from three different measurements were reported. The amount of the protein loaded in encapsulation and adsorption was calculated using this calibration curve. The enzyme loading efficiency (%) and protein in silica (wt %) was determined as follows equation (Eq. 8) and (Eq. 9):

(Eq. 8) $$Loading\ efficiency\ (\%) = \frac{E_{tot} - (E_{recovery} + W1 + W2 + W3)}{E_{tot}} x\ 100$$

(Eq. 9) $$Protein\ in\ silica\ (\%) = \frac{Protein\ loading(g)}{Support\ yield(g)} x\ 100$$

Where E_{tot} is the initial enzyme quantity present in the mixture (during encapsulation or adsorption), $E_{recovery}$ is the amount of enzyme in the supernatant immediately after encapsulating and adsorbing. While the *W1*, *W2*, and *W3* are the amounts of enzymes present in the washing solutions. The protein in silica is the ratio of the total mass of protein loaded and the mass of support obtained after dying (which is the total quantity of the support plus protein after the encapsulation or adsorption protein).

2.4.4.2 Endoglucanase assay

The enzyme activity was evaluated through the analysis of reducing sugar that formed in the solution after the catalytic action of the enzyme on Carboxymethylcellulose sodium salt (CMC). The concentrations of the reducing sugar were analyzed by the reaction with 3,5-Dinitrosalicylic acid (DNS) reagent [34], [35].

❖ *DNS reagent preparation*

The DNS reagent was prepared following the work of T. K. Ghose et.al [143]. In a falcon tube, 3,5-Dinitrosalicylic acid (0.05 M) was dissolved in a 50 ml of water and NaOH (0.55 M) solution and mixed until completely dissolved obtaining a yellow-orange color solution. An amount of potassium sodium tartrate tetrahydrate (1.2 M), phenol (0.1 M), and sodium metabisulfite (0.05 M) were added to the solution and mixed at room temperature for 30 min.

❖ *Endoglucanase assay protocol*

In a tube, 0.05 ml of protein solution (0.2 mg/ml of the Cell_EG in 0.05 M citrate buffer at pH 4.8) and 0.05 ml of CMC solution (2 % w/v CMC in 0.05 M citrate buffer) were mixed at 50 °C for 30 min. Then DNS reagent (0.3ml) was added. The final solution was boiled for 10 min and then immediately transferred to a cold-water bath and 1.6 ml of distilled water were added. The color formed was monitored at a wavelength of 540 nm. A calibration curve with glucose standard was used to evaluate the amount of reducing glucose produced in solution. The kinetic parameters K_m, V_{max} was used to evaluate enzyme activity. The relative activity (RA %) of the different confinement systems and their recycled (RASR %) were calculated following the (Eq. 10) and the (Eq. 11).

(Eq. 10) $$RA\ (\%) = \frac{Reducing\ glucose\ from\ confinement\ system\left(\frac{mg}{ml}\right)}{Reducing\ glucose\ from\ free\ enzyme\left(\frac{mg}{ml}\right)}\ x\ 100$$

(Eq. 11) $$RASR\ (\%) = \frac{Reducing\ glucose\ from\ \ system\ reused\left(\frac{mg}{ml}\right)}{Reducing\ glucose\ from\ confinement\ system\left(\frac{mg}{ml}\right)}\ x\ 100$$

2.4.4.3 PETase assay

The PETase assay has been performed using a para-nitrophenol acetate as substrate. In a tube was prepared a solution of Na_2HPO_4 -HCl (45 mM) at pH 7.0, NaCl (90 mM) , and DMSO 10 % (v/v). Para-nitrophenol acetate (1 mM) was added to the solution and mixed until completely dissolved. An aliquot of PETase protein (370 nM) was added and mixed for 5 min at 30 °C. Para nitrophenol (pNP) produce by the reaction was monitored at 415 nm.

CHAPTER 3

RESULTS AND DISCUSSIONS

3.1 NON-POROUS SILICA PARTICLES.

Non-porous spherical silica particles were synthesized in ammonia solution by the Stöber method (**Fig. 33a**). Different ratios of water (H_2O), ammonia (NH_3), and TEOS and different reaction times were tested to evaluate their effects on the particles size. The influence of these parameters on the morphology of the particles was analyzed by FE-SEM microscopy and the data elaboration was carried out by ImageJ software (**Fig. 33b**). The concentrations of NH_3, H_2O and TEOS were based on literature data [96], [156]. As shown in **Table 8**, keeping the reaction time constant (2 h), lower concentrations of NH_3, H_2O and TEOS cause a reduction of the particle size.

Table 8

Sample	H_2O (mol/L)	NH_3 (mol/L)	TEOS (mol/L)	Particles size (nm)
S1	4.94	1.65	0.11	**275±28**
S2	4.94	0.83	0.11	**178±17**
S3	4.94	0.41	0.11	**53±6**
S4	2.46	1.65	0.11	**200±21**
S5	1.23	1.65	0.11	**177±18**
S6	0.61	1.65	0.11	**70±4**
S7	4.94	1.65	0.028	**163±15**
S8	4.94	1.65	0.05	**250±20**
S9	4.94	1.65	0.014	**86±9**
S10	4.94	3.85	0.11	**Aggregate**

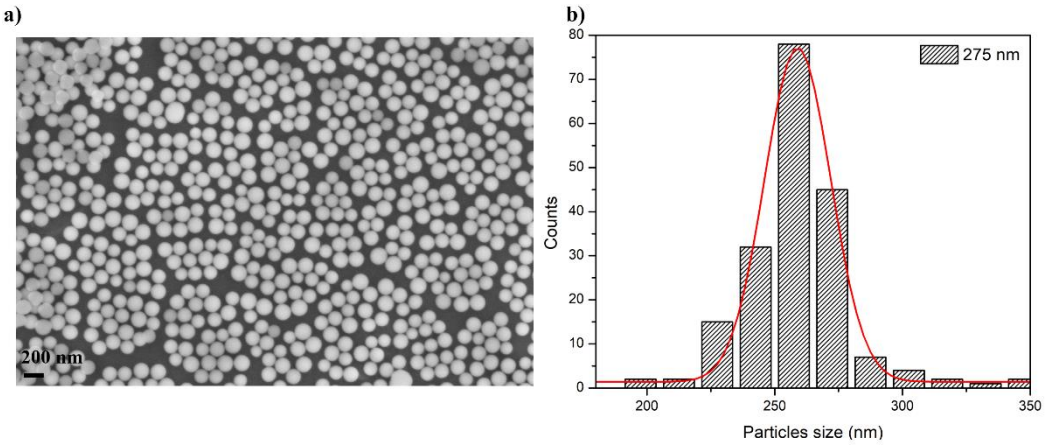

Fig. 33 a) SEM image of sample S1 synthetized following Stöber method, **b)** Particles size distribution.

Fig. 34a summarized the results of **Table 8**. Three distinct behaviors can be clearly evidenced. The increase of the catalyst concentration can also produce a particles conglomeration as shown in **Fig. 34b**.

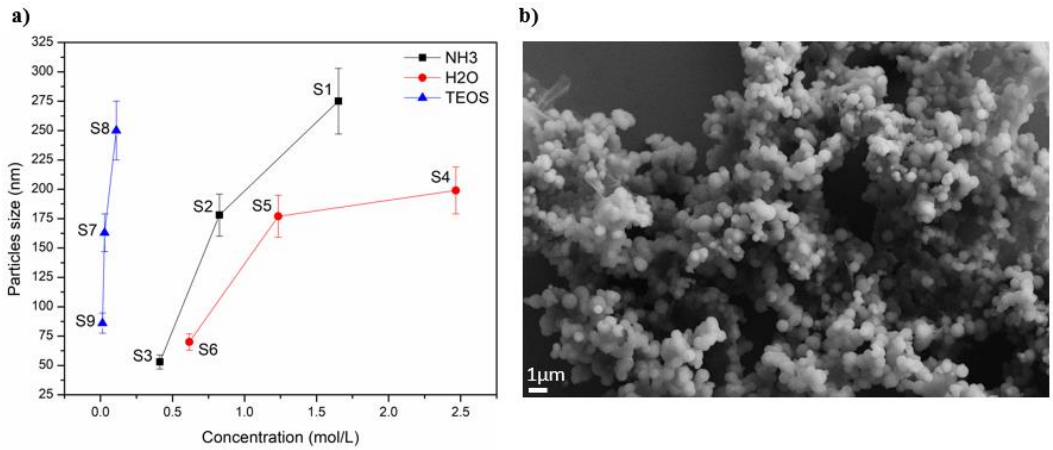

Fig. 34 a) Effect of different concentration of the NH_3, H_2O and TEOS, **b)** FE-SEM image of the S10 with increase of the catalyst concentration.

The influence of the reaction time on sample S1 was also analyzed. **Fig. 35** shows the growth of the particle size during the reaction time. After 1440 minutes the size reaches a value of 350 nm defined as the limit diameter of the particle growth.
As shown by Masalov et al. [157] the particles does not grow further after reaching a certain critical diameter.

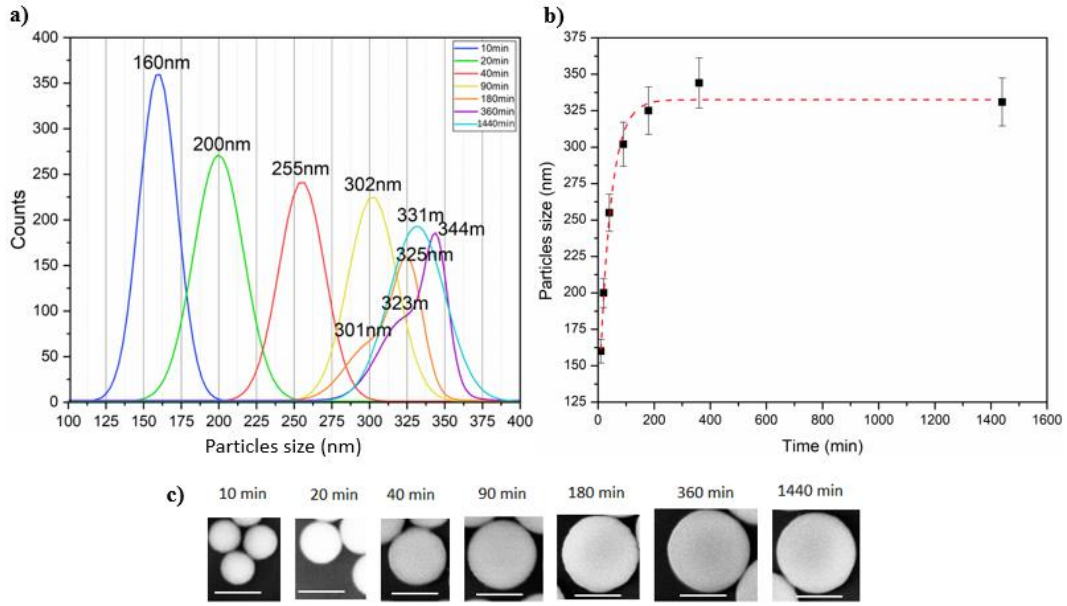

Fig. 35 Evaluation of particle size during the synthesis reaction, **a)** Different distribution of the particle sizes, **b)** Plot of particle size (nm) vs time, **c)** FE-SEM image of the particle growth over time.

However, the possibility to prepare particles with larger size was also investigated. In this case, the growth of the particle was controlled by dropping TEOS precursor with a 0.2 ml/min rate using a piston pump. A final particle size of 1 and 2 μm was obtained, in the presence of an electrolyte (KCl) in solution. The experimental conditions are listed in **Table 9** and the experimental setup are represented in **Fig. 36.**

Table 9

Sample	H_2O (mol/L)	NH_3 (mol/L)	TEOS (mol/L)	KCl (mol/L)	Dripping speed (mL/min)	Particles size (nm)
S15	3.18	4.05	0.08	n/a	0.20	238±19, 360±23, 441±13
S18	3.18	4.05	0.08	0.002	0.20	1180±25
S19	3.21	2.73	0.16	0.002	0.20	2081±49

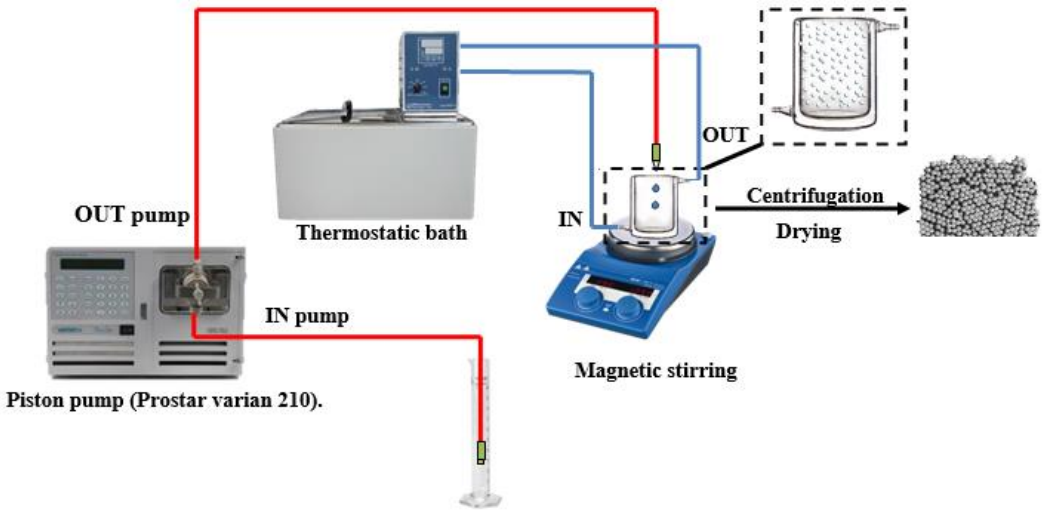

Fig. 36 Experimental setup of the growth technique.

Sample S15 (see **Fig. 37**) was synthetized without the electrolyte and the growth of the particles was investigated during 4 hours of TEOS dripping. As shown in **Fig. 38a,** after 1 hour, the particle size distribution is centered at about 230 nm. The continuous addition of TEOS, after 2 and 3 hours (**Fig. 38b** and **Fig. 38c**), generates different distribution size of particles centered at different values. The average size of the distribution containing the larger particles increases when the dripping time is increased. After 3 hours, four distributions centered at 189, 233, 305 and 375 nm are clearly present. After 4 hours (see **Fig. 38d**), the size distribution of the larger particles is centered at about 441 nm.

The presence of a cationic species (K^+) promotes the aggregation of small spheres on the surface of the growing particles causing crucial effects on the distribution and the final size of the particles. Keeping the TEOS, H_2O, and NH_3 concentrations constant, sample S18 was prepared in presence also of KCl. As a result, a single size distribution centered at about ~1 μm is obtained (see **Fig. 39a**).

Still, in presence of KCl, but changing the NH_3 and TEOS concentrations, sample S19 identified an increased particle size up to ~2 μm (**Fig. 39b**).

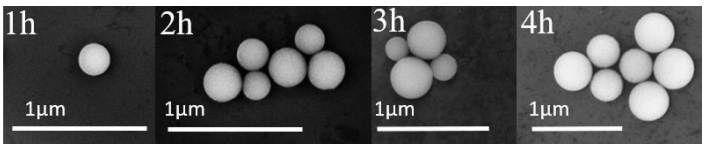

Fig. 37 FE-SEM images of the S15 sample at different times.

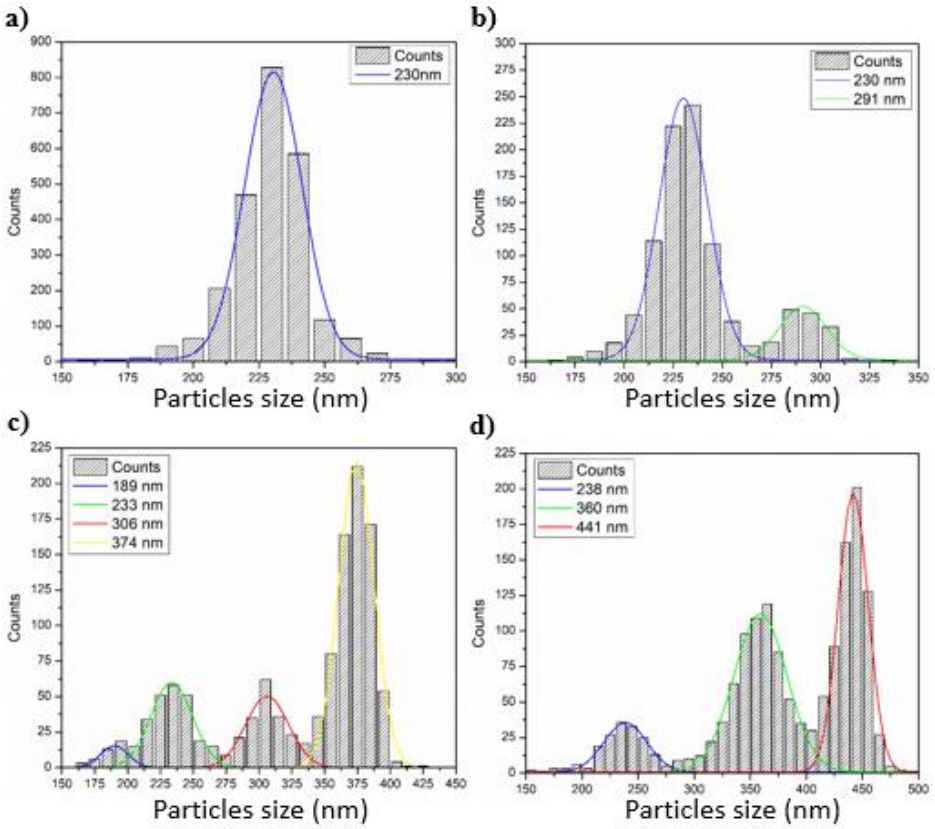

Fig. 38 size distributions of the sample S15 during the growth over time, **a)** 1 h, **b)** 2 h, **c)** 3 h and **d)** 4 h.

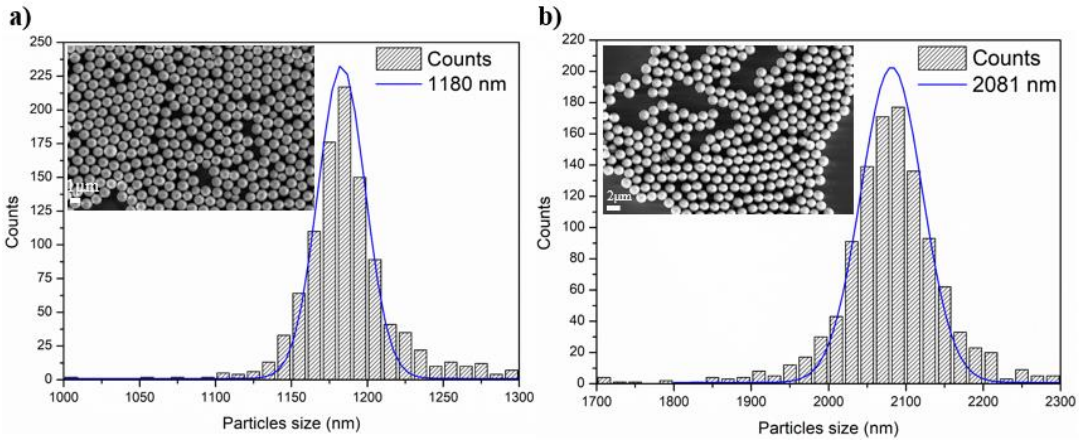

Fig. 39 Size distribution and FE-SEM images of the **a)** S18 and **b)** S19 samples.

3.2 MESOPOROUS SILICA PARTICLES VIA SOFT AND HARD TEMPLATING

Table 10

Soft method (MC samples)

Sample	H_2O (mol/L)	EtOH (mol/L)	NH_3 (mol/L)	TEOS (mol/L)	Template* (mol/L)	Particles size (nm)
MC 1[1]	18	9	5.3	0.15	0.05	Aggregate
MC 10[2]	40	4.1	0.33	0.12	0.08	85±6.0
MC 11[3]	45	2.2	1.1	0.13	0.09	291±19.5; 345±9.1
MC 12[4]	0.04	0.004	0.1	0.0002	0.01	Aggregate
MC 13[5]	4.48	14.6	1.57	0.11	0.0001	Aggregate

*(1), (2), (3) CTABr, (4) Methyl 2-hydroxyethyl cellulose (MHEC), (5) Sodium stearate (Na-STE)

Hard method (MS samples)

Sample	H_2O (mol/L)	NaOH (mol/L)	Swelling agents* (mol/L)	TEOS (mol/L)	CTABr (mol/L)	Particles size (nm)
MS 1[6]	53	0.003	0.23	0.01	0.001	103±8.2, 122± 12.3
MS 2[7]	47	0.003	1.17	0.01	0.001	Not spheric

*(6) Hexane (7) Cyclohexane

Hard method (KCC1 sample)

Sample	H_2O (mol/L)	Urea (mol/L)	Toluene (mol/L)	n-butanol (mol/L)	TEOS (mol/L)	CTABr (mol/L)	Particles size (nm)
KCC 1	19.2	0.12	3.2	0.16	0.14	0.03	~400

The best confinement process depends on the morphological properties (shape, surface area, and size) of the porous support. Soft and hard templates are the main methods to produce suitable mesoporous silica systems. **Table 10** summarizes the samples synthesized by soft and hard method.

Soft method (MC series) is similar to the Stöber method, but in this case, during the hydrolysis and condensation reactions of TEOS, a surfactant is added as template to generate, after calcination, a mesoporous structure (see **Fig. 40**).

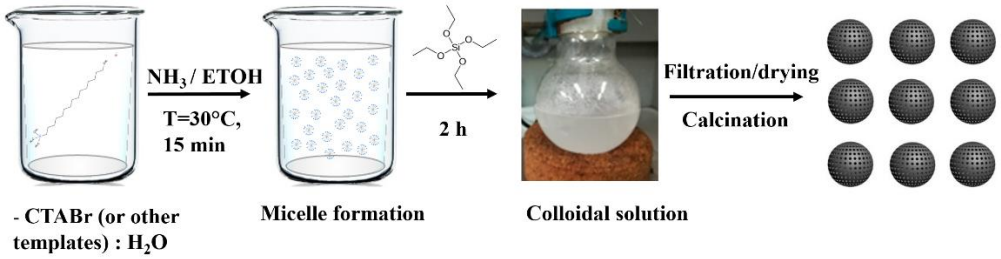

Fig. 40 scheme of the reaction by soft template.

In order to prepare mesoporous systems with monodisperse nanoparticles size and high surface areas, we optimized the reaction conditions and the template (chosen among Methyl 2-hydroxyethyl cellulose, MHEC, and sodium stearate (Na-STE)). The hard template method (MS and KCC1 samples) was performed using different swelling agents (hexane, cyclohexane, and toluene) to increase the pore diameter (**Fig. 41**) and the surface area. For the detail of the synthesis see § 2.1.2.3 and 2.1.2.4. At basic condition: NaOH was added to hexane or cyclohexane, meanwhile urea and a co-solvent (n-Butanol) to toluene. All the samples were analyzed by nitrogen physisorption and SEM microscopy. For each sample, the measurement for each analysis was performed three times.

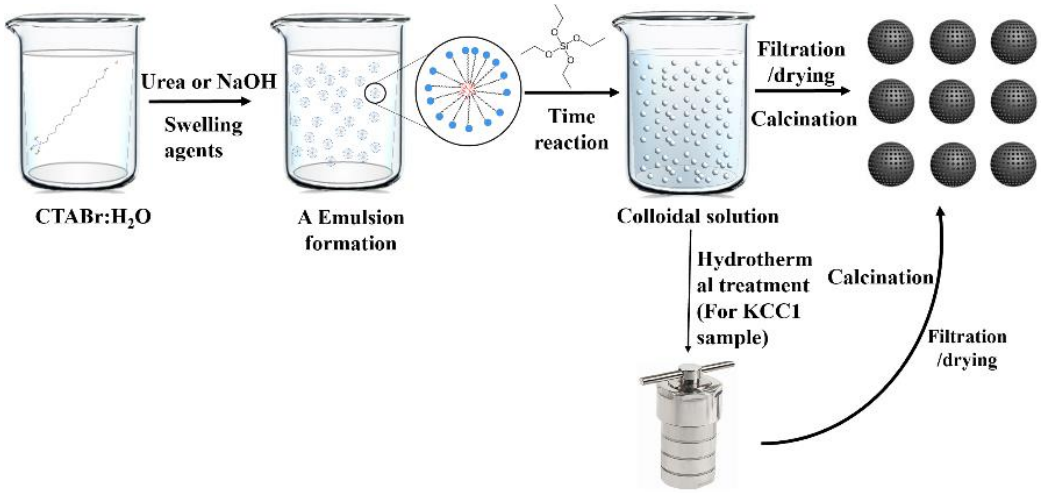

Fig. 41 scheme of the reaction by hard template.

The analysis of MC samples often showed the formation of aggregates and conglomerates, with irregular shapes (**Fig. 42**), due probably to the thermal treatment at 550°C and to the reaction conditions. Only samples MC 10 (**Fig. 43)** and MC 11 (**Fig. 44**), showed spherical particles with size of about 85 and 290 nm and little aggregation (see **Fig.45**).

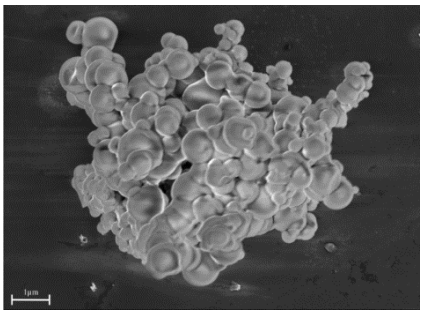

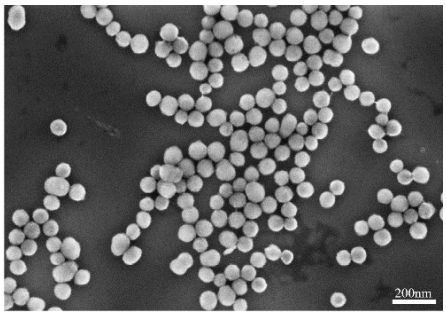

Fig. 42 FE-SEM image of the MC 1 sample. **Fig. 43** FE-SEM image of the MC 10 sample.

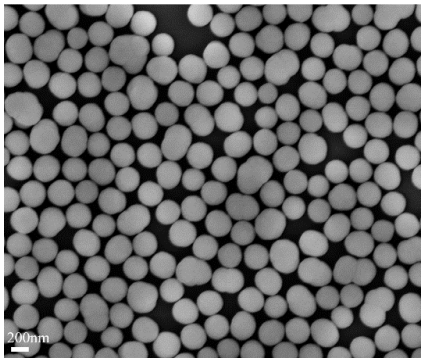

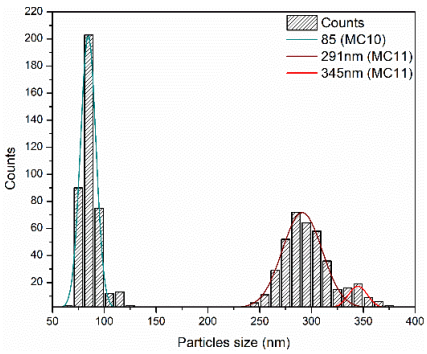

Fig. 44 FE-SEM image of the MC 11 sample. **Fig. 45** Dimensional analysis of the MC 10 and MC 11samples.

Using the same optimized conditions of MC 10 and MC 11 but changing the templates (MHEC and Na-STE), the particles form aggregates as clearly observed in **Fig. 46** and **Fig.47**.

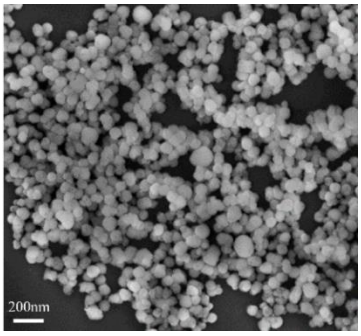

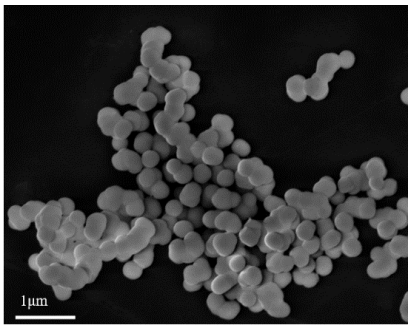

Fig. 46 FE-SEM sample MC 12. **Fig. 47** FE-SEM sample MC 13.

Concerning the hard template method, samples MS 1and MS 2 were prepared with two different swelling agents (n-hexane and cyclohexane). As a result, the

morphology of the samples drastically changes. Sample MS 1 (**Fig. 48**) showed the presence of aggregated spherical nanoparticles with an average size of about 103 nm (**Fig.49**). The use of cyclohexane (sample MS 2 **Fig. 50**) led to a total loss of sphericity probably due to a structural change of the reverse micelle during the formation of the emulsion.

Sample KCC 1 was prepared by hydrothermal method using toluene and N-butanol for the formation of reverse micelles. The obtained particles showed a fibrous morphology (see **Fig. 51**) and an average size of ~ 400 nm. This morphology, as explained by Febriyanti et al. [151], was generated through a cooperative action between the growth of the inverse micelle and the hydrolysis and condensation processes of TEOS that occurred inside the emulsion/bath.

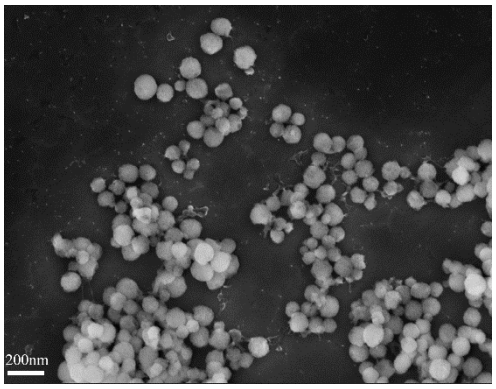

Fig. 48 FE-SEM of the MS 1 sample.

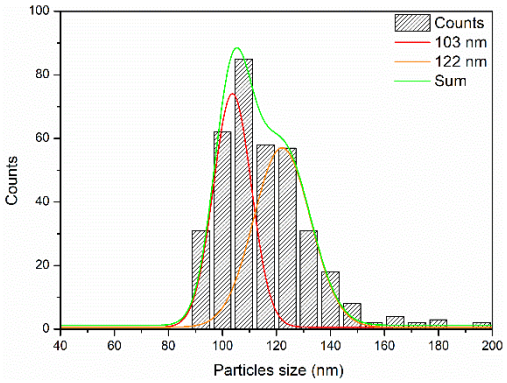

Fig. 49 Dimensional analysis of the MS 1 sample.

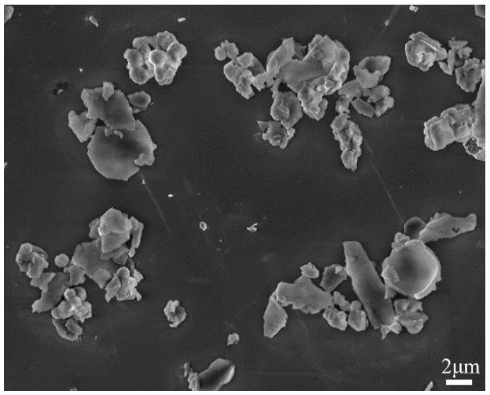

Fig. 50 FE-SEM of the MS 2 sample.

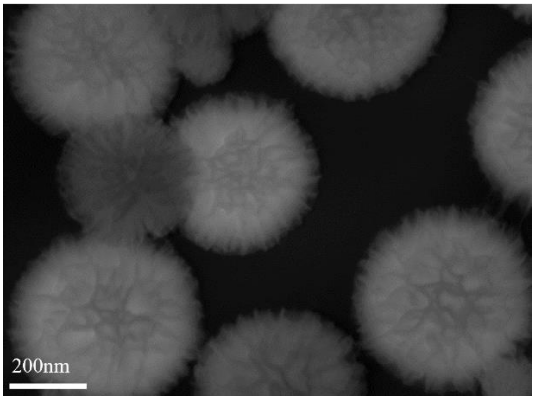

Fig. 51 FE-SEM of the KCC 1 sample.

Nitrogen adsorption isotherms of MC 11 and MS 1 showed type IV profiles with a H1 hysteresis loop (according to the IUPAC classification), typical of mesoporous materials, whereas KCC 1 presents a type II profile and H4 hysteresis loop typical

of micro-mesoporous material. MC 12 and MS 2 show a type III isotherm, characteristic of a non-porous material. Some isotherms are reported in **Fig. 52**.

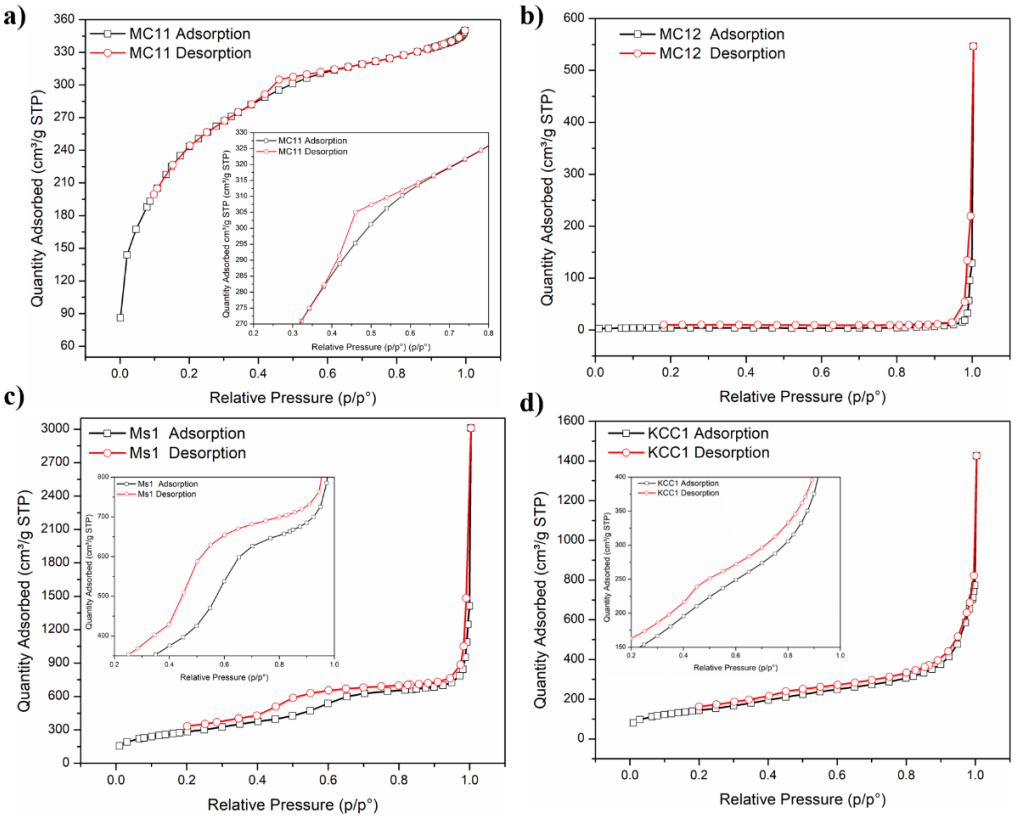

Fig. 52 Adsorption and desorption curve of the **a)** MC11, **b)** MC12, **c)** MS1 and **d)** KCC1.

Table 11 summarizes the results of the samples obtained by soft and hard methods. For both the methods the specific surface area and the pore size distributions (**Fig. 53**) are within a wide range of values.

Table 11				
Soft method				
Sample	BET Surface area (m^2g^{-1})	Total Pore volume (cm^3g^{-1})	BJH Pore diameter (nm)	Particles size (nm)
MC-1	1552±62.1	0.80±0.04	2.3±0.9	Aggregate
MC-10	1165±46.1	1.15±0.1	2.6±1.0	85±6.0
MC-11	810±32.2	0.18±0.02	1.1±0.05	291±19.5; 345±9.1
MC-12	50±2.5	0.06±0.02	n/a	Aggregate
MC-13	256±10.1	0.17±0.04	2.8±1.1	Aggregate
Hard method				
MS1	1029±40.6	1.30±0.05	4.2 ±1.6	103±8.2, 122± 12.3
MS2	123±4.9	0.18±0.01	n/a	Not spheric
KCC1	507±20.3	1.01±0.04	3±1.1	~400

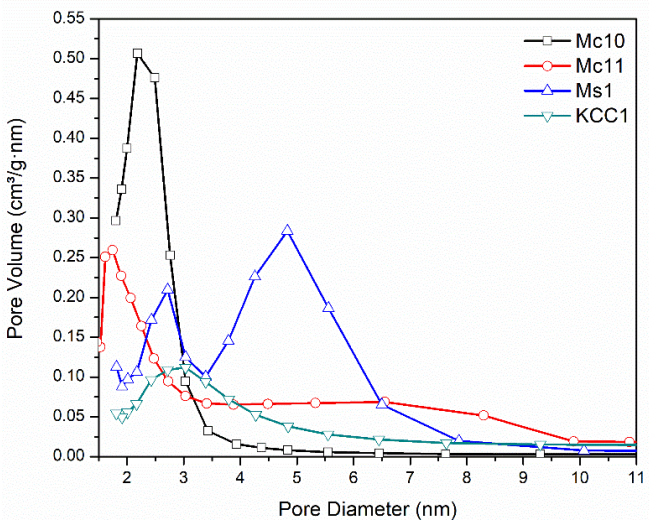

Fig. 53 Pore size distribution of the samples from BJH model.

3.3 SILICA SUPPORTS PREPARED BY BIOINSPIRED METHOD

The bioinspired method was used as an alternative process to produce silica supports in a water environment without organic solvents. Compared to the procedures followed for the synthesis of mesoporous materials, that required drastic reaction conditions (e.g., high temperatures or different organic compounds), the bio-inspired synthesis was carried out in water solution using a metasilicate salt ($(Na_2SiO_3)•5H_2O$) as precursor, in presence of an additive (usually an amine or polyamine) at room temperature. In general, the initial pH of the reaction was about 12, but it depended on the used additive. The condensation process (**R. 5**) of the silicic precursor started when a stoichiometric amount of hydrochloric acid was added to the solution. Around 5 minutes later, a colloidal solution with pH=7 was obtained. At the end of the synthesis in presence of an acid pH, the amine can be removed as shown in **Fig. 54**. All the samples were analyzed by nitrogen physisorption, SEM microscopy. For each sample, the measurement for each analysis was performed three times. The removal of the additive from the supports was analyzed by FTIR-DRIFT.

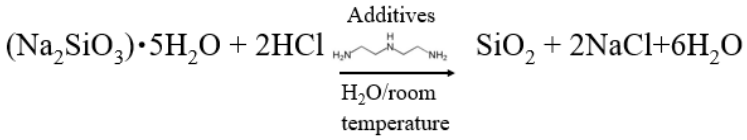

R. 5 The reaction from sodium metasilicate to formation of the silica support.

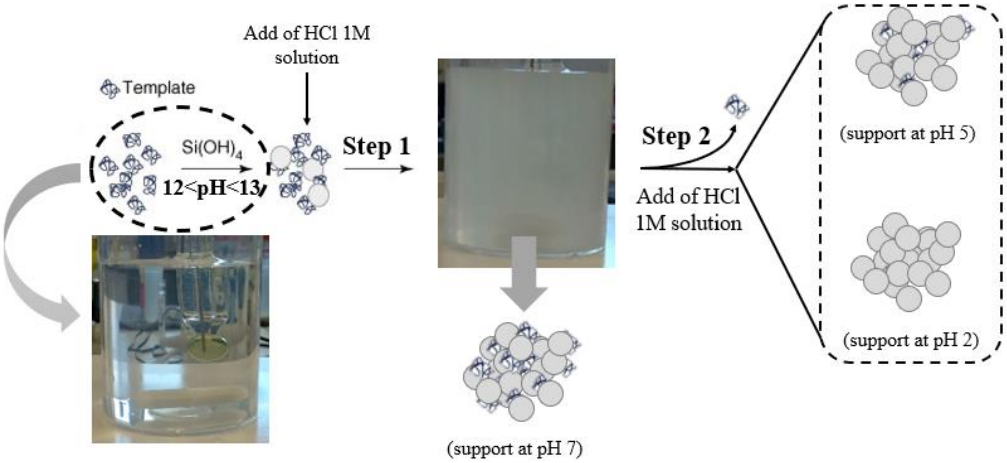

Fig. 54 Scheme of the bio inspired silica synthesis.

In **Table 12** are listed: the samples, the final pH (7,5,2) and the different additives (i.e., DETA, TETA, PEHA, PEI, and PAA) chosen for the preparation.

Table 12		
Sample	Additive	pH
BIS_DETA_7	DETA	7 - 5- 2
BIS_DETA_5		
BIS_DETA_2		
BIS_TETA_7	TETA	
BIS_TETA_5		
BIS_TETA_2		
BIS_PEHA_7	PEHA	
BIS_PEHA _5		
BIS_PEHA _2		
BIS_PEI_7	PEI	
BIS_PEI_5		
BIS_PEI_2		
BIS_PAA_7	PAA	
BIS_PAA_5		
BIS_PAA_2		

The supports were characterized by FE-SEM microscopy and by nitrogen physisorption, whereas the purification degree was verified by FTIR-DRIFT. All the samples showed aggregates of particles, especially when PAA (**Fig. 55a)** and PEI (**Fig. 55b**) are used.

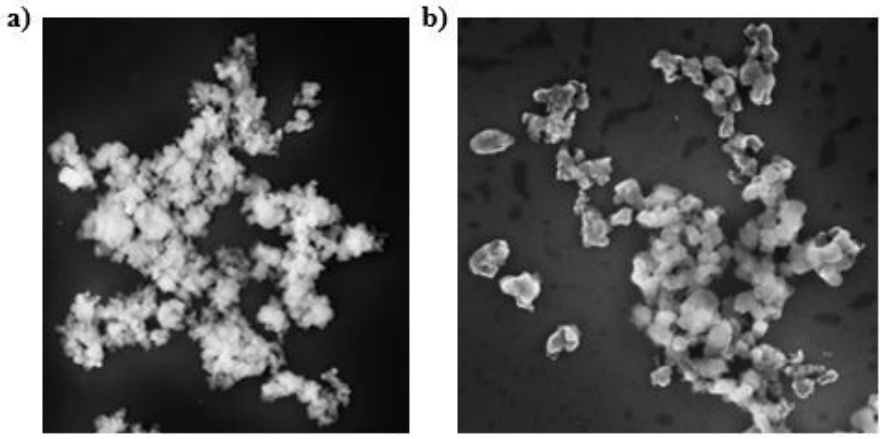

Fig. 55 a) FE-SEM images of the BIS-PAA, **b)** and BIS-PEI at pH7.

At pH 7 and 5, the particles of the supports synthesized with other additives (DETA, TETA, PEHA) do not completely lose their spherical shape. On the other hand, at pH=2 the morphology of the particles was completely changed. As an example, **Fig. 56** shows the FE-SEM images for the supports synthesized with DETA additive at different pHs.

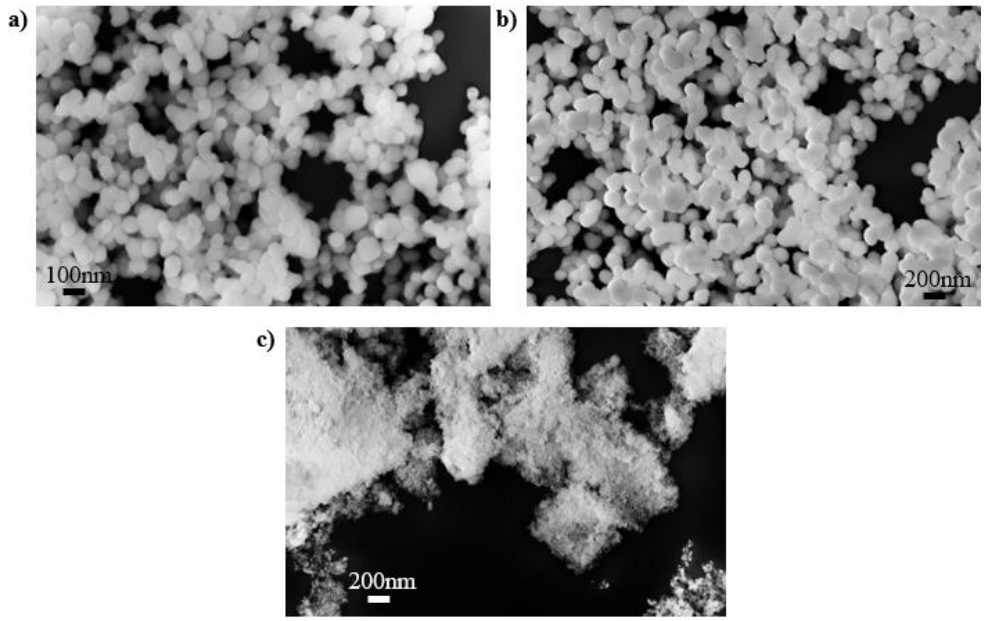

Fig. 56 FE-SEM images of the sample BIS-DETA at **a)** pH 7, **b)** 5 and **c)** 2.

The samples show isotherms of type II and III, typical of the non-porous or macroporous materials (see **Fig. 57a-b)**.

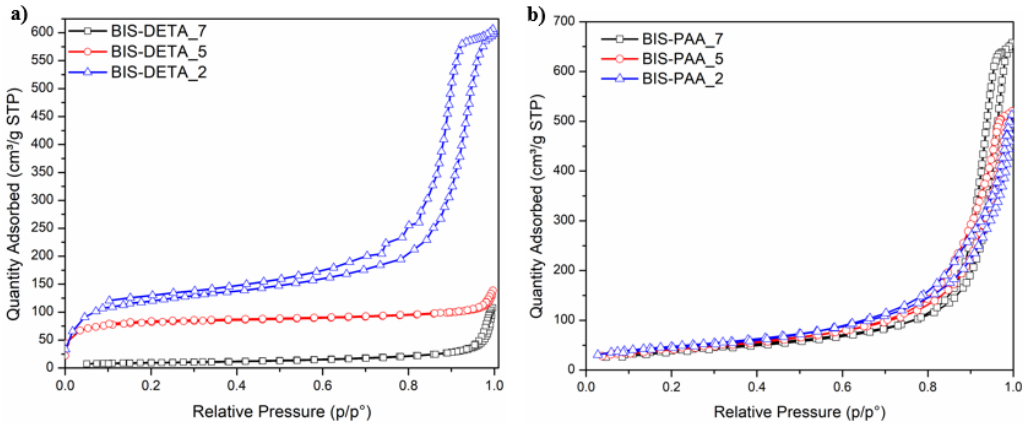

Fig. 57 Adsorbed and desorbed curves of the BIS-DETA **a)** and **b)**BIS-PAA at different pH.

At pH 2, the specific surface area of samples synthesized by DETA, TETA and PEHA are larger than the values obtained at pH 7 and 5 (**Fig. 58a**). These differences could be related to the best removal of the additives from the support after the treatment at pH 2. This difference is also supported by the increased pore volume for supports synthesized at pH 2, as indicated in **Fig. 58b**. The supports synthesized with PAA and PEI at pH 2, 5 and 7 do not show evident changes.

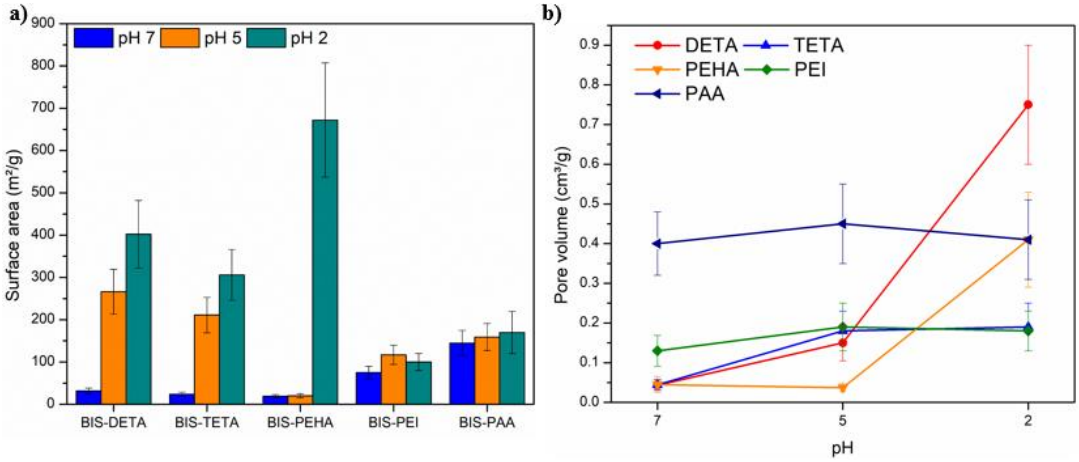

Fig. 58 a) Specific surface area, **b)** pore volume of the different silica supports.

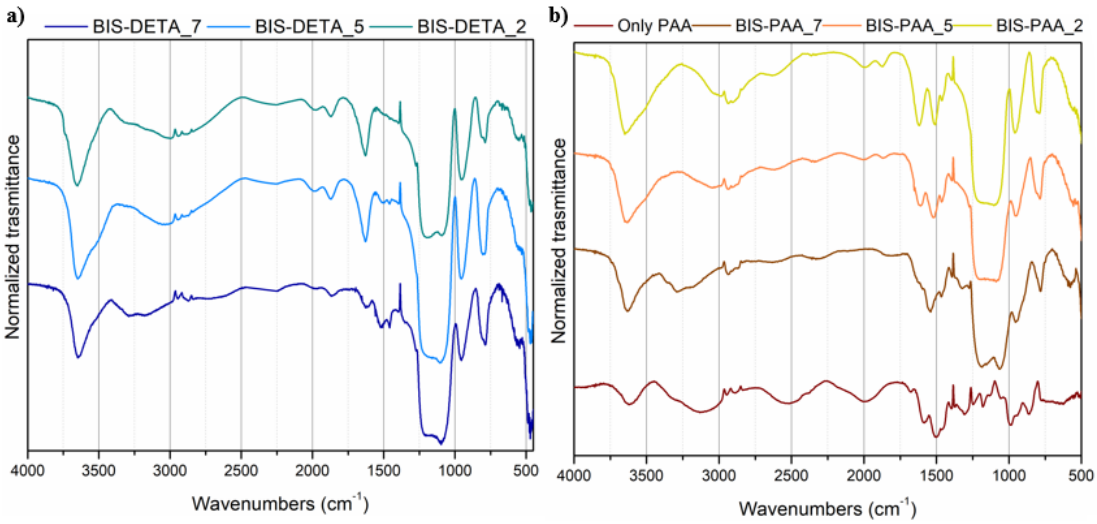

Fig. 59 FTIR-DRIFT analysis of the **a)** BIS-DETA, **b)** BIS-PAA samples.

From FTIR analysis it is possible to have a further evidence of the removal of the additive from the supports synthesized at pH 2. As shown in **Fig. 59**, supports prepared at pH 7, show the characteristic signals of the additive (1440-1480 CH bending, 1650-1600 bending of primary amines, 3000-3330 NH stretching of

secondary amines) in addition to those of the silica (1100-1000 Si-O-Si stretching, > 3500 Si-OH stretching). The intensity of the additive bands decreased for supports synthesized at pH 5 and 2. In the supports produced by PAA (**Fig. 59b**) at pH 2, the additive is not completely removed as confirmed by the bands at 1500-1450 of the C-H bending.

3.4 CHEMICAL FUNTIONALIZATION OF THE NON-POROUS AND MESOPOROUS SILICA SUPPORT

Chemical functionalization is an important step to obtain silica supports containing organic groups on the surface able to interact with proteins.
The non-porous silica supports were functionalized with APTES and CPTMS with an azide group. In the first case, the density effect of NH_2 groups and the use of some silanization methods have been investigated (see § 2.2.2) on the particle size; in the second one, the quality of the surface functionalization has been studied. Samples functionalized with APTES were characterized by CHSN elemental analysis and the Ninhydrin assay. The samples functionalized with CPTMS with azide group, were investigated by Thermogravimetric Analysis (TGA), Differential Scanning Calorimetry (DSC) and FTIR-DRIFT data.
Mesoporous supports were functionalized using different organosilnes ((3-Aminopropyl) triethoxysilane (APTES), 3-(Trimethoxysilyl)-1-propanethiol (MPTMS), (3-Glycidyloxypropyl)trimethoxysilane(GPTMS), N-[(3-trimethoxysilyl)propyl] ethylenediaminetriacetic acid (TMS-EDTA)). The sample functionalized with GPTMS was further modified with PEI.
The samples were characterized with TGA, DSC, CHNS elemental analysis and the Ninhydrin assay (for the APTES case). For the sample functionalized with GPTMS and PEI, also FTIR-DRIFT analysis was performed. In **Table 13** are reported the details of the samples used. For each sample, the measurement for each analysis was performed three times.

Table 13

Sample	Oragnosilanes	Functionalization method	Particles size (nm)	Density (NH_2/nm^2)	Linkers (mmol/g)
S8-PrNH$_2$	APTES	Acid silanization (method A)	250±20	1.5±0.23	0.17±0.03
S18-PrNH$_2$	APTES	Acid silanization (method A)	1180±25	0.97±0.15	0.21±0.04
S19-PrNH$_2$	APTES	Acid silanization (method A)	2081±49	1.74±0.26	0.22±0.03
S19-PrCl	CPTMS	Grafting in organic solvent (method B)	2081±49	n/a	n/a

S19-PrN$_3$	Sodium azide	Grafting in organic solvent (method B)	2081±49	n/a	n/a
S8-PrNH$_2$ (A)	APTES	Acid silanization (method A)	250±20	1.5±0.23	0.17±0.03
S8-PrNH$_2$ (B)	APTES	Grafting in organic solvent (method B)	250±20	27.50±4.13	3.78±0.60
S8-PrNH$_2$ (C)	APTES	Acid silylation using a controlled dripping (method C)	250±20	1.72±0.26	1.23±0.18
S8-PrNH$_2$ (D)	APTES	Co-condensation synthesis (method D)	250±20	64.50±9.67	7.92±1.20
MC10-PrNH$_2$	APTES	Acid silanization (method A)	85±6.0	0.71±0.10	6.23±0.93
MC10-PrSH	MPTMS	Grafting in organic solvent (method B)	85±6.0	0.65±0.10	6.82±1.02
MC10-GP-PEI	GPTMS and PEI	Grafting in organic solvent (method B)	85±6.0	1.07±0.16	10.70±1.60
MC10-EDTA	EDTA-TMS	Acid silanization (method A)	85±6.0	0.50±0.07	4.8±0.72

3.4.1 APTES and CPTMS cases on different non-porous supports.

The APTES functionalization on non-porous silica particles, was carried on particles of 250 (sample S8), 1000 (S18) and 2000 nm (S19). S8 was also used for testing different silanization methods.

As shown in **Table 13**, the density of the NH_2 groups increases for larger particles, indicating a correlation between the APTES functionalization and the particle size. However, the total density in all the samples is low. In order to increase the NH_2 density several silanization methods were tested.

In the method B a grafting solvent (toluene) was used; method C was similar to method A, with the difference that an acidic solution was used to keep the pH constant and the APTES precursor was added controlling the drop rate via a piston pump. Finally, method D concerned the co-condensation reaction of APTES in presence of TEOS in a basic environment. **Table 14** summarized the results of the

CHNS analysis, the linkers concentration and the values of the density of NH_2 groups obtained by different functionalization methods. The methods B and D displayed the higher density of NH_2 groups and the higher concentrations of functional groups (linkers). Even using ninhydrin assay to detect primary amines, methods B and D still showed the higher linkers concentration.

Table 14

Element	Element content (%)[1]				
	S8	S8-$PrNH_2$ (A)	S8-$PrNH_2$ (B)	S8-$PrNH_2$ (C)	S8-$PrNH_2$ (D)
C	0.025	0.10±0.02	2.38±0.35	0.70±0.10	7.60±1.15
H	2.140	1.64±0.25	1.92±0.28	1.50±0.23	2.70±0.40
N	0.01	0.43±0.07	0.96±0.15	0.06±0.01	2.25±0.33
S	0.035	0.04±0.01	0.05±0.01	0.04±0.01	0.038±0.01
Linkers (mmol/g)	0.04±0.01	0.17±0.03	3.78±0.60	1.72±0.23	7.92±1.20
Density (NH_2/nm^2) [3]	0.3±0.05	1.50±0.23	27.5±4.13	1.23±0.20	64.50±9.60
Ninhydrin assay[2]					
Linkers (mmol/g)	negligible	0.05±0.01	7.20±1.08	1.48±0.22	27.2±4.10
Density (NH_2/nm^2) [4]	negligible	0.3±0.05	28.40±4.26	1.82±0.27	91.36±13.70

1-2 Analysis were performed on two different batches.
3-4 Different density values (NH_2/nm^2) obtained with the two different methods [1-2] can be due to large batch-to-batch variability in amine content available.

As revealed for APTES case, the functionalization can be influenced by silanization method. The functionalization with CPTMS and azide groups was performed on micro non-porous particles with a size of about 2081 nm. In this case, the graft mechanism can be divided in two steps: in the first step, the silica surface is modified using CPTMS [158]; in the second step, the surface is modified with sodium azide in a DMF solution obtaining a substitution (S_N2) of the halogen group (Cl^-) with an azide group as shown in **R. 6**.

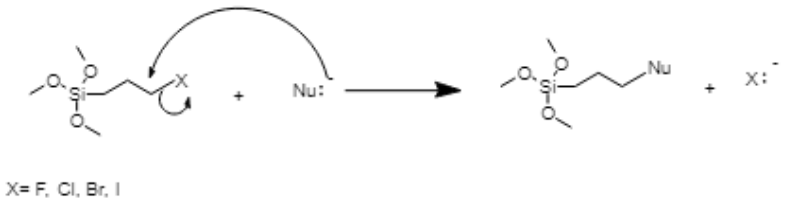

R. 6 S_N2 reaction mechanism between halogen group of the CPTMS and azide group of the sodium azide.

IR spectra (**Fig. 60**) show signals mainly attributed to the silica support (1100-1000 cm^{-1} Si-O-Si stretching, > 3500 cm^{-1} Si-OH stretching). Samples S19-PrCl and S19-PrN_3 also show a weak band around 2975-2845cm^{-1} attributed to the stretching of the C-H bond.

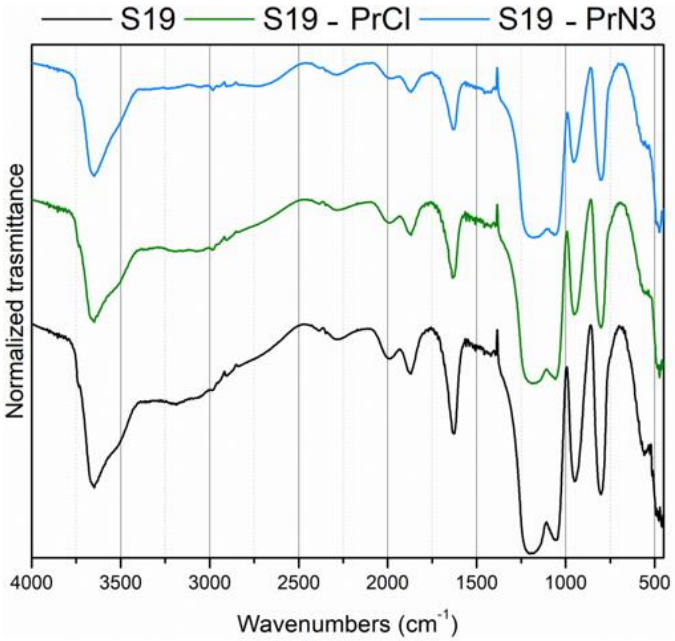

Fig. 60 FTIR-DRIFT analysis on the samples S19, S19-PrCl and S19-PrN_3.

DSC curves (**Fig. 61a**) and thermograms (**Fig. 61b**) of S19-PrCl and S19-PrN_3 evidence a small weight variation of the residual mass (3-4 %), indicating a low density of the organic groups on the surface of the support.

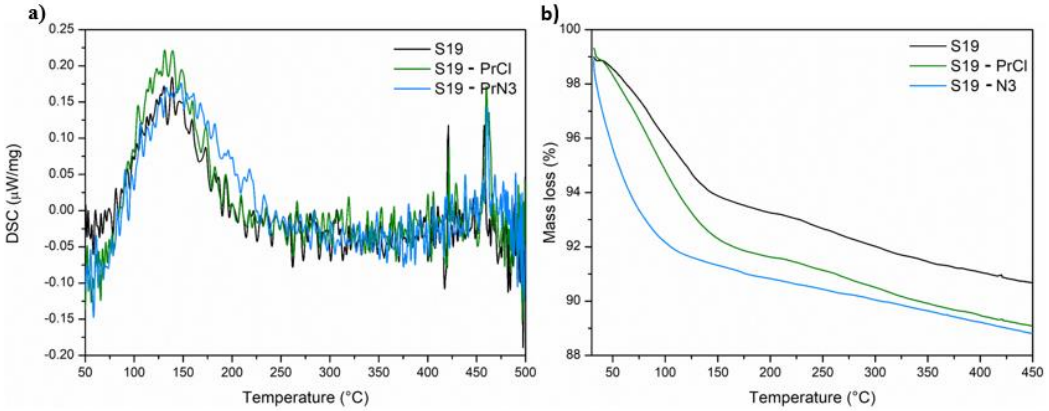

Fig. 61 a) Thermograms, **b)** DSC curves of the samples S19, S19-PrCl and S19-PrN_3.

3.4.1.1 Biotinylation of the azide silica by CuAAC Click reaction

In order to verify the substitution of the halogen with an azide group, that was not always clearly visible by FTIR and DSC analysis, biotin was bound to the azide-functionalized silica supports via Cu-Catalyzed Azide-Alkyne Cycloaddition (CuAAC). The analysis of the amount of bind biotin was carried out by adsorption of fluorescent streptavidin.

The click reaction was carried out between non-porous silica particles (sample S19-PrN_3) and biotin (Btn). The reaction is catalyzed by Cu (I) obtained from the reduction of Cu (II) in $CuSO_4$, using sodium ascorbate as reducing agent. As shown in **R. 7**, the cycle started with the coordination of the alkyne 1 with the Cu (I) species forming the acetylide via the formation of an acetylene π-complex with a loss of the terminal hydrogen of the alkyne group.

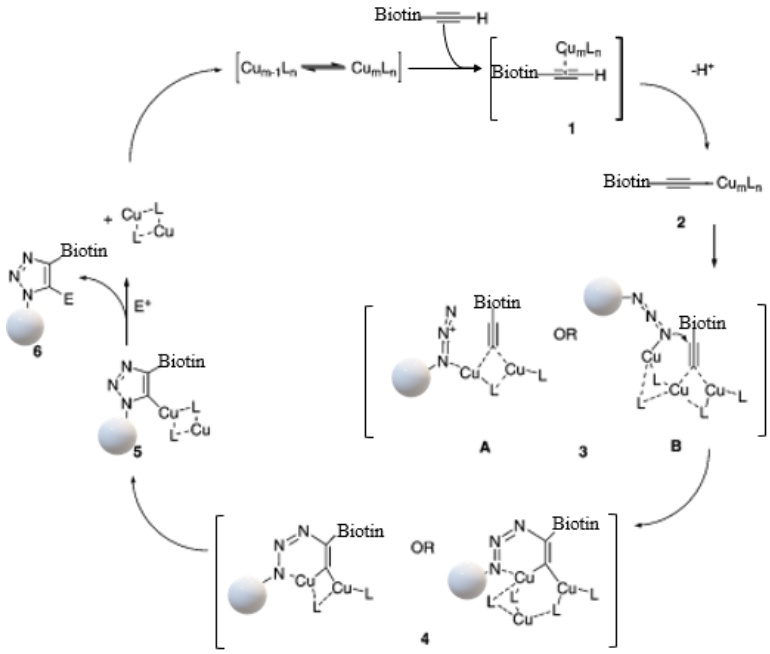

R. 7 Cycloaddition mechanism between silica azide particles and alkyne group of the biotin [159]

Consequently, one of the copper ligands was replaced by the azide compound. The nitrogen proximal to the carbon forms the bond with the copper species giving intermediate 3. Subsequently, the C-2 carbon of the alkyne was attacked by the distal nitrogen of the azide in 3 giving a six-membered Cu (III) metallacycle (4). This step was endothermic. The energy barrier was much lower than the barrier for the uncatalyzed reaction explaining the accelerating effect of the Cu (I) catalysis.

As a result, Species 5 is formed via a ring contraction reaction. Finally, triazole compound is produced by a proton transfer reaction completing the catalytic cycle.

3.4.1.2 Analysis with fluorescent streptavidin of the binding efficiency of biotinylated silica support

The Azide-functionalized silica supports (S19 PrN_3) were used to bind biotin (Btn) containing an alkyne group via Cu-Catalyzed Azide-Alkyne Cycloaddition (CuAAC) in order to evidence the presence of functional groups on the surface of the particles. The binding efficiency between biotin and support was detected by adsorption of 10 mM of streptavidin (Strep) containing a fluorescent compound and analyzed by flow cytometry. The analysis for each sample was performed three times.

In **Fig. 62,** the bioconjugation process between biotin and STREP is represented. Tests of the binding efficiency was performed on sample S19-PrN_3 whereas the bioconjugate and cytofluorimetric analysis were carried out on samples S19-PrCl, S19-PrN_3 and S19-Pr-triazole-B with a negative control with S19.

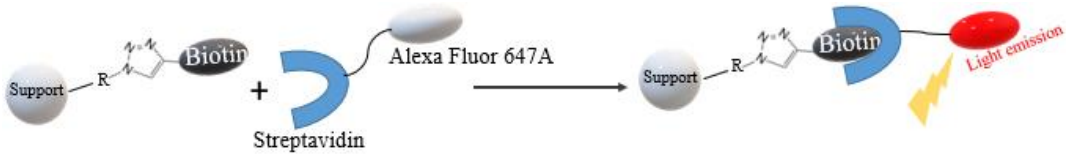

Fig. 62 Bioconjugation between Streptavidin and biotin bound on silica particles.

Further, in **Fig. 63** is reported the fluorescence counts on the single micro particles for sample S19. The same analysis was made also for sample S19-Pr-triazole-Btn treated with STREP protein in order to identify the biotin on the particles. In this case, as shown in **Fig. 63a-4** and **Fig. 63b-4**, the high counts related to the quantity of streptavidin, indicated that part of streptavidin interacts with the surface of the biotinylated particles.

In order to verify a possible adsorption affinity between streptavidin and the surface of the silica particles, the adsorption of streptavidin on the non-biotinylated support S19-$PrN_3$was also tested (**Fig. 63b-3**). The final amount of the adsorbed protein was very low. A further test was carried out on sample S19-PrCl (see **Fig. 63b-2**): in this case the adsorption of both biotin and streptavidin was tested. Also, in this case the adsorption was low, confirming that the result obtained for the biotinylated

sample S19-Pr-triazole-Btn is not only due to the absorption of streptavidin, but also to the presence of biotin covalently linked to the functionalized particles.

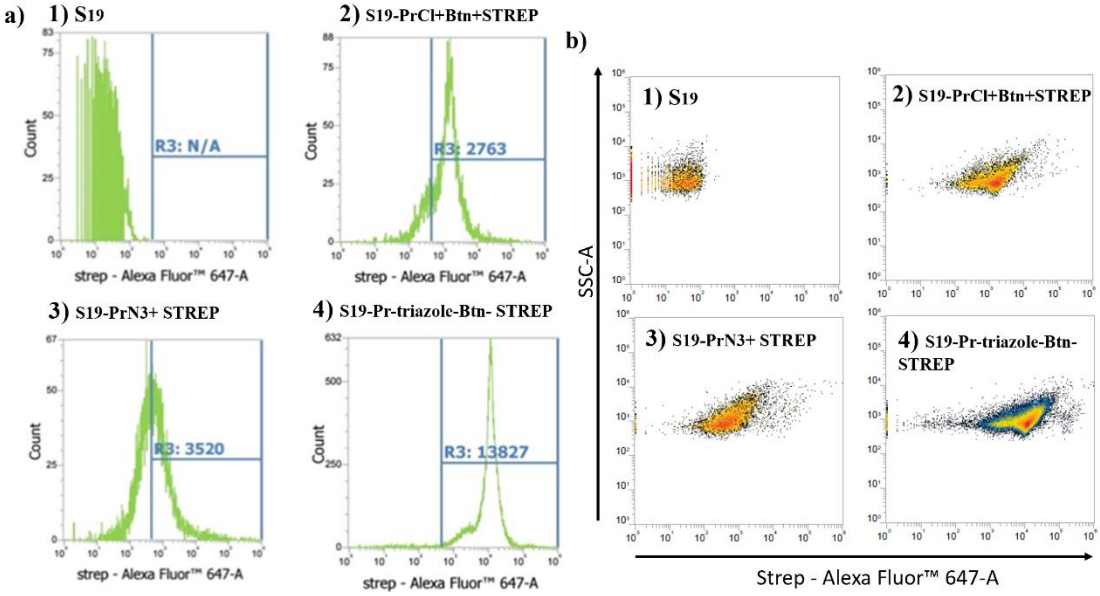

Fig. 63 Flow cytometric analysis of the samples: **a)** graphics of the counts in function of fluorescence intensity and **b)** graphics of the particles scattering intensity.

3.4.2 Functionalization of Mesoporous silica supports.

The functionalization of mesoporous silica supports with different organosilanes (APTES, MPTMS, GPTMS and EDTA-TMS) was performed on MC and MS series. Since the results are similar for all the mesoporous support series, only the results of MC 10 sample are discussed as representative of the data reported in **Table 15.**

Table 15

Sample	Organosilanes	Functionalization method	Density (NH_2/nm^2)	Linkers (mmol/g)
MC10-PrNH$_2$	APTES	Acid silanization (method A)	0.71±0.10	6.23±0.93
MC10-PrSH	MPTMS	Grafting in organic solvent (method B)	0.65±0.10	6.82±1.02
MC10-GP	GPTMS	Grafting in organic solvent (method B)	1.07±0.16	10.70±1.60
MC10-GP-PEI*	PEI	Grafting in organic solvent (method B)	0.50±0.07	4.8±0.72
MC10-EDTA	EDTA-TMS	Acid silanization (method A)	1.30±0.20	12.30±1.85

*The analysis was performed after functionalization with Ninhydrin assay
* For each sample, the measurement was performed three times.

DSC curves (**Fig. 64a**) of all (MC10-) samples exhibited both endothermic and exothermic peaks that correspond to crystallization and melting events of the material. The relative thermograms (**Fig. 64b**) showed the weight loss compared to the non-functionalized sample (MC-10). The calculated residual mass of the samples ranges from 13.44%±2.01 (MC10-PrNH2) to 27.93%±4.20 (MC10-EDTA), as reported in **Table 16**.
Elemental analysis was performed to confirm the presence of the functional groups on the MC samples. The corresponding values are listed in **Table 16**.

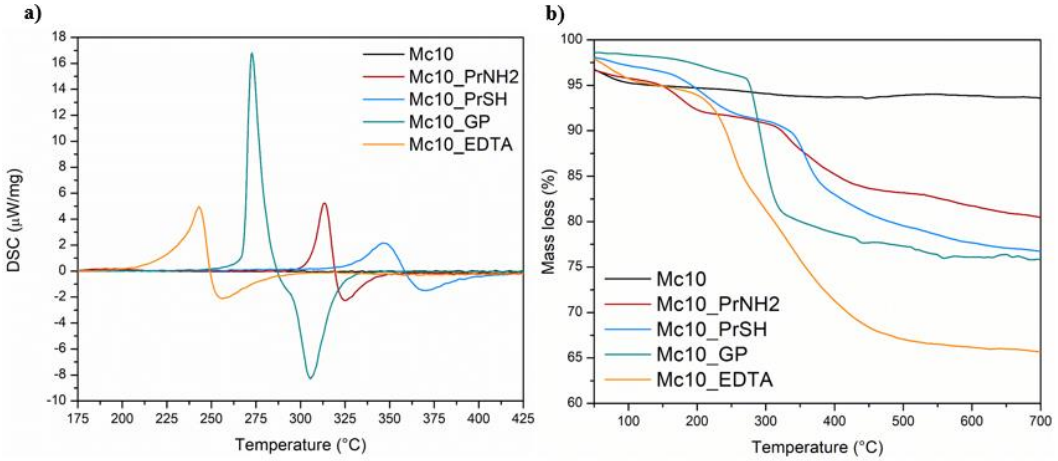

Fig. 64 a) Thermograms and **b)** DSC curves of the sample MC10 functionalized

Table 16

Element	Element content (%)				
	MC10	MC10-$PrNH_2$	MC10-PrSH	MC10-GP	MC10-EDTA
C	0.02±0.005	5.26±0.80	7.90±	14.97±	15.65±
H	2.14±0.43	3.02±0.45	7.30±	1.18±	1.21±
N	0.01±0.002	1.86±0.28	0.01±	0.11±	3.48±
S	0.03±0.007	0.02±	4.00±	0.03±	0.01±
Mass(%)	0	10.17±	17.00±	16.29±	20.35±
Linkers (mmol/g)	0	6.23±	6.82±	10.70±	12.30±
Density (groups/nm^2)	0	0.71±	0.65±	1.07±	1.30±
TG analysis					
Mass (%)	0	13.44±	17.10±	17.21±	27.93±
* For each sample, the measurement was performed three times.					

FTIR spectra (**Fig. 65**) show the typical peaks related to silica systems together with CH bond peaks, both of stretching at 2975-2845 cm^{-1} and bending at 1480-1440 cm^{-1} (even tough of weak intensity) especially in MC10-PrSH, MC10-GP and MC10-GP-PEI samples. In addition, MC10-PrSH, MC10-GP and MC10-EDTA samples show also the absorption related to the stretching of the C-C bond of the acyl group at 1636-1653 cm^{-1}. The peak at 1350cm^{-1} of MC10-GP sample is ascribable to the stretching of the C-O bond of the ether groups. This signal disappears with the C-C bond at 1600-1650cm^{-1} when the sample is functionalized with PEI, indicating that the surface is further modified.

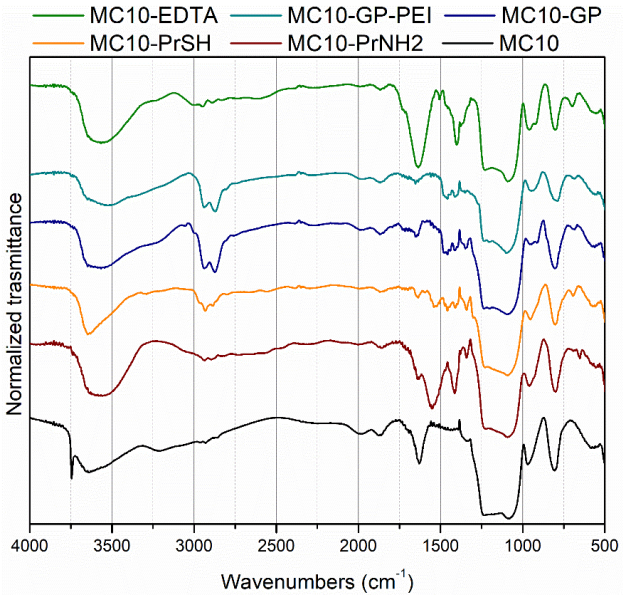

Fig. 65 FTIR analysis of mesoporous silica support (MC10) with different functionalization.

3.5 PROTEIN EXSPRESSION AND PURIFICATION

3.5.1 PETase

The pET21b(+)-PETase-W159H-S238F pET-21b(+) plasmid was used of PETase. The gene from *Ideonella sakaiensis* 201-F6 (Genbank GAP38373.1) contains W159H and S238F mutations.

The expression tests were carried out with different expression strains of *E. Coli* (C41(DE3)), Rosetta, Lemo 21 (DE3), Shuffle® T7); the final concentration of IPTG was 0.4 mM for 20h at16°C. A small-scale purification with Nickel -NTA resin was performed and enzyme was eluted with 500 mM imidazole. The purification has been performed by gravity-flow. The Lemo 21 strain obtained a greater yield as shown by SDS-PAGE gel in **Fig. 66a.**

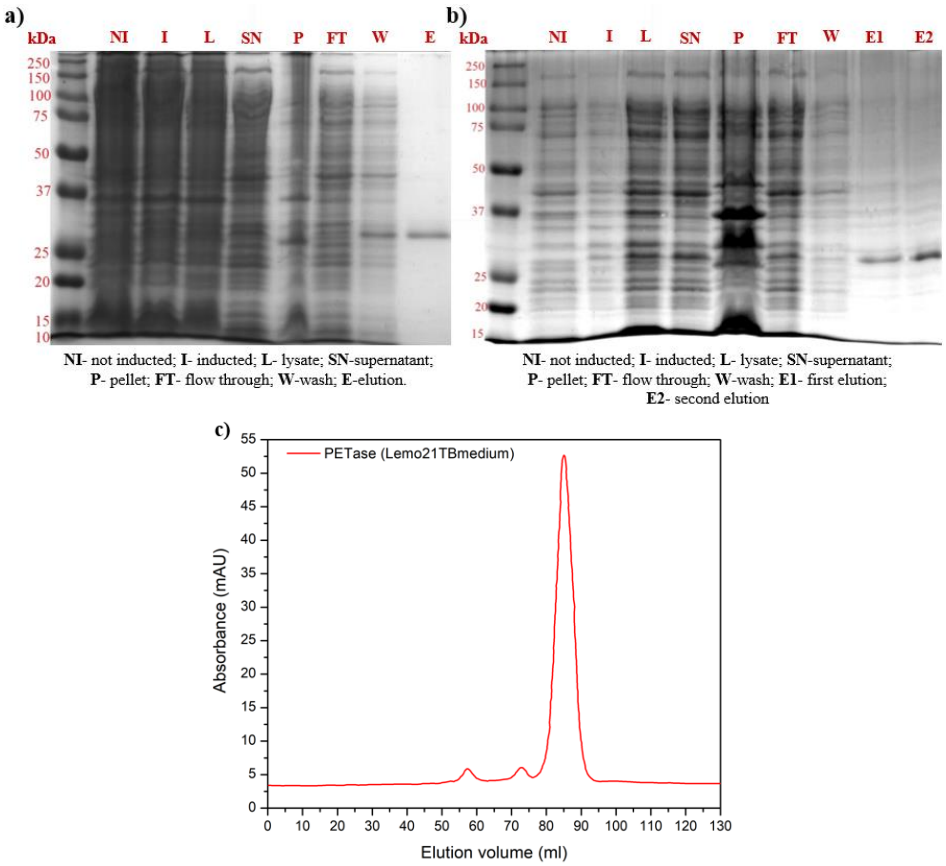

Fig. 66 SDS-PAGE gels of the expression strains, **a)** Lemo21 PETase TB medium (100mL), **b)** Lemo21 PETase TB medium (1L), **c)** Chromatogram of the Lemo21 PETase TB medium (1L and 2L).

After the first small-scale test expression, the protein was purified as describe in § 2.3.2, from 1 L of TB medium, using the Lemo 21 (DE3) induced with 0.4 mM IPTG and grown at 16°C for 20 hours. The final yield of the protein was 1.1mg (**Fig. 66b**). In the **Fig. 66c** shown the result of the size exclusion chromatography, where it is observable the narrow peaks came out at around 85 ml on the Hi Load Superdex 75 16/600.

3.5.2 Purification of Endo-β-1,4-glucanase (Cell_EG)

Purification of the cellulase Endo-β-1,4-glucanase was performed with size exclusion chromatography as described in § 2.3.3. In this case a higher level of purity compared to the commercially available form is reached, showing a co-elution with narrow peak at ca 68 ml of the elution volume and a smaller peak at around 75 ml corresponding to the dimeric and monomeric form of the protein, respectively (**Fig. 67a)**. The protein showed an equilibrium between the two forms that are both catalytically active, as reported in the literature [160][161]. In addition, in **Fig. 67b** shown the principal bands of SDS PAGE gel before and after purification of the Cell_EG protein. After purification, the protein displayed a more intense band at 65KDa and a second, less intense, nearby 50kDa. This weak band could be due to impurities still present in the protein.

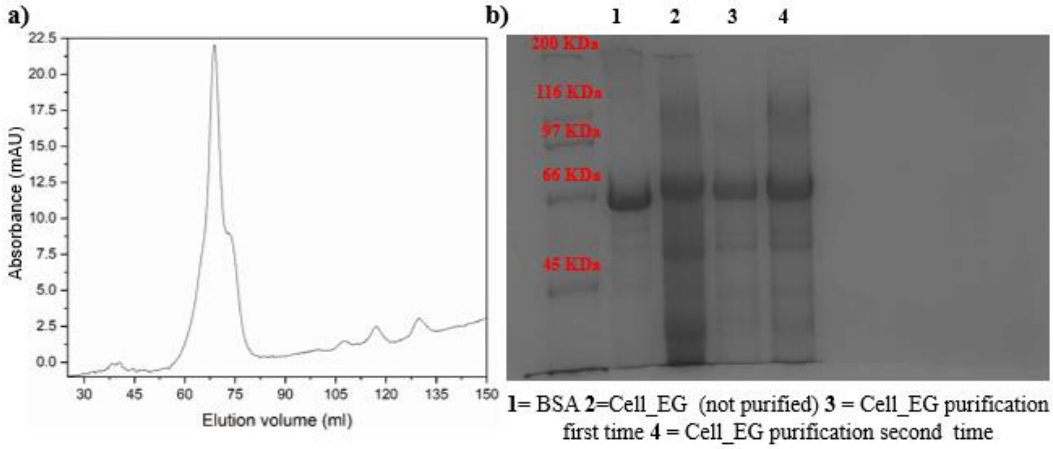

Fig. 67 a) Chromatogram of the Cell_EG after second time purification, b) SDS-PAGE gel of the Cell_EG after first and second time purification.

3.6 COVALENT CONFINEMENT

3.6.1 Cross-linking reaction

3.6.1.1 Protein cross-linking

Cross-linking is a method to generate a covalent bond between protein molecules or protein and functionalized support. In general, the reaction involves a bifunctional molecule such as Glutaraldehyde (Glu) and the lateral groups of the protein. The reactivity of the dialdehyde depends on the reactive moieties of the amino acids. The reactivity follows the following order: ε-amino (lysine) > α-amino (contained in all amino acids) > guanidinyl (arginine) > secondary amino (Arginine, Histidine, Proline, Tryptophan) > hydroxyl groups (Serine and Threonine) [162]. Glu residues react with amine by two principal mechanism, the Schiff base formation and Michael-type addition as shown in **R. 8**.

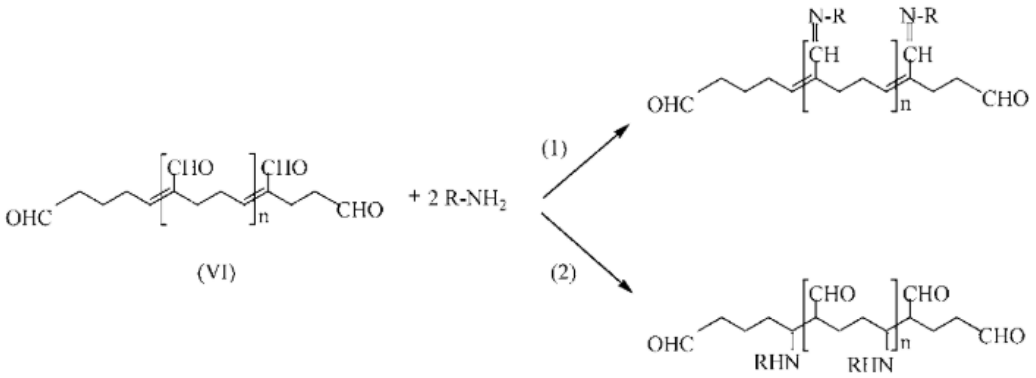

R. 8 Schiff base (1) and Michael-type (2) reactions of glutaraldehyde with proteins [163].

Tests on the cross-linking were performed with BSA and Cell -EG proteins and were carried out at different concentrations of glutaraldehyde. The study on Cell_EG was used to optimize the pH of the reaction. Once the reaction was over, the solutions were analyzed by UV spectrophotometry to verify the formation of bonds among the proteins thorough the crosslinker Glu. For each sample, the measurement was performed three times.

❖ ***BSA protein without support***

Table 17		
Sample	**Glu concentration (mol)**	**Time and temperature**
BSA	n/d	2 h at room temperature
BSA@Glu_1	2.5×10^{-5}	
BSA@Glu_2	5.3×10^{-5}	
BSA@Glu_3	1.06×10^{-4}	
BSA@Glu_4	2.1×10^{-4}	

Table 17 reports the details of the samples. The protein, without the crosslinker, evidences a maximum absorption at 280 nm (UV-visible). The maximum is due to the absorbance of the aromatic amino acids tryptophan (Trp), tyrosine (Tyr), phenylalanine (Phe). When the proteins start to cross-link, due to a hyperchromic effect, the intensity of the peak at 280nm decreases and a new peak near 275 nm starts to increase. The shift of the peak is generated by the π-π* transition of ethylenic double bond conjugated with an adjacent double bond (R 1 - C=C(R2)-C=N or Rs- C=C(R4)- C=O) as reported by Kawahara et al. [163] or by Glu polymerization by aldol condensation. As shown in **Fig. 68a**, the absorbance at 275 nm increases with the concentration of the Glu indicating a larger number of cross-linking among the proteins.

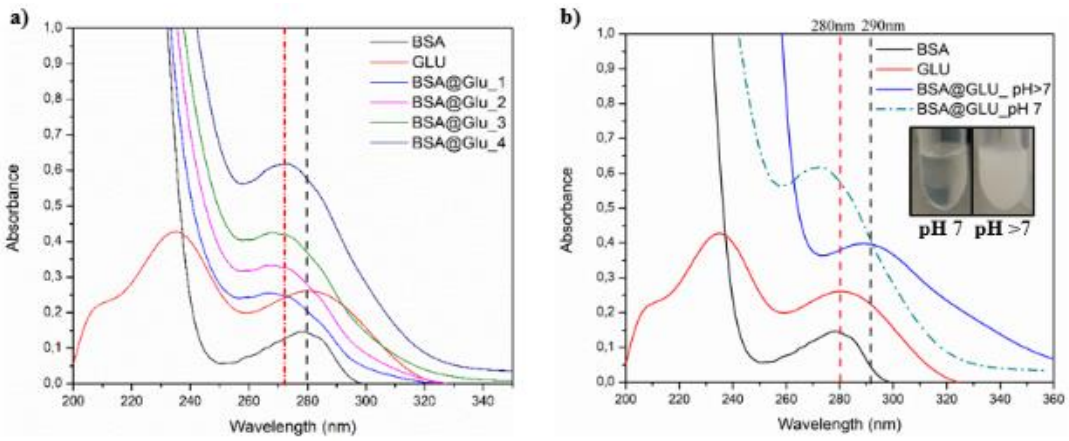

Fig. 68 UV-visible spectra of BSA cross-linked **a)** at different GLU concentrations and **b)** at pH 7 and pH > 7

The addition of NaOH 1 M, used to increase the protein aggregation, also influences the aspect of the final solution; in particular, at pH > 7, the transparent solution become white due the formation of aggregates. In **Fig. 68b,** a redshift of the peak from 275 nm to 290-300 nm is very clear and probably due to an n-π^* transition of a C=O bond in an α-β unsaturated formyl group.

In order to verify the cross-linking among the proteins, for the present evaluation was used the electrophoresis analysis (SDS-PAGE gels). **Table 18** reports the details of the analysis. Gels show that, when the protein interacts with glutaraldehyde, different long smeared bands are formed. The smearing is due to the formation of aggregates of BSA that migrate in different ways along the gel. These bands present in the lines (1,2,3,4 in **Fig. 69a**) are already formed in the upper part of the gel. This result indicates that the BSA starts to aggregate and to migrate in a different way with respect to the not cross linked BSA (line 5 **Fig. 69b**).

Table 18

Sample	Glu concentration (mol)	Line
BSA@Glu_1	2.5×10^{-5}	Line 1
BSA@Glu_2	5.3×10^{-5}	Line 2
BSA@Glu_3	1.06×10^{-4}	Line 3
BSA@Glu_4	2.1×10^{-4}	Line 4
BSA	n/d	Line 5

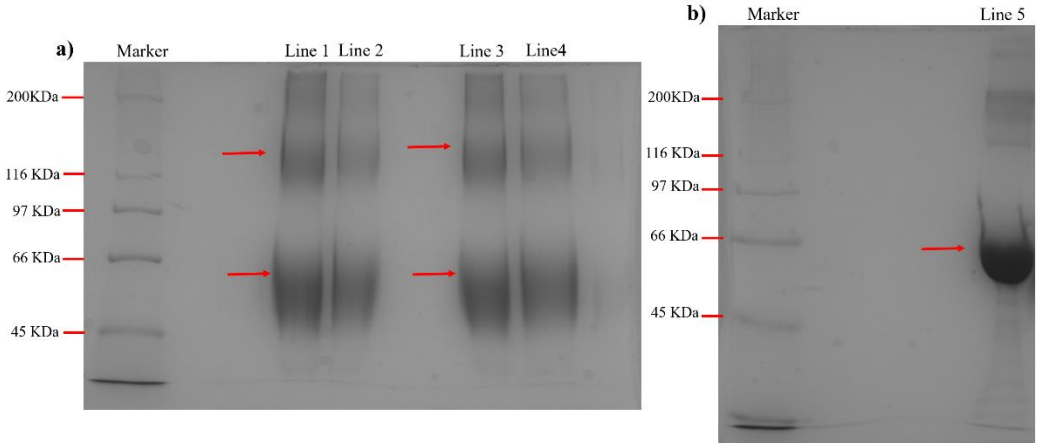

Fig. 69 SDS-PAGE gels on **a)** BSA crosslinked at different concentration of Glu **b)** BSA without Glu (line 5)

❖ ***Cell_EG protein without support***

The results for Cell_EG are similar to the BSA results. The peak at 280 nm increased with the increase of the amount of Glu (**Fig. 70**a). At different pH, up to pH 7, the solution is transparent and shows two peaks at 275-280 nm and 230 nm (UV-Vis spectra, **Fig. 70b-c**). At pH 8-9, the transparent solution become white indicating the formation of aggregates and the peak shifts from 280nm to 290-300 nm.

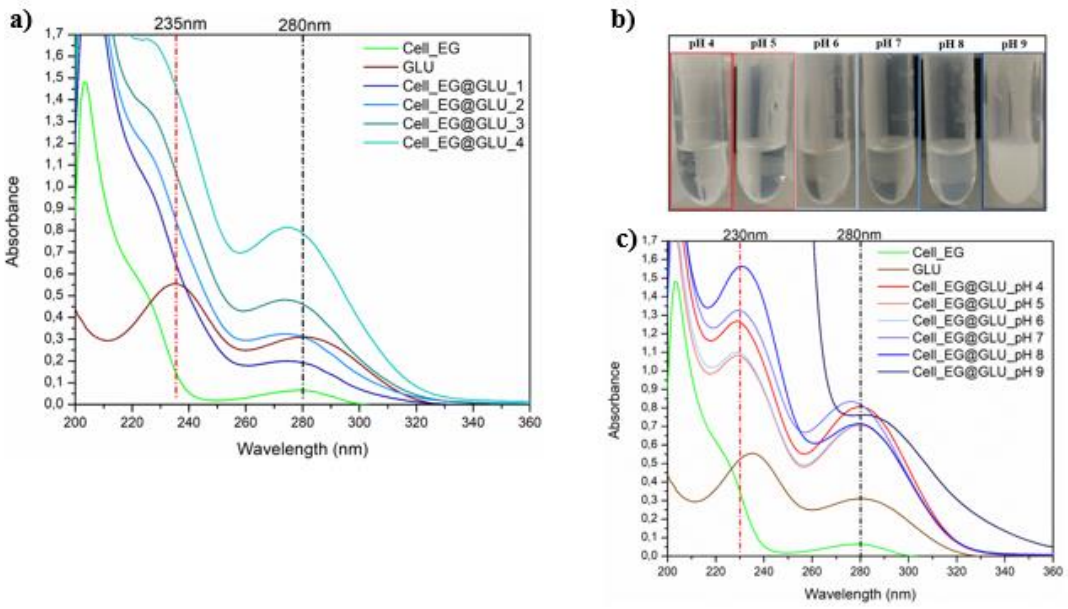

Fig. 70 a) Cell_EG UV spectra at different Glu concentrations **b)** solutions and **c)** Cell_EG UV spectra at different pH.

3.6.1.2 Protein cross-linking on functionalized silica particles

The covalent confinement via cross-linking was carried out on the solid supports in two steps, the former involves the bond of a cross linking agent on the solid support and the second concerns the attachment of the protein on the functionalized supports (see **R. 9**). Glu was used as cross-linking agent and the reaction was carried out at pH 7,4 and room temperature.

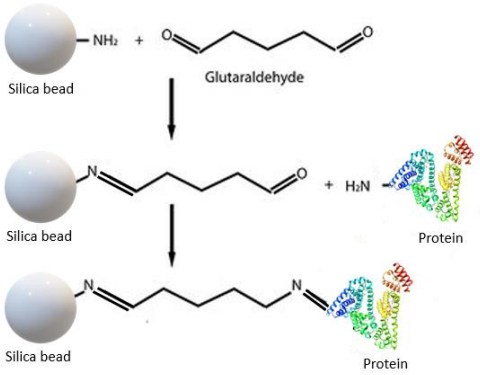

R. 9 Cross-linking reaction between the silica support and the protein.

❖ ***BSA systems on non-porous support***

The functionalized supports and the results of the BSA loading efficiency are listed in **Table 19.**

Table 19

Sample[1]	Support	Functionalization method	Quantity of organic groups (mmol/g)	Loading efficiency (%) BSA[2]
S8@PrNH$_2$_A	Non-porous (250nm)	Acid silanization (method A)	0.17±0.03	13.0±2.6
S8@PrNH$_2$_B		Grafting in organic solvent (method B)	3.78±0.60	52.3±12.6
S8@PrNH$_2$_C		Acid silylation using a controlled dripping (method C)	1.23±0.18	27.5±5.4
S8@PrNH$_2$_D		Co-condensation synthesis (method D)	7.92±1.20	35.2±6.4

1 For each sample, the measurement was performed three times.
2 The loading efficiency is measured after 3 washing

The maximum loading efficiency and the protein yield were calculated according to the equation (8) in §2.4.4.1. Equation (8) is applied on the recovery supernatant after immobilization reaction and different washing. The supernatants were analyzed with Bradford assay and UV-Vis spectrophotometry at 280nm. As reported in **Table 19**, the loading efficiency depends on the silanization methods.
The BSA loading efficiency at different time reports in **Fig. 71a**. S8-PrNH$_2$_A reaches the maximum loading efficiency after 4 hours. This value remains constant also after 24 hours. S8@PrNH2_B reaches the maximum efficiency after 2 hours, then the efficiency decreases and, after 24 hours, it stabilizes at about 43%.
The behavior of the loading efficiency is the same for samples prepared with methods C and D. After a maximum of 3 hours, a constant loss of protein, probably due to its low interaction with the support, is well detectable. The maximum loading of the different non-porous silica supports shows in **Fig. 71b**.

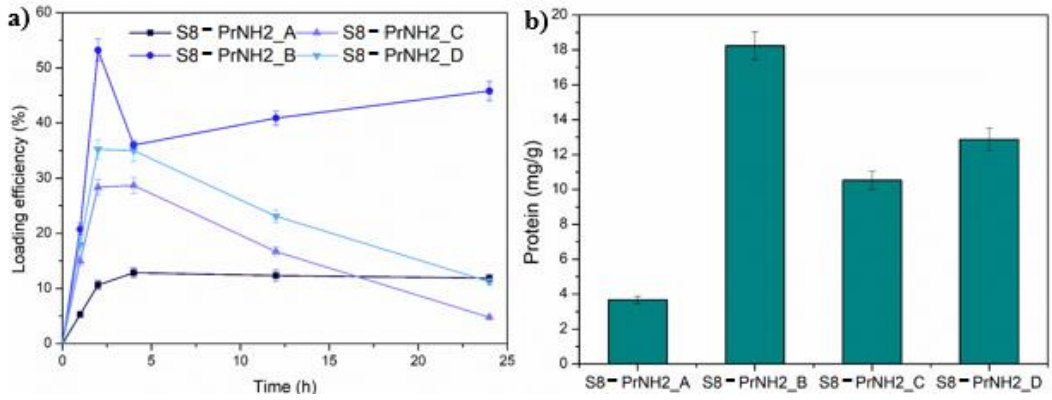

Fig. 71 a) BSA Loading efficiency at different time, **b)** BSA amount on different non-porous silica supports.

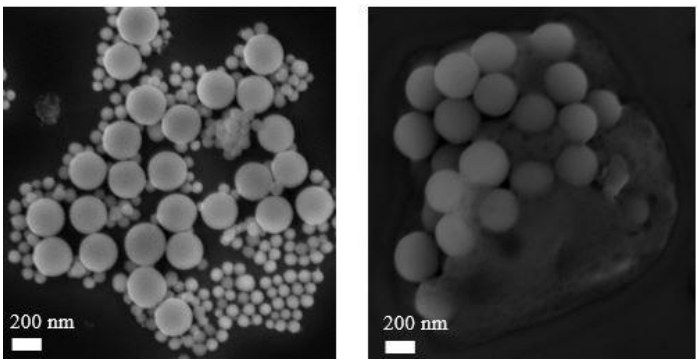

Fig. 72- Fig. 73 FE-SEM image of the S8@NH2_A before and after BSA immobilization

We can conclude that for the cross-linking, S8-PrNH_2_B and S8-PrNH_2_D are the best support for the BSA loading.
After the immobilization process an increased aggregation of the particles is well detectable (see **Fig. 72** and **Fig 73)**.

❖ ***BSA systems on mesoporous supports***

Table 20 reports the loading efficiency on mesoporous silica supports with different grafted group ($PrNH_2$, PrSH, and GP-PEI). The best protein loading is achieved by MC10-$PrNH_2$@BSA (37%) and MC10-PrSH@BSA (54%).

Table 20

Sample[1]	Support	Functionalization method	Quantity organic groups (mmol/g)	Loading efficiency (%) BSA[2]
MC10-$PrNH_2$	Mesoporous	Acid silanization (method A)	6.23±0.93	36.7±3.7
MC10-PrSH		Grafting in organic solvent (method B)	6.82±1.02	54.0±6.1
MC10-GP-PEI		Grafting in organic solvent (method B)	10.70±1.60	25.0±3.4

1 For each sample, the measurement was performed three times.
2 The loading efficiency is measured after 3 washing

❖ ***Cell_EG systems on non-porous and mesoporous supports***

Cell EG cross-linking was performed on the best loading supports found for BSA. The loading efficiency results are summarized in **Table 21**. In this case the loading efficiency is much lower respect to BSA, probably due to a lower affinity of the protein with the support.

Table 21

Sample[1]	Support	Functionalization method	Quantity of organic groups (mmol/g)	Loading efficiency (%) Cell_EG[2]
S8@$PrNH_2$_D	Non-porous	Co-condensation synthesis (method D)	7.92±1.20	42.0±8.4
S8@PrSH_B		Grafting in organic solvent (method B)	3.78±0.60	17.0±3.3
MC10-$PrNH_2$	Mesoporous	Acid silanization (method A)	6.23±0.93	10.5±1.88
MC10-PrSH		Grafting in organic solvent (method B)	6.82±1.02	10.5±2.1

1 For each sample, the measurement was performed three times.
2 The loading efficiency is measured after 3 washing

3.7 THE NON-COVALENT CONFINEMENT

3.7.1 Protein adsorption

The adsorption confinement uses the non-covalent bond to generate an interaction between protein and the surface of the support. It was carried out in a single-step process at pH 7.4 and room temeperature (see §2.4.3.1) using BSA (see **Fig. 74a**) and Cell_EG (**Fig. 74b**). The protein adsorption was performed on the different supports with different particles size and functionalized with different methods.

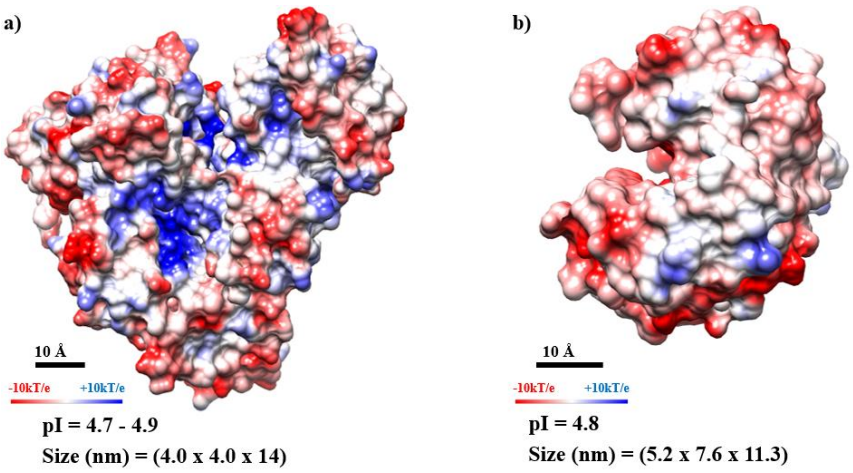

Fig. 74 Potential surface, Isoelectric point (pI) and size of the **a)** BSA and **b)** Cell_EG

3.7.1.1 Adsorption on non-porous silica support

❖ ***BSA protein***

In **Table 22** are listed the samples, the particle size and the loading efficiency.

Table 22			
Sample[1]	**Particle size (nm)**	**Quantity organic groups on the surface (mmol/g)**	**Loading efficiency (%)**[2]
S8-PrNH_2@ BSA	250±20	0.17±0.03	11.5±2.1
S18-PrNH_2@ BSA	1180±25	0.21±0.04	4.8±0.9
S19-PrNH_2@ BSA	2081±49	0.22±0.03	28.8±0.6
1 For each sample, the measurement was performed three times. 2 The loading efficiency is measured after 3 washing			

The adsorption kinetics[6] (**Fig. 75a**) were performed after reaction before washing, while the quantity of the protein loaded on the systems was evaluated after three washing.
The figure below showed similar trends and the amount of BSA adsorbed increases proportionally to the size of the particles. A maximum is well detectable after 4 hours for the two samples with larger size. After the maximum, the amount of the protein decreases and after 24 hours an equilibrium state is almost reached. Sample S8-PrNH_2@BSA shows a small maximum and the system reaches the equilibrium after 4 hours.

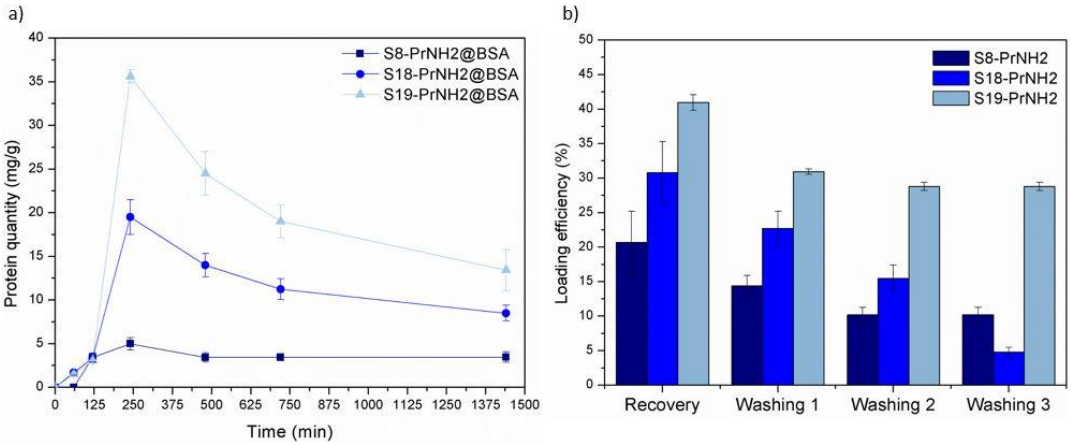

Fig. 75 a) BSA kinetic adsorption on samples with different size particles **b)** loaded amount of protein after recovery and washing.

The trends of **Fig. 75a** can be analyzed by the model descried by Wertz et.al [32]. This model, called "*Rollover model*", considers that the protein is rapidly adsorbed, but rather weakly on the surface in its end-on orientation, and then it is slowly, but tightly adsorbed in its side-on orientation. A possible scheme of the model is shown in **Fig. 76**. The surface is initially in the non-equilibrium state, mainly covered with proteins in the end-on orientation. Then, the side-on oriented proteins dominate, their surface affinity is higher, and their desorption rate is slower. The slow desorption explained the decreasing behavior of the protein quality (**Fig. 75a)**. As expected, the loading efficiency (**Fig. 75b**) decreased after the washing cycles.

[6] The kinetics study was performed to evaluate: the equilibrium state between the protein and the supports and the time needed to have a maximum amount of protein adsorbed on the supports.

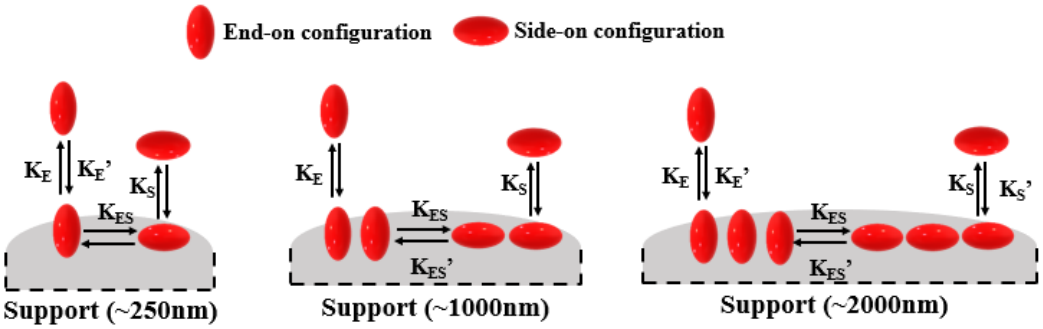

Fig. 76 Rollover model scheme on different size particles

The presence of the protein on the particles was further investigated by SDS-PAGE gels analysis.

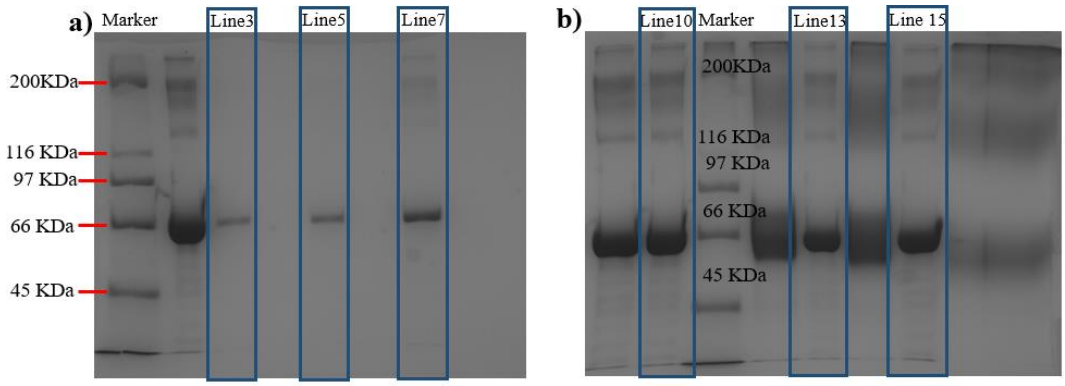

Fig. 77 SDS-PAGE gels **a)** BSA adsorption on S8 -$PrNH_2$_A at 2h, 4h and 24h, **b)** Amount of BSA in the supernatant of the recovery and after washings.

Fig. 77a shows the gel (Lines 3,5,7) of the BSA residues on the S8-$PrNH_2$@BSA sample (previously washed) after 2, 4 and 24 h of adsorption. **Fig. 77b** shows the gel (Lines 10,13,15) of the protein in the recovery solution (supernatant) immediately after adsorption. The analysis indicates that a large amount of protein is still present in solution.

❖ ***Cell_EG protein***

Table 23 reports the loading efficiency and the details of the samples.

Table 23			
Sample[1]	**Particle size (nm)**	**Quantity organic groups on the surface (mmol/g)**	**Loading efficiency (%)[2]**
S8-PrNH$_2$@ Cell_EG	250±20	0.17±0.03	Negligible
S18-PrNH$_2$@ Cell_EG	1180±25	0.21±0.04	5.5±1.5
S19-PrNH$_2$@ Cell_EG	2081±49	0.22±0.03	Negligible
1 For each sample, the measurement was performed three times. 2 The loading efficiency is measured after 3 washing			

The adsorption kinetics (**Fig. 78a**) of samples S8-PrNH$_2$@Cell_EG and S18-PrNH$_2$@Cell_EG have similar trends, but different loadings.

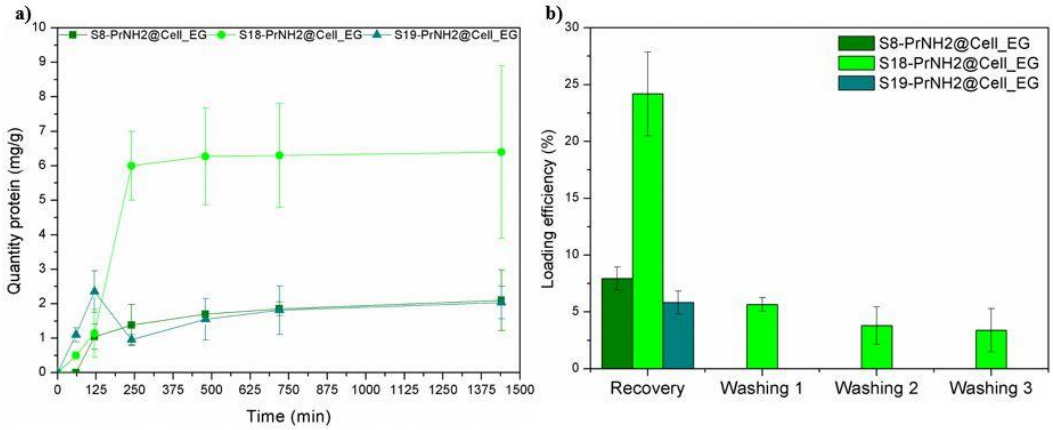

Fig. 78 Cell_EG adsorption on silica supports with different size: **a)** kinetic of adsorption, **b)** loading efficiency after recovery and different washing cycles

The behavior, can be described by the "*Surface Cluster model*" introduced by Minton et al. [164]. The model describes the growth of two-dimensional protein clusters on the surface. Each surface can interact with monomers, dimers, trimers, etc.. (**Fig.79**) and it has a specific tendency to attract a further incoming protein that increases the cluster size by one unit. Proteins can be adsorbed as individual species and then they can diffuse and aggregate to a pre-existing cluster or they can be deposited directly on the edge of a two-dimensional surface cluster via a piggyback

pathway (S8-PrNH$_2$@BSA). In both the steps the predicted adsorption kinetics exhibit an S-shaped curve with an increasing adsorption rate at the beginning (a positive cooperative adsorption) followed by a decreasing adsorption rate when the available surface becomes a limiting factor.

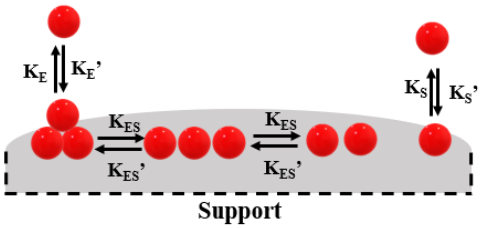

Fig.79 Surface cluster model scheme.

The behavior of S19-PrNH$_2$@Cell_EG can be described with the "*Rollover model*". After some washing, the loading efficiency of S19-PrNH$_2$@Cell_EG and S8-PrNH$_2$@Cell_EG samples is negligible (see **Fig. 78b** and **Table 23**).

3.7.1.2 Adsorption on functionalized non porous silica supports

The adsorption tests performed on the samples are reported in **Table 24**.

Table 24

Sample[1]	Functionalization method	Particles size (nm)	Quantity linker on the surface (mmol/g)	Loading efficiency (%)[2]
S8-PrNH$_2$_A@BSA	Acid silanization (method A)	250±20	0.17±0.03	13.0±2.6
S8-PrNH$_2$_A@Cell_EG				Negligible
S8-PrNH$_2$_B@BSA	Grafting in organic solvent (method B)	250±20	1.23±0.18	Negligible
S8-PrNH$_2$_B@Cell_EG				Negligible
S8-PrSH_B@Cell_EG				22.5±1.3%.
S8-PrNH$_2$_C@BSA	Acid silylation using a controlled dripping (method C)	250±20	3.78±0.60	Negligible
S8-PrNH$_2$_C@Cell_EG				Negligible
S8-PrNH$_2$_D@BSA	Co-condensation synthesis (method D)	250±20	7.92±1.20	Negligible
S8-PrNH$_2$_D@Cell_EG				Negligible

1 For each sample, the measurement was performed three times.
2 The loading efficiency is measured after 3 washing

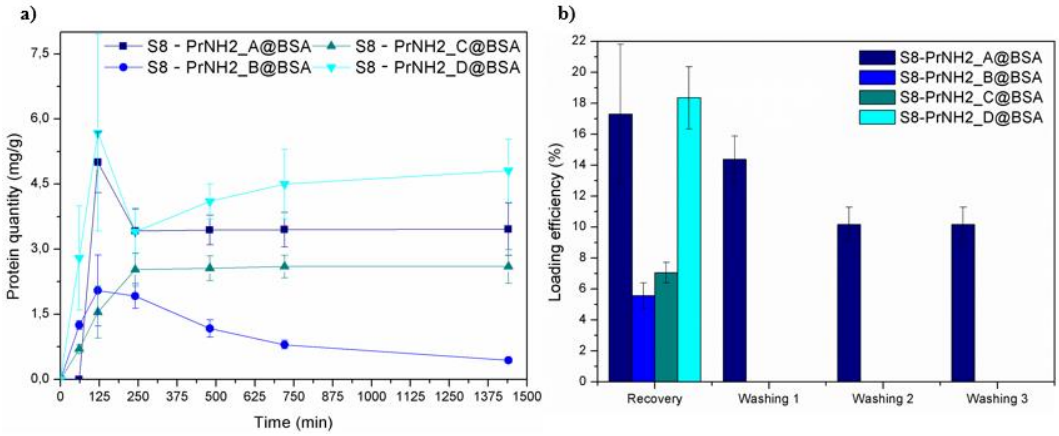

Fig. 80 a) BSA kinetics on different functionalized surface **b)** BSA loading efficiency after different washings.

The trends of the adsorption kinetics relative to the BSA protein(**Fig. 80a**) can be analyzed by the "*Rollover model*" and "*Surface Cluster model*".

The loading efficiency (about 13.0% **Fig. 80b**) is positive only for S8-$PrNH_2$_A@BSA sample.

Concerning the adsorption of Cell_EG, only S8-PrSH_B@Cell_EG shows a positive value (about 22.5%). In this case, the protein seems to have more affinity with thiol group then with the amine.

3.7.1.3 Adsorption on functionalized mesoporous supports

Table 25 lists the samples and the loading efficiency of the proteins.

Table 25				
Sample[1]	**Functionalization method**	**Particles size (nm)**	**Quantity linker on the surface (mmol/g)**	**Loading efficiency (%)[2]**
MC10-$PrNH_2$@BSA	**APTES** by Acid silanization (method A)	85±6.0	6.23±0.93	34.1±3.5
MC10-$PrNH_2$@Cell_EG				4.75±1.5
MC10-PrSH@BSA	**MPTMS** by Grafting in organic solvent. (method B)	85±6.0	6.82±1.02	40.3±4
MC10-PrSH@Cell_EG				4.25±0.7
MC10-PEI@BSA	**GPTMS** and **PEI** by Grafting in organic solvent. (method B)	85±6.0	16.29±2.5	10.5±2.3
MC10-PEI@Cell_EG				8.5±1.0
1 For each sample, the measurement was performed three times. 2 The loading efficiency is measured after 3 washing				

The adsorption process of the proteins on functionalized mesoporous supports is described by different trends (**Fig. 81**).

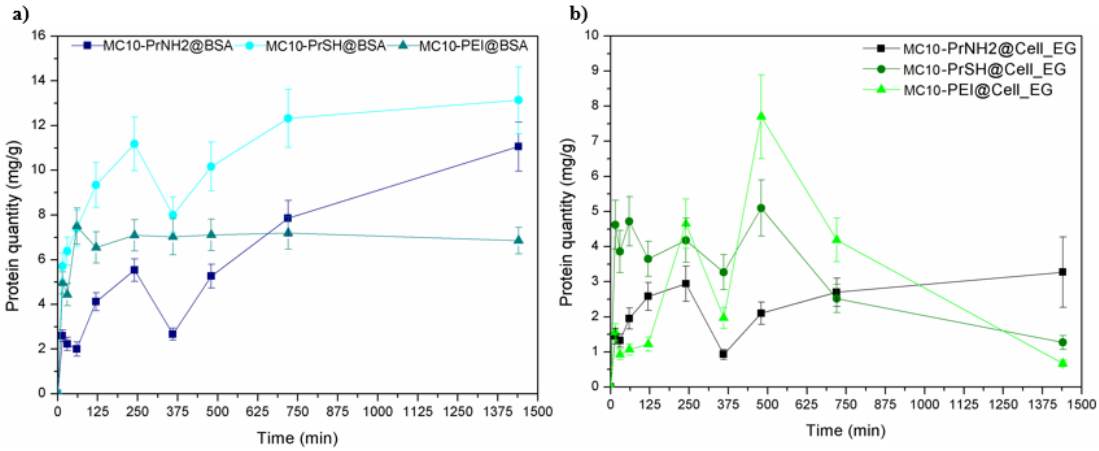

Fig. 81 Adsorption kinetics for **a)** BSA and **b)** Cell_EG proteins.

The trends of MC10-PrNH2@BSA and MC10-PrSH@BSA are similar (**Fig. 81a**) and they can be described by the "*Three-states model*" according to Rabe et al., (**Fig. 82**) [165]. In this case the protein continues to be adsorbed as long as the surface is empty or when it is covered not homogeneously. The proteins are adsorbed on the surface only via the ***initial state***. The transition between ***initial*** and ***intermediate state*** is a result of lateral protein–protein interactions and takes place once a critical surface coverage is exceeded. According to the authors, this transition proceeds rapidly suggesting an orientational change rather than a (multistep) conformational rearrangement. Proteins in the ***intermediate state*** undergo further transition into the ***final relaxed state***. This transition is much slower and therefore involves most likely some conformational rearrangements. The last step is divided in two transition states, changing their surface affinity from irreversible to reversible state which is the key element of the overshooting effect in this model.

The adsorption kinetic of MC10-PEI@BSA sample can be descried by the "*Rollover model"* as reported above.

The adsorption kinetic of MC10-PrNH$_2$@Cell_EG (**Fig. 81b**), has a trend close to MC10-PrNH2@BSA and MC10-PrSH@BSA. The specific behavior evidenced by MC10-PEI@Cell_EG and MC10-PrNH$_2$_Cell_EG can be explained by the fact the protein is always in a different state of reversible equilibrium.

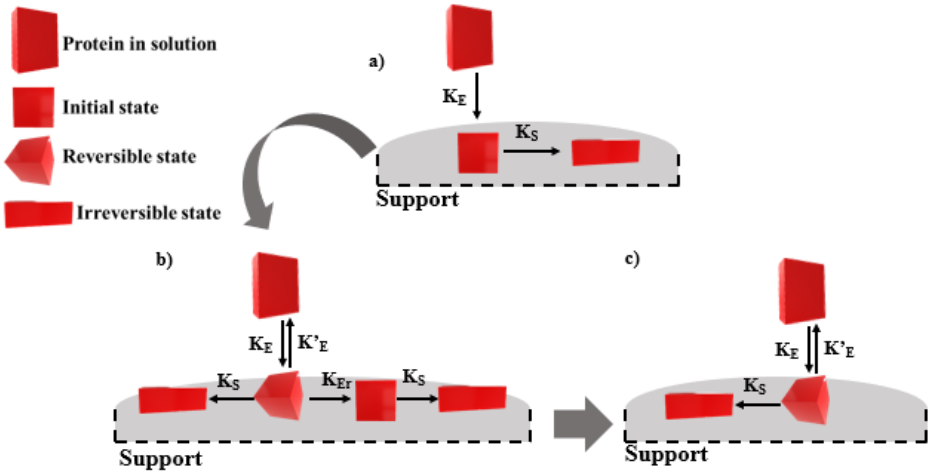

Fig. 82 Three-states model scheme **a)** at the beginning **b)** around critical coverage and **c)** after a long-term adsorption.

3.7.1.4 Adsorption on silica bioinspired with different polyamine additives.

The adsorption strategy was performed, in two steps, also on silica supports synthesized via the bio-inspired method. The first step concerns the synthesis of the supports. At pH 7, the additives (see section § 3.3) are completely entrapped in the silica network, resulting in a functionalized surface of the support. At pH 2, the amines are soluble, and they can be eliminated from the silica network by washings; the polyamines, due to their size and to their closer interaction with the silica network, are not completely eliminated by washings. The second steps concern the protein adsorption on the bio-inspired supports. The adsorption tests were carried out only for 2h at room temperature using water as solvent.

- ***BSA protein***

Table 26 summarizes the samples, some morphological features and the loading efficiency.

Table 26

Sample[1]	Surface area (m^2/g)	Pore volume (cm^3/g)	Loading efficiency (%)[2]
BIS_DETA_7@BSA	32±4.80	0.043±0.01	2.79±0.85
BIS_DETA_5@BSA	266±40	0.15±0.02	Negligible
BIS_DETA_2@BSA	402±60.34	0.75±0.10	14.55±0.33
BIS_TETA_7@BSA	24±3.63	0.044±0.01	27.42±10.50
BIS_TETA_5@BSA	211±31.72	0.18±0.02	1.34±0.44
BIS_TETA_2@BSA	306±46.00	0.19±0.03	1.66±1.47
BIS_PEHA_7@BSA	19±2.80	0.044±0.01	26.07±1.63
BIS_PEHA_5@BSA	20±3.00	0.18±0.03	7.10±2.04
BIS_PEHA_2@BSA	672±100.85	0.19±0.03	Negligible
BIS_PEI_7@BSA	75±11.30	0.13±0.02	71.66±4.58
BIS_PEI_5@BSA	117±17.65	0.19±0.03	52.16±22.21
BIS_PEI_2@BSA	100±15.00	0.18±0.02	Negligible
BIS_PAA_7@BSA	145±21.75	0.4±0.06	32.00±3.12
BIS_PAA_5@BSA	159±23.85	0.45±0.07	52.69±3.59
BIS_PAA_2@BSA	170±25.50	0.41±0.06	71.66±4.58

1 For each sample, the measurement was performed three times.
2 The loading efficiency is measured after 3 washing

The best loading (**Fig. 83**) is obtained with the supports synthesized at pH 7 (BIS_PEI_7 and BIS_TETA_7) and at pH 2 (BIS_DETA_2 and BIS_PAA_2). The additives (ammine and polyamine) are still present in the two samples prepared at pH 7, revealing a certain affinity related to the interaction between negative charges of the protein and positive charges of the additives.

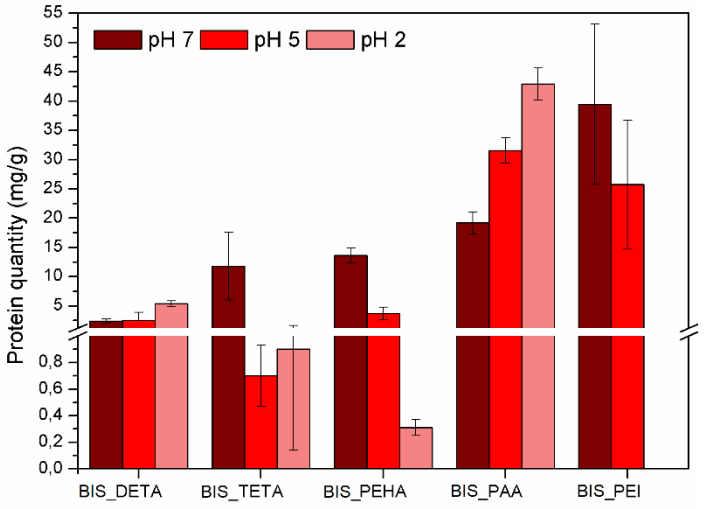

Fig. 83 BSA amount (mg/g) after adsorption on different bio-inspired supports.

For the two samples prepared at pH 2 we can consider that: a) the absence of the additives changes the morphology features of the support (pore volume and surface area) influencing the adsorption amount of the protein (sample BIS_DETA_2); b) when the additives are not completely eliminated a surface, positive charged, can be obtained (sample BIS_PAA_2)

❖ *Cell_EG protein*

The supports, with the best BSA performance, were chosen also for the Cell_EG. **Table 27** reports the samples and the loading efficiency.

Table 27			
Sample[1]	**Surface area (m^2/g)**	**Pore volume (cm^3/g)**	**Loading efficiency (%)[2]**
BIS_DETA_2@Cell_EG	402±60.34	0.75±0.10	Negligible
BIS_TETA_7@Cell_EG	24±3.63	0.044±0.01	10.4±0.8
BIS_PEI_7@Cell_EG	75±11.30	0.13±0.02	4.9±1.5
BIS_PAA_2@Cell_EG	170±25.50	0.41±0.06	28.3±0.5
1 For each sample, the measurement was performed three times. 2 The loading efficiency is measured after 3 washing			

Keeping the same adsorption conditions of BSA, the Cell_Eg loading is lower. BIS_PAA_2@Cell_EG shows the best loading efficiency (28.3%). The adsorption kinetics (see **Fig. 84)** can be analyzed by the Three-state model (BIS_PAA_2) and the Rollover model (others).

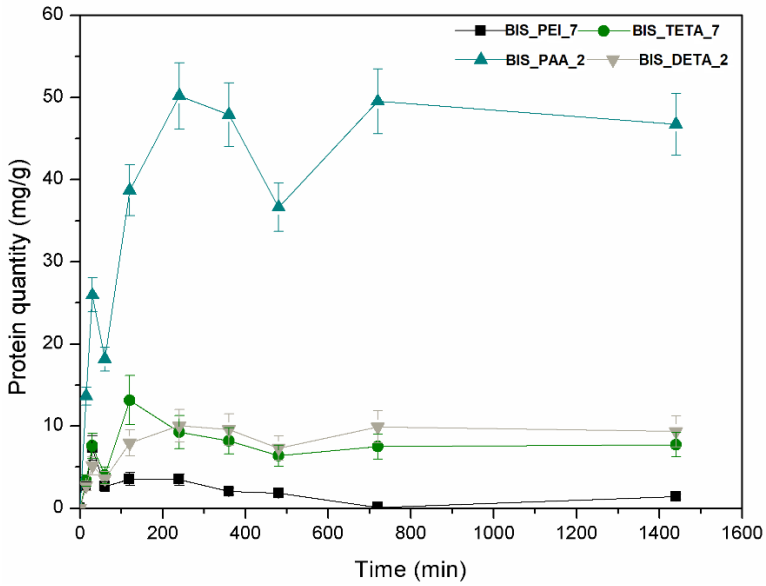

Fig. 84 Adsorption kinetics of the Cell_EG.

3.7.2 Protein entrapment.

The non-covalent confinement via entrapment method was carried out *in situ* with one-pot step reaction and the protein is caged into the silica network.
Fig. 85 shows a scheme of the general reaction. The entrapment strategy was performed in water, at room temperature, at pH 7, with a time reaction of 5-10 minutes and with five additives (**Table 28**).

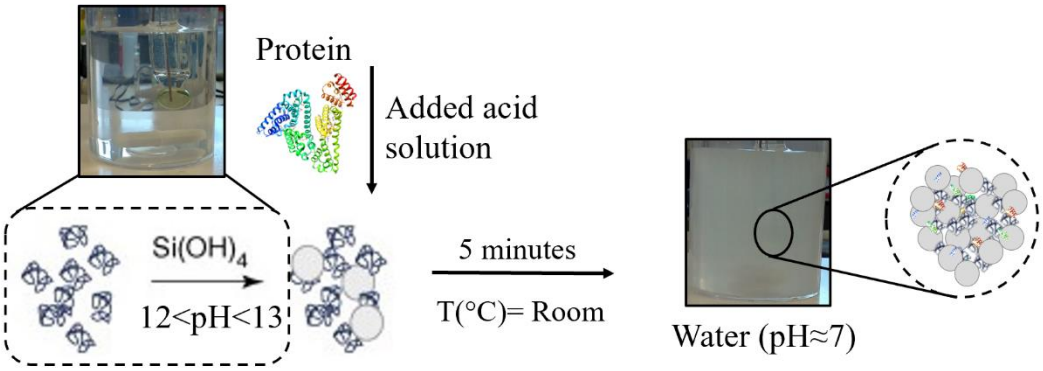

Fig. 85 Protein entrapment reaction

Table 28	
Sample	**Additives**
BSA Protein	
BIS_DETA@BSA	DETA
BIS_TETA@BSA	TETA
BIS_PEHA@BSA	PEHA
BIS_PEI@BSA	PEI
BIS_PAA@BSA	PAA
Cell_EG Protein	
BIS_DETA@Cell_EG	DETA
BIS_TETA@Cell_EG	TETA
BIS_PAA@Cell_EG	PAA

The mechanism of the protein entrapment with bio-inspired synthesis (see **Fig. 86**), can be analyzed according to the model proposed by Manning et al [166]. In presence of an additive and the silica precursor, the entrapment reaction starts when protein and acid are added to the solution. The acid has the role to reduce the pH of the solution (from 13-12 to 7), allowing the additive to activate the silica polymerization via condensation of the precursor ($Na_2SiO_3 \bullet 5H_2O$). During the

reaction, the protein interacts with the additive by charge attractions. Then, protein and additive interact with the moieties on the surface. However, during polymerization, the SiO^- fractions can also interact forming oxygen Si-O-Si bridges. During the condensation, the slow elimination of the SiO^- fractions, can cause the desorption of the additive and of the protein from the surfaces. At the end of reaction (pH 7), the protein and the additive remain in close contact with the surface, obtaining an entrapment or embedded state.

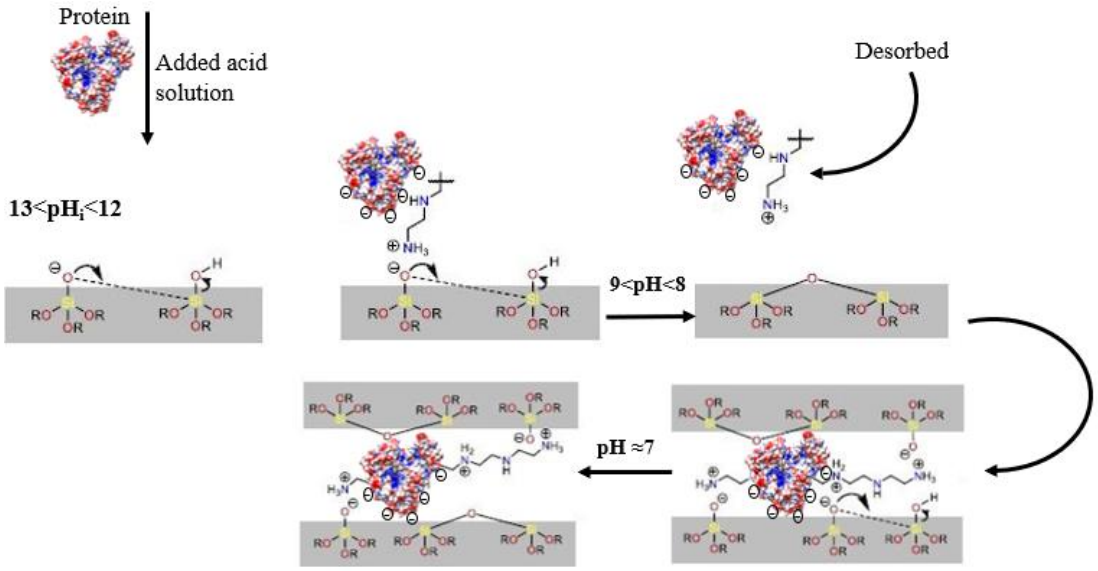

Fig. 86 Possible mechanism of the protein entrapment with bio-inspired synthesis.

❖ *BSA protein*

Table 29 reports the samples and the results of the loading efficiency.

Table 29

Sample[1]	Additives	Loading efficiency (%)[2]
BSA PROTIEN		
BIS_DETA@BSA	DETA	50.6±13.1%
BIS_TETA@BSA	TETA	16.6±2.1%
BIS_PEHA@BSA	PEHA	10.5±5.3%
BIS_PEI@BSA	PEI	6.4±2.4 %
BIS_PAA@BSA	PAA	87.2±7.2%

1 For each sample, the measurement was performed three times.
2 The loading efficiency is measured after 3 washing

The best loading (87.2%) is obtained with PAA. This result is due to the strong interaction between polyamine, positively charged, and protein, negatively charged. As the number of secondary amines increases (PEI>PHEA>TETA>DETA), the loading decreases since the additives, with higher numbers of secondary amine, interact better with the silica polymeric network.

The FTIR -DRIFT was performed only on the system with the maximum loading (taken as reference). **Fig. 87** shows the spectra of: BIS-PAA@BSA, BIS-PAA_7 (support without BSA), BSA protein powder and polyamine powder. The entrapped protein shows signals at 3280, 1650-1550 and 1400-1200, cm^{-1}. Peaks at 1400-1200 cm^{-1} are due to the combination of the NH bending with the C-N stretching vibration with small contributions from the C-C stretching vibration. The 1650-1550 cm^{-1} peaks are mainly due to the stretching of the double bond C=O and C-N bond, whereas the 3280 cm^{-1} band represents the NH stretching vibration. However, the intensity of the signals (in particular at 1400-1200 and 3280 cm^{-1}) can be affected by the presence of polyamine into the support. The other peaks at 3600 cm^{-1} and 1100-800 cm^{-1} represent the OH stretching vibration and stretching and bending of the Si-O-Si.

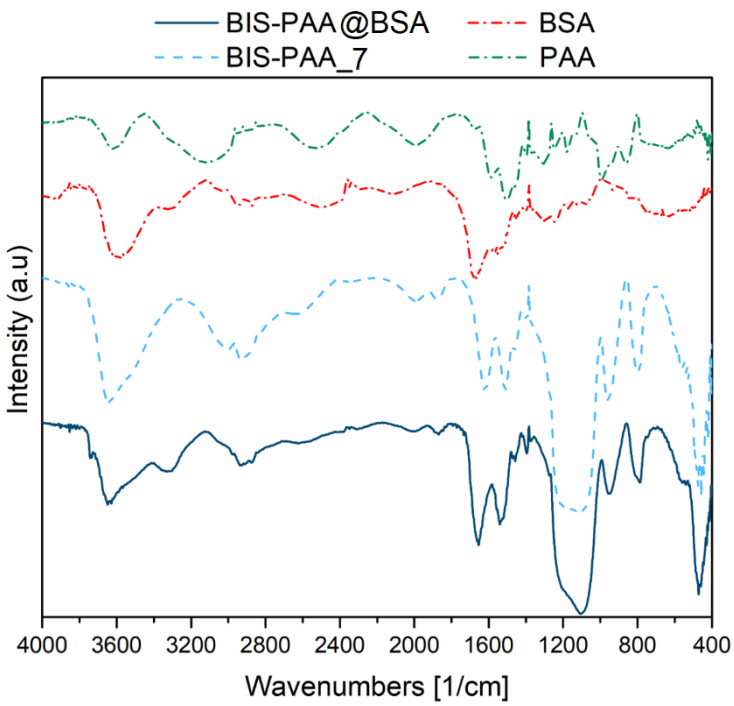

Fig. 87 FTIR spectra of BIS-PAA@BSA (solid blue line), BIS-PAA_7 (system without BSA light blue), protein powder (BSA, red) and polyamine powder (PAA, green).

❖ ***Cell_EG protein***

The three supports (BIS_DETA, BIS_TETA, BIS_PAA), with the best BSA performance, were used also for the entrapment of Cell_EG protein. All these new samples evidence a lower loading even though the trends are very similar (**Table 30**). The maximum loading (34.3 %) is obtained with the BIS_PAA support.

Table 30

Sample[1]	Additives	Loading efficiency[2] (%)
Cell_EG PROTEIN		
BIS_DETA@Cell_EG	DETA	5.35±2.4%
BIS_TETA@Cell_EG	TETA	16.0±1.6%
BIS_PAA@Cell_EG	PAA	34.3 ± 6.7%

1 For each sample, the measurement was performed three times.
2 The loading efficiency is measured after 3 washing

3.8 CATALYTIC ACTIVITY ON DIFFERENT CONFINMENT SYSTEMS OF THE Cell_EG PROTEIN

Table 31 summarizes the samples, the confinement strategy, the loading efficiency, and the catalytic activity. The activity test of the Cell_EG confinement was performed on the best samples of each confinement technique.

Table 31

Samples	Confinement Strategy	Loading efficiency (%)*	Relative activity (%)*
1 S8@PrNH2_D@Cell_EG	Covalent via crosslinking	42.2±8.6	negligible
2 Mc10-PrNH2-Glu @ Cell_EG		8.5±1.0	35.5±7.0
3 Mc10-PrSH @ Cell_EG		10.5±2.1	14.3±3.0
4 S8-PrSH_B@ Cell_EG	Adsorption	22.5±2.5	negligible
5 Mc10-PEI@ Cell_EG		8.5±1.0	10.0 ±0.2
6 BIS-TETA_7@ Cell_EG		10.4±0.8	22.5±0.1
7 BIS-PAA_2@ Cell_EG		28.3±0.50	54.7±0.7
9 BIS-DETA@ Cell_EG	Entrapment	5.35±2.4	negligible
10 BIS-TETA@ Cell_EG		16.0±1.6	43.3±10.8
8 BIS-PAA@ Cell_EG		35.24±5.2	90.4±10

* For each sample, the measurement was performed three times.

The Cell_EG activity was carried out with the Endoglucanase assay (CMCase) that produces the amount of reducing sugars by hydrolysis of the substrate sodium carboxymethyl cellulose (CMC). The reducing sugar was evaluated by the DNS method. The DNS method consists of a redox reaction between the 3,5- dinitro salicylic acid (DNS) and the reducing sugars (see **Fig. 88**).

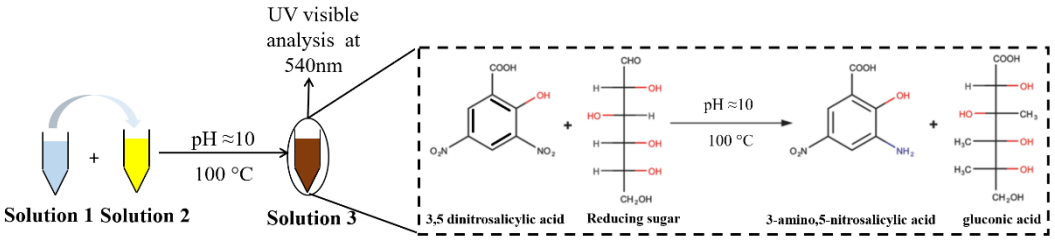

Solution 1 = Reducing sugar solution
Solution 2 = Solution 1+DNS reagent
Solution 3 = Resulting solution after DNS reaction

Fig. 88 Scheme of the reducing sugar process by DNS method.

The reducing power of these sugars derives from their carbonyl group, which can be oxidized to carboxyl group by mild oxidizing agents, whereas the DNS (of yellow color) is reduced to 3-amino-5-nitrosalicylic acid (red brown). The intensity of the color is proportional to the concentration of the sugars in the solution [135], [167].

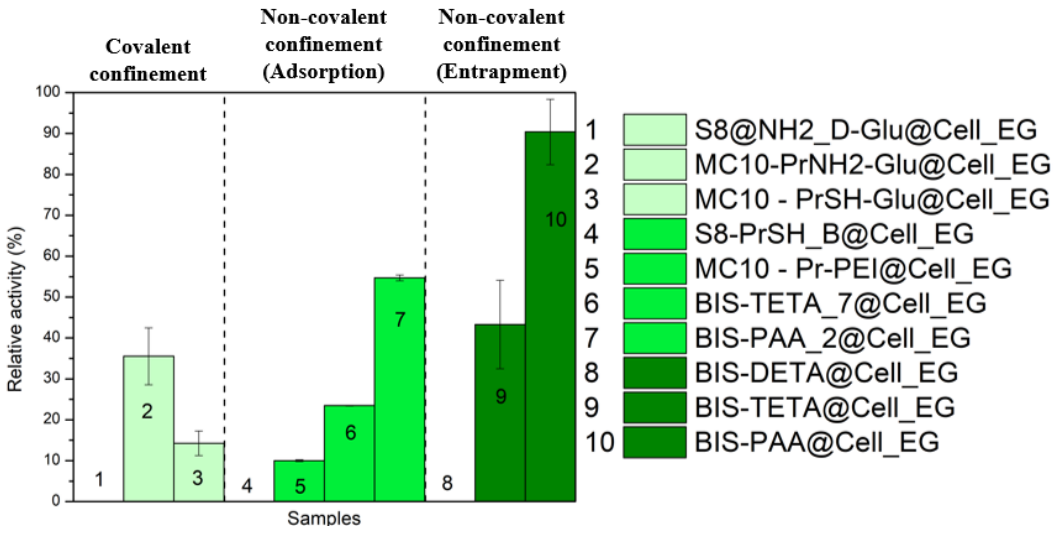

Fig. 89 Relative activity of the different Cell_EG confinement systems

Fig. 89 shows the activity of all the samples. BIS-PAA@Cell_EG (entrapment) and BIS - PAA_2@Cell_EG (adsorption) prepared by bioinspired method show the best performance. Among the samples prepared by covalent strategy, only sample Mc10-PrNH$_2$-Glu@Cell_EG still evidences a residual activity. In the covalent strategy the enzyme fails to maintain its natural conformation and suffers the unfolding process. **Fig. 90a-b** show the Michaelis Menten curves and the Lineaweaver-Burk plot of the samples with the best activity. The Michaelis Menten curves report the reaction rate of the enzyme at different substrate concentrations. The curves of the entrapment system and the free enzyme are very close, meanwhile the curves of the adsorption and the covalent systems show a decrease of the reaction rate. The kinetic parameters are extrapolated linearizing the Michaelis curves by the Lineaweaver-Burk plot (Eq. 12).

(Eq. 12) $$\frac{1}{V_0} = \frac{K_m}{V_{max}} \frac{1}{[S]} + \frac{1}{V_{max}}$$

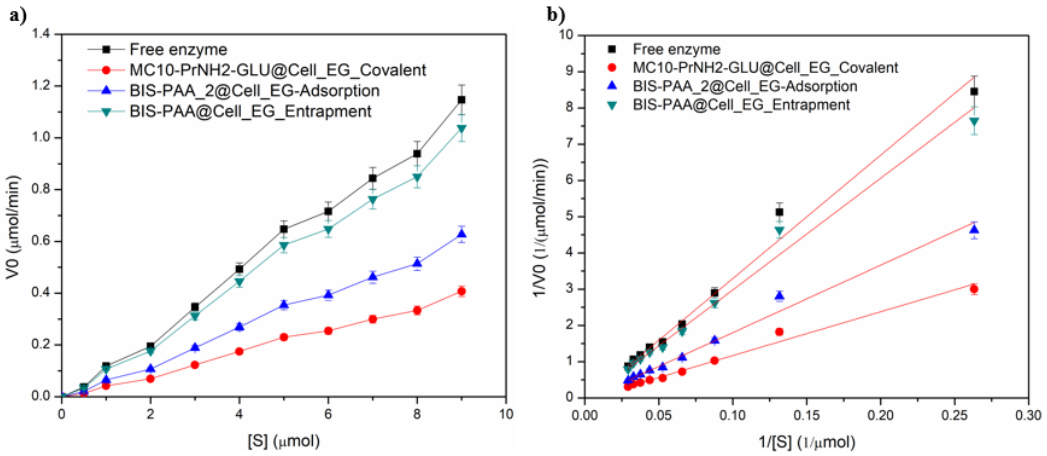

Fig. 90 a) Michaelis Menten curves and **b)** Lineaweaver-Burk plot of the Cell_EG.

Table 32 reports the kinetic parameters of the confined systems compared to the free enzyme.

Table 32		
Samples	K_m*	V_{max}*
Free enzyme	11.45± 0.57	0.72± 0.03
MC10-PrNH_2-GLU@Cell_EG	11.70± 0.70	2.05±0.15
BIS- PAA_2@Cell_EG	11.5± 0.45	1.33±0.06
BIS- PAA@Cell_EG	11.46± 0.80	0.80±0.05
* For each sample, the measurement was performed three times.		

The K_m parameter (Michaelis constant) represents the affinity between enzyme and substrate and V_{max} is the point where the enzyme is complexed with substrate. The larger K_m and V_{max} values for the adsorption and covalent systems are related to the loss of affinity between confined enzyme and substrate. On the contrary, the kinetic parameters of the entrapment system, close to free enzyme parameters, show a good affinity between confined enzyme and substrate.

The pH and thermal stabilities of the samples are shown in **Fig. 91a**. The trends of the entrapment and the covalent systems, at different pH, are similar, but lower than the free enzyme. The adsorbed system shows a different trend: at pH=3 and pH=9 the activity is larger or comparable to the free enzyme activity. The trends of the thermal stability (**Fig. 91b**) are similar, even though the values of the confined systems are always lower than the values of the free enzyme.

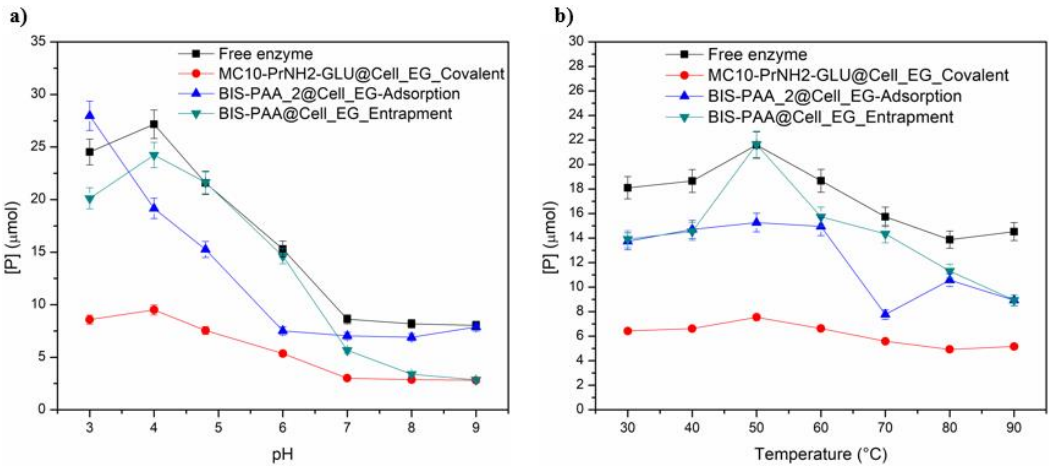

Fig. 91 a) Chemical stability and **b)** thermal stability of Cell_EG.

As underline in the previous paragraphs, one of the advantages of the confinement systems is the possibility of recycling the enzyme after the catalytic process.
In order to verify this possibility, the confined enzyme systems were recycled for a maximum of 5 recycles (**Fig. 92a**). The adsorption and the covalent confinement systems show a low residual activity after 2 recycles, preserving, after the last recycle, only the 5% ca of the activity. The entrapped enzyme maintains the 40-45% ca of the activity after 2 recycles, losing the residual activity after the last three recycles. The missing activity after each recycles may be due to a further unfolding or a leaching effect of the enzyme.
Since the entrapped confinement gives the best results, we use this strategy also for the PETase confinement.

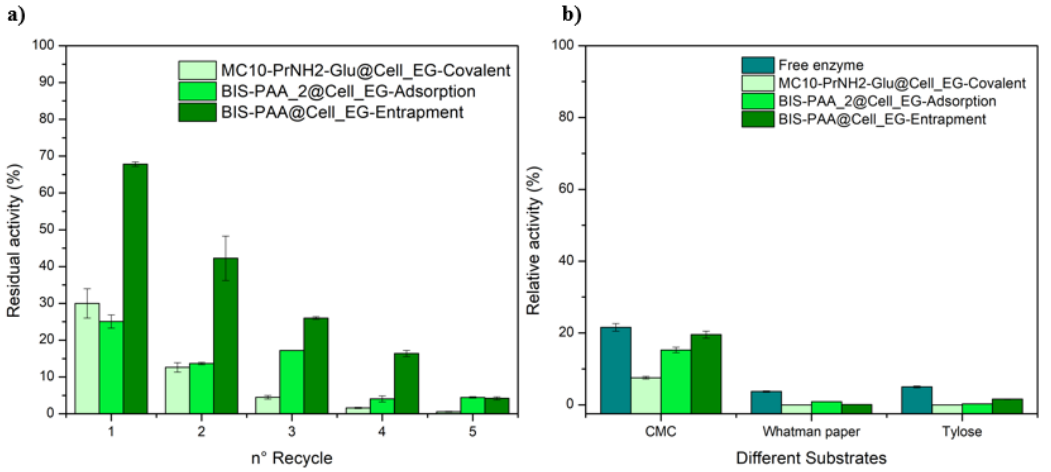

Fig. 92 a) residual activity after recyclings **b)** relative activity of Cell_EG systems with different substrates

The confinement systems were tested also with Tylose (methyl-hydroxyethyl cellose ethers (MHEC)) and Whatman Filter Paper (**Fig. 92b**). However, the use of these two substrates reduces the activity also for free Cell_Eg. This negative effect can be due to the non-ionic nature of the substrate which requires more drastic conditions for the activation of the enzyme.

3.9 ENTRAPMENT CONFINEMENT OF PETase PROTEIN

As previously reported for the Cell_EG, the entrapment via bio-inspired method is an easy and valid method to confine the enzyme and allows to preserve its activity. We use the same procedure also for PETase enzyme (sample BIS- PAA@PETase) and a loading efficiency of about **80%** was obtained. After the entrapment process the evaluation of the enzymatic activity was performed by hydrolysis of para-nitrophenyl acetate (reaction scheme **Fig. 93**).

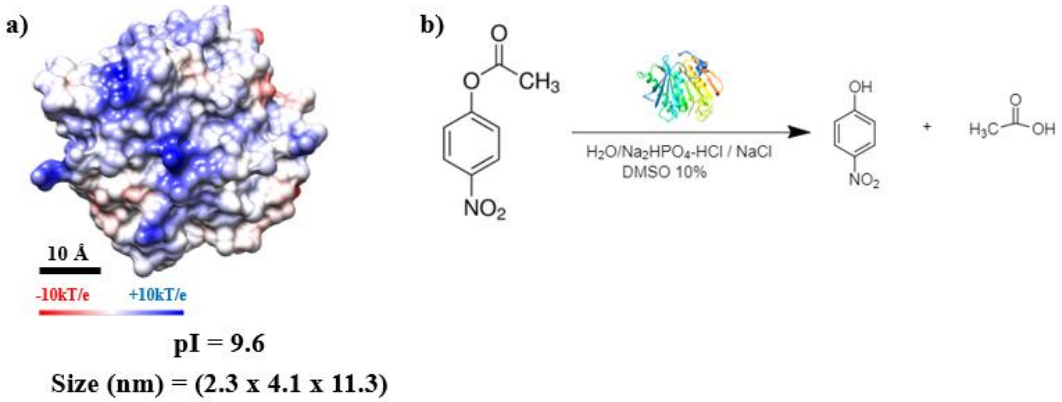

Fig. 93 a) Potential surface, Isoelectric point (pI) and size, **b)** PETase hydrolysis reaction with P-nitrophenyl acetate

Sample BIS- PAA@PETase shows an enzyme activity of about 95%, suggesting that the enzyme entrapped preserves most of its activity. The Michaelis curves (**Fig. 94**) of the free and entrapped systems show that the reaction velocity of the entrapped enzyme tends to decrease. This indicates that the confined enzyme loses some of its efficiency. However, the catalytic parameters, K_m and V_{max} (**Table 33**), do not change. The same K_m values show a high affinity between the enzyme and the substrate.

Table 33		
Samples	K_m	V_{max}
Free enzyme	0.76± 0.1	0.04± 0.03
BIS-PAA@PETase	0.8± 0.06	0.05±0.05
* For each sample, the measurement was performed three times.		

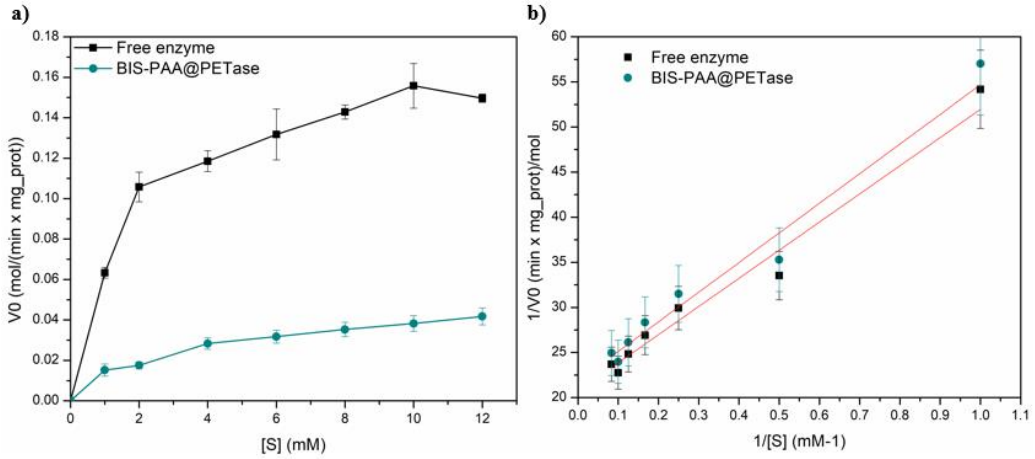

Fig. 94 a) Kinetics PETase of free enzyme and entrapped system **b)** Lineaweaver-Burk plot

The chemical (**Fig. 95a**) and thermal stability (**Fig. 95b**) show similar trends evidencing that the enzyme maintains its stability after entrapment.

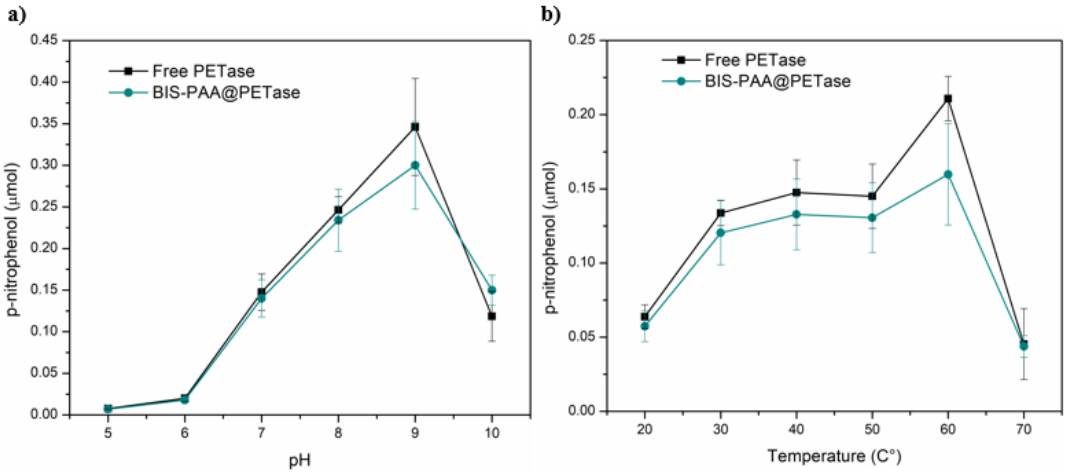

Fig. 95 Free PETase and PETase entrapped **a)** chemical stability **b)** thermal stability

The recycling process of the entrapped system (**Fig. 96**) indicated that the enzyme after the second recycles loose half of its activity (52.1%), but after 5 recycles the activity remain high (about 42.3 %). The activity loss after first and second recycles may be due to a further strong unfolding of the enzyme.

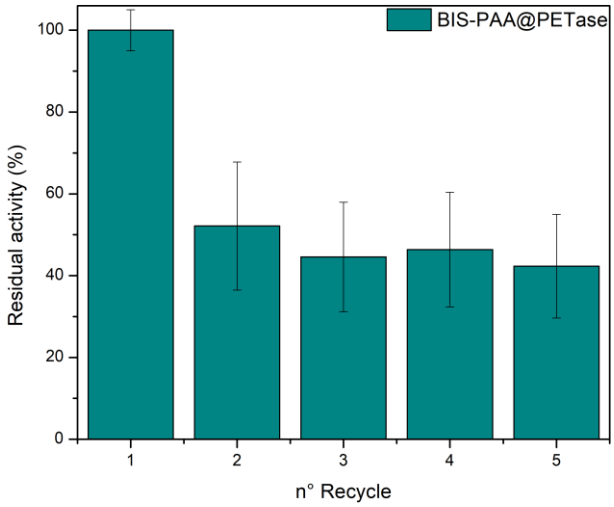

Fig. 96 Residual activity of the recycling system of the entrapped PETase sample.

CHAPTER 4

CONCLUSIONS

4.1 FINAL REMARKS AND FURTHER PERSPECTIVES

The thesis is focused on the study of some methods to confine Bovine Serum Album (BSA), Cellulase-endo-β 1,4-glucanase (Cell-EG), PETase, and streptavidin (Strep) proteins on different silica supports. The project is divided in three parts: the first part concerns the synthesis of some non-porous and mesoporous silica systems prepared by different methods; the second part is focused on some functionalization processes of the supports; the third part compares the yield of the different protein confinement strategies.

The synthesis of the non-porous supports was carried out following the Stöber method. The research investigated the role of the concentration of the components (TEOS, H_2O, NH_3) on the final morphology: particles size of 50- 350 nm (samples S1-S10) were obtained. By controlling the dropping rate of the precursor, in presence of an electrolyte (KCl), it was possible to synthesize particles with larger diameters of 1-2 μm (samples S18 and S19).

The synthesis of the mesoporous materials was carried out by the soft and the hard template methods, using surfactants as templating agents to generate pores inside the support.

The Soft method (MC series) is similar to the Stöber method, but, during the hydrolysis and the condensation reactions of TEOS, a surfactant is added as template to generate, after calcination, a mesoporous structure. When CTABr was used as surfactant, it was possible to synthesize spherical particles with pores size of 2 nm, with diameters of 80-345 nm and surface areas of 50-1500 m^2g^{-1}. The change of the templates (sodium stearate and methyl cellulose) causes particles aggregation with the loss of sphericity.

The hard-templating method uses different swelling agents (hexane, cyclohexane and toluene) to increase the pore diameter and the surface area. The syntheses were carried out with CTABr as template and NaOH or urea as catalysts for the silica polymerization. Using hexane and cyclohexane (MS series) and NaOH, we

obtained spherical shapes (except for the samples synthesized with cyclohexane), pore sizes of about 3-5 nm and surface area of 120-1000 m^2/g.
Using toluene and urea, we obtained supports with spherical shape (with fibrous morphology), pore sizes of about 3 nm and surface area of 500 m^2/g.
Bioinspired method (BIS series) was an alternative method to produce silica materials. In this case the reaction was carried out in an aqueous solution, at room temperature, using sodium metasilicate as precursor and an additive (usually an amine or a polyamine). With this method it is possible to prepare samples with the additive into the silica network. Different amines (DETA, TETA and PEHA) and polyamines (PEI, PAA) at different pH (7, 5, 2) were used. Thanks to the soluble nature of the amine, it was possible to eliminate the additive by decreasing the pH of the solution (pH=2). On the contrary, the supports synthesized with polyamines (PEI and PAA) at pH 2 still contained the additive as evidenced by the FTIR analysis. The supports with the amines show high values of surface area at pH 2 especially with the additive PEHA (BIS-PEHA_2 672 m^2/g). This high value of surface is probably related to the complete removal of the additive from the support. The removal is also confirmed by FTIR-DRIFT characterization: no peaks related to the amino additive are present.
As reported above, the second part of the research is focused on the functionalization of non-porous and mesoporous support with several organosilanes precursor such as APTES, MPTMS, GPTMS, EDTA-TMS. We would like to remember that this part does not consider the bioinspired systems that have the surface already functionalized.

1) Non-porous supports functionalization

   The functionalization of non-porous supports was performed with APTES as the elective organosilane compound. Initially the functionalization was performed on particles with different sizes (i.e., 250 nm sample - S8, 1000 nm - S18 and 2000 nm - S19) using an acid silanization (method A). For larger particles, the NH_2 groups increases, indicating that the APTES functionalization can be influenced by the particle size.

   The functionalization process with APTES was optimized using other methods (B, C and D) on sample S8. Method B was carried out by grafting process in an organic solvent, without a catalyst; method C is similar to the acid silanization, but in this case the organosilane precursor was dripped by piston pump, and method D was performed by a single step reaction using TEOS and APTES to synthetize supports already functionalized. Methods B and D evidence the

higher density of NH_2 groups and the higher concentrations of functional groups (linkers) (3.78 and 7.92 mmol/g)

The functionalization of the supports with larger particles, was further carried out with CPTMS and then, with sodium azide. In order to verify the functionalization (CPTMS and azide group), biotin was bound to the azide-functionalized silica supports via Cu-Catalyzed Azide-Alkyne Cycloaddition (CuAAC).

The bond between the support with azide groups and biotin was evidenced by the adsorption of the fluorescent streptavidin and analyzed by flow cytometer. The analysis confirms that biotin was covalently linked to the support.

2) Mesoporous supports functionalization

The mesoporous supports were functionalized with some organosilanes (APTES, EDTA-TMS, GPTMS and MPTMS).

The final part of the research is focused on the covalent and non-covalent confinement of Bovine Serum Albumin (BSA) used as reference, Cellulase-endo-β 1,4-glucanase (Cell-EG) and PETase on the silica supports.

Before the use: Cell_EG protein was purified and analyzed by size exclusion chromatography, PETase protein was expressed using the pET21b(+)-PETase-W159H-S238F pET-21b(+) plasmid and the gene from *Ideonella sakaiensis* 201-F6 (Genbank GAP38373.1) contains W159H and S238F mutations. This expression was optimized and then scaled to obtain a greater amount of protein after purification (1.1 mg).

Different confinement methods (covalent via cross linking reaction, adsorption, and entrapment) were tested first on BSA and then on Cell_EG. Methods used to confine Cell_EG with the best activity were also employed for PETase protein.

Covalent confinement

Glutaraldehyde was used as cross-linking agent. The reaction was performed on two systems: among proteins (with crosslinker) and among protein and silica support.

For the systems containing only proteins (BSA and Cell_EG) and cross-linker the effect of the cross-linker concentration and of pH on the reaction was studied. Samples, with higher crosslinker concentration and at acid pH, showed a blue shift (from 280 to 275 nm) of the UV-visible peak. This shift could be due to the imino bond or ethylene bond between protein and crosslinker. At basic pH, the peak shifts from 280 nm to 290-300 nm and the transparent solution became white, indicating

the formation of protein aggregates.

The systems containing protein and silica supports (non-porous and mesoporous) were prepared by two steps cross-linking reaction. During the first step, the crosslinker is bound to the support and then (second step) the protein can interact with functionalized support. The measures of the loading efficiency for BSA and Cell_EG proteins gave the following results:

1) Non-porous support:
   - BSA protein. Samples (S8@PrNH2_B) and (S8@PrNH2_D) functionalized with APTES and prepared by method B and D showed the best values of loading efficiency.
   - Cell_EG protein. Samples (S8@PrNH2_D) and (S8@PrSH_B) functionalized with APTES and MPTMS and prepared by method D and B showed the best value of loading efficiency.
2) Mesoporous supports:
   - BSA protein. Samples (MC10-PrSH) and (MC10-PrNH_2) functionalized with MPTMS and APTES evidenced the best loading efficiency. The support with the best BSA loading was used for Cell_EG protein.
   - Cell_EG protein. The loading efficiency of MC10-PrSH and MC10-PrNH_2 samples was lower with respect to BSA. This result is probably due to the lower affinity between Cell_EG and the support.

Non-covalent confinement

Non- covalent confinement was performed by ***adsorption*** and ***entrapment*** of BSA and Cell_EG.

The ***adsorption*** method was carried out using different silica support (non-porous, mesoporous, and support synthesized by bio-inspired method).

1) Non-porous supports. First the adsorption was performed on supports with different particle sizes and functionalized only with APTES and then on supports functionalized with different silanization methods using APTES and MPTMS.

- Supports with different sizes.
  BSA protein. Sample S19-PrNH$_2$_A (with larger particle sizes- 2000nm), evidenced the better loading efficiency.
  Cell_EG protein. Sample S18-PrNH$_2$_A (with 1 μm particle sizes) had the better loading efficiency.

- Supports functionalized with different silanization methods.
  BSA protein. Sample S8-PrNH2_A@BSA, functionalized with APTES and prepared by A method, showed the better loading.
  Cell_EG protein. Sample S8-PrSH_B@Cell_EG functionalized with MPTMS and prepared by B method had the better loading.

2) Mesoporous supports.
   BSA protein. Samples MC10-PrSH@BSA and MC10-PrNH$_2$ @BSA functionalized with MPTMS and APTES gave the better values of the loading efficiency.
   Cell_EG protein. Samples MC10-GP-PEI@Cell_EG (functionalized by GPTMS and PEI) and MC10-PrNH$_2$_Cell_EG (functionalized by APTES) gave the better values of the loading efficiency.
3) Bioinspired supports
   The better loading for BSA was obtained with the supports synthesized at pH 7 (BIS_PEI_7 and BIS_TETA_7) and at pH 2 (BIS_DETA_2 and BIS_PAA_2). These supports were used also for Cell_EG protein, but in this case only sample BIS_PAA_7 evidenced a good loading efficiency.

The adsorption kinetics of all samples could be described by three kinetic models: the "Rollover model", the "Three-states model" and the “Surface Cluster model”.

The ***Entrapment*** method was performed on supports prepared by bioinspiration method using five additives (amines and polyamines). The confinement was carried out, at pH 7, with one-pot step reaction. The best loading efficiency was obtained with polyamine PAA for BSA and Cell_EG. This result can be explained by a better charge affinity between polyamine PAA (positive charge) and the proteins (negative charge).

The final catalytic activity tests of the Cell_EG confined systems was performed on the best loaded support of each confinement techniques (covalent via cross linking reaction, adsorption, and entrapment). The Cell_EG maintained about 90% of the initial activity using the entrapment method (BIS-PAA@Cell_EG), while for the adsorption (BIS-PAA_2@Cell_EG) and covalent methods (Mc10-PrNH2-Glu@Cell_EG) the residual activity decreased to 54% and 35%. The lower activity of the samples prepared by the covalent and adsorption methods probably derives by a decrease of the enzyme stability after the confinement process.

This finding was also confirmed by the Michaelis Menten curves and the kinetic parameters (K_m and V_{max}) that show as the entrapment method keeps the protein more stable with respect to the adsorption and covalent confinement.

The best catalytic activities of the Cell_EG confined systems were tested at different pH values (1), temperature (2), different recycles (3) and substrates (4).

1) **Different pH**: The entrapment and the covalent systems have similar activity, even if lower of the free enzyme. The activity is larger or comparable to the free enzyme for the adsorbed systems prepared at pH=3 and pH=9.
2) **Thermal stability**: The activity values of the confined systems are always lower than the values of the free enzyme.
3) **Different recycles**: The adsorption and the covalent systems show a low residual activity after 2 recycles and after the last recycles the activity is about of 5%.The entrapment method maintains the activity of about 40-45% after 2 recycles, but the residual activity after the last recycles is lower than 5%.
4) **Different substrates**: The substrates (MHEC and Whatman filter paper) reduce the activity of the confined systems also for free Cell_EG protein.

As reported above, BIS-PAA@Cell_EG sample is the systems with the best performance to confine the Cell_EG protein. The same method was used to entrap the PETase protein.

Sample BIS_PAA@PETase showed a loading efficiency of about 80% and a residual activity of 95%. The sample was recycling for five time maintaining a residual activity of about 45%.

Also, the catalytic activity of this samples was compared to the catalytic activity of the free enzyme at different pH (1) and thermal stability (2).

1) At different pH, the trend of the entrapment system was similar to free enzyme. Only at pH10 the entrapped enzyme was more stable.
2) The thermal stability of the entrapped system showed similar trend to the free enzyme.

In conclusion, we can underline that the entrapment via bioinspired method could be very interesting technique for future applications. This strategy shows promising results thanks to easy preparation and the green environment, preserving the catalytic activity and stability of the enzyme. In particular, interesting results are observed with Cell_EG and PETase (proteins used in the recycling field of biomass and plastic PET waste) entrapped into silica network.
Further research can be addressed to find new methods to improve the stability of entrapped proteins and to scale up the relative process.

ACKNOWLEDGEMENTS

Dopo questi tre anni di dottorato è arrivata l'ora di fare i consueti ringraziamenti alle persone che mi hanno accompagnato in questo particolare percorso di dottorato e alla stesura della tesi. Un grandissimo ringraziamento va dovuto alla mia famiglia che mi ha sostenuto in tutti i miei percorsi di studi e mi ha tirato su nei momenti di assoluto bisogno.

Al mio supervisore prof. Alvise Benedetti per avermi dato l'opportunità di svolgere il dottorato nel suo gruppo di ricerca e per avermi dato un grandissimo supporto sia nella fase sperimentale che nella stesura della tesi di dottorato. Ai professori Pietro Riello, Elti Cattaruzza, Patrizia Canton, Elisa Moretti e Aldo Talon per la loro accoglienza e soprattutto per il loro supporto scientifico. Al prof. Alessandro Angelini e al suo gruppo di ricerca, in particolare ad Arianna e Matteo per il gradissimo supporto e aiuto biotech.

Al professor di Sheffield Siddharth V. Patwardhan che mi ha accolto nel suo gruppo di ricerca e mi ha dato l'occasione di confrontarmi con altre persone, qui saluto i ragazzi del green nanomaterial group (Max, Jake, Amber, Eleni, Luc, Justin) e i ragazzi di Sheffield con la quale ho passato delle bellissime serate tra partite a bigliardo e balli sfrenati al cubana (Francesco, Naomi, Solange, Ludovica, Federica, Vittoria, Angelo, Kostas)

Un saluto grandissimo ai ragazzi dell'ETA (Tiziano, Davide, Martina, Mirena, Lorenzo, Michele, Emmanuele, Riccardo, il Biondo (Falza), Benedetta, Elisa, Irene, Gabriele, Leonardo, Federica, Dafne, Eleonora), ai ragazzi del gruppo feste (Matteo, Pietro, Lorenzo, Sambo, Diego, Ciano) e ai ragazzi di Potenza (Valentina Emanuele, Daniele, Rosa, Francesco, Rosario, Tania).

Ringrazio veramente tutti per il vostro sostegno e per il bellissimo supporto che mi avete dato in questi anni.

Vincenzo

BIBLIOGRAPHY

[1] A. Illanes, *Enzyme biocatalysis: Principles and applications*. 2008.

[2] R. DiCosimo, J. McAuliffe, A. J. Poulose, and G. Bohlmann, “Industrial use of immobilized enzymes,” *Chem. Soc. Rev.*, vol. 42, no. 15, p. 6437, 2013.

[3] D. M. Liu and C. Dong, “Recent advances in nano-carrier immobilized enzymes and their applications,” *Process Biochem.*, vol. 92, no. December 2019, pp. 464–475, 2020.

[4] S. D. M. Editor and J. M. Walker, *Enzyme Stabilization and Immobilization IN Series Editor*. .

[5] J. N. Talbert and J. M. Goddard, “Enzymes on material surfaces,” *Colloids Surfaces B Biointerfaces*, vol. 93, pp. 8–19, 2012.

[6] R. A. Sheldon, “Enzyme immobilization: The quest for optimum performance,” *Adv. Synth. Catal.*, vol. 349, no. 8–9, pp. 1289–1307, 2007.

[7] Y. Zhou, Y. Fang, and R. P. Ramasamy, “Non-covalent functionalization of carbon nanotubes for electrochemical biosensor development,” *Sensors (Switzerland)*, vol. 19, no. 2, 2019.

[8] E. Katchalski-Katzir, “Immobilized enzymes--learning from past successes and failures.,” *Trends Biotechnol.*, vol. 11, no. 11, pp. 471–8, 1993.

[9] M. Pegueroles, C. Tonda-Turo, J. A. Planell, F. J. Gil, and C. Aparicio, “Adsorption of fibronectin, fibrinogen, and albumin on TiO2: Time-Resolved Kinetics, structural changes, and competition study,” *Biointerphases*, vol. 7, no. 1–4, pp. 1–13, 2012.

[10] B. C. C. Pessela *et al.*, “Increasing the binding strength of proteins to PEI coated supports by immobilizing at high ionic strength,” *Enzyme Microb. Technol.*, vol. 37, no. 3, pp. 295–299, 2005.

[11] F. Wang, C. Guo, L. rong Yang, and C. Z. Liu, “Magnetic mesoporous silica nanoparticles: Fabrication and their laccase immobilization performance,” *Bioresour. Technol.*, vol. 101, no. 23, pp. 8931–8935, 2010.

[12] R. R. Naik, M. M. Tomczak, H. R. Luckarift, J. C. Spain, and M. O. Stone, “Entrapment of enzymes and nanoparticles using biomimetically synthesized silica.,” *Chem. Commun. (Camb).*, no. 15, pp. 1684–1685, 2004.

[13] M. Tarhini, H. Greige-Gerges, and A. Elaissari, “Protein-based nanoparticles: From preparation to encapsulation of active molecules,” *Int. J. Pharm.*, vol. 522, no. 1–2, pp. 172–197, 2017.

[14] R. Ahmad and M. Sardar, “Immobilization of cellulase on TiO2 nanoparticles by physical and covalent methods: A comparative study,” *Indian J. Biochem. Biophys.*, vol. 51, no. 4, pp. 314–320, 2014.

[15] T. Heck, G. Faccio, M. Richter, and L. Thöny-Meyer, “Enzyme-catalyzed protein crosslinking,” *Appl. Microbiol. Biotechnol.*, vol. 97, no. 2, pp. 461–475, 2013.

[16] Q. Husain, “Nanomaterials Immobilized Cellulolytic Enzymes and their Industrial Applications : A Literature Review,” *JSM Biochem. Mol. Biol.*, vol. 4, no. 3, p. 1029, 2017.

[17] V. L. Sirisha, A. Jain, and A. Jain, *Enzyme Immobilization: An Overview on Methods, Support Material, and Applications of Immobilized Enzymes*, 1st ed., vol. 79. Elsevier Inc., 2016.

[18] M. Falahati, A. A. Saboury, L. Ma’mani, A. Shafiee, and H. A. Rafieepour, “The effect of functionalization of mesoporous silica nanoparticles on the interaction and stability of confined enzyme,” *Int. J. Biol. Macromol.*, vol. 50, no. 4, pp. 1048–1054, 2012.

[19] H. Suo, L. Xu, Y. Xue, X. Qiu, H. Huang, and Y. Hu, “Ionic liquids-modified cellulose coated magnetic nanoparticles for enzyme immobilization: Improvement of catalytic performance,” *Carbohydr. Polym.*, vol. 234, no. November 2019, 2020.

[20] N. Arabacı, T. Karaytuğ, A. Demirbas, I. Ocsoy, and A. Katı, “Nanomaterials for Enzyme Immobilization,” *Green Synth. Nanomater. Bioenergy Appl.*, pp. 165–190, 2020.

[21] M. Egli and S. Sarkhel, “Lone pair-aromatic interactions: to stabilize or not to stabilize.,” *Acc. Chem. Res.*, vol. 40, no. 3, pp. 197–205, Mar. 2007.

[22] P. C. Hiemenz and R. Rajagopalan, “Principles of Colloid and Surface Chemistry, 3rd Ed, Revised, and Expanded_Paul C. Hiemenz_1997_Marcel Dekker, Inc._New York.pdf,” *Marcel Dekker, Inc. New Yorl*. 1997.

[23] A. Küchler, M. Yoshimoto, S. Luginbühl, F. Mavelli, and P. Walde, “Enzymatic reactions in confined environments,” *Nat. Nanotechnol.*, vol. 11, no. 5, pp. 409–420, 2016.

[24] M. Rabe, D. Verdes, and S. Seeger, “Understanding protein adsorption phenomena at solid surfaces,” *Adv. Colloid Interface Sci.*, vol. 162, no. 1–2, pp. 87–106, 2011.

[25] M. Malmsten, “Formation of Adsorbed Protein Layers,” *J. Colloid Interface Sci.*, vol. 207, no. 2, pp. 186–199, 1998.

[26] C. A. Haynes and W. Norde, “Globular proteins at solid/liquid interfaces,” *Colloids Surfaces B Biointerfaces*, vol. 2, no. 6, pp. 517–566, Jul. 1994.

[27] C. Czeslik, “Factors Ruling Protein Adsorption Protein Adsorption / Neutron Reflectometry / TIRF / FCS / Polyelectrolyte Brush,” *Z. Phys. Chem*, vol. 218, pp.

771–801, 2004.

[28] J. M. Sarkar, A. Leonowicz, and J.-M. Bollag, “Immobilization of enzymes on clays and soils,” *Soil Biol. Biochem.*, vol. 21, no. 2, pp. 223–230, Jan. 1989.

[29] J. O. Hardesty, L. Cascão-Pereira, J. T. Kellis, C. R. Robertson, and C. W. Frank, “Enzymatic proteolysis of a surface-bound alpha-helical polypeptide.,” *Langmuir*, vol. 24, no. 24, pp. 13944–56, Dec. 2008.

[30] T. Arai and W. Norde, “The behavior of some model proteins at solid-liquid interfaces 1. Adsorption from single protein solutions,” *Colloids and Surfaces*, vol. 51, no. C, pp. 1–15, Jan. 1990.

[31] W. Norde, “Driving forces for protein adsorption at solid surfaces,” *Macromol. Symp.*, vol. 103, pp. 5–18, 1996.

[32] C. F. Wertz and M. M. Santore, “Adsorption and reorientation kinetics of lysozyme on hydrophobic surfaces,” *Langmuir*, vol. 18, no. 4, pp. 1190–1199, 2002.

[33] V. Ball and J. J. Ramsden, “Absence of surface exclusion in the first stage of lysozyme adsorption is driven through electrostatic self-assembly,” *J. Phys. Chem. B*, vol. 101, no. 28, pp. 5465–5469, 1997.

[34] M. D. Alves, F. M. Aracri, É. C. Cren, and A. A. Mendes, “Isotherm, kinetic, mechanism and thermodynamic studies of adsorption of a microbial lipase on a mesoporous and hydrophobic resin,” *Chem. Eng. J.*, vol. 311, pp. 1–12, Mar. 2017.

[35] Z. Li, “Protein Interactions with Mixed Poly (ethylene glycol)/ Polyacrylic Acid Brushes,” 2008.

[36] E. E. Ghadim, F. Manouchehri, G. Soleimani, H. Hosseini, S. Kimiagar, and S. Nafisi, “Adsorption Properties of Tetracycline onto Graphene Oxide: Equilibrium, Kinetic and Thermodynamic Studies,” *PLoS One*, vol. 8, no. 11, p. e79254, Nov. 2013.

[37] W. Norde and J. Lyklema, “The adsorption of human plasma albumin and bovine pancreas ribonuclease at negatively charged polystyrene surfaces. I. Adsorption isotherms. Effects of charge, ionic strength, and temperature,” *J. Colloid Interface Sci.*, vol. 66, no. 2, pp. 257–265, 1978.

[38] J. G. Kirkwood, “Theory of solutions of molecules containing widely separated charges with special application to zwitterions,” *J. Chem. Phys.*, vol. 2, no. 7, pp. 351–361, 1934.

[39] W. Norde and J. Lyklema, “Thermodynamics of protein adsorption. Theory with special reference to the adsorption of human plasma albumin and bovine pancreas ribonuclease at polystyrene surfaces,” *J. Colloid Interface Sci.*, vol. 71, no. 2, pp. 350–366, 1979.

[40] F. L. Barroso Da Silva, M. Boström, and C. Persson, “Effect of charge regulation and ion-dipole interactions on the selectivity of protein-nanoparticle binding,” *Langmuir*, vol. 30, no. 14, pp. 4078–4083, 2014.

[41] K. Chen *et al.*, “Electrostatic selectivity in protein-nanoparticle interactions,” *Biomacromolecules*, vol. 12, no. 7, pp. 2552–2561, 2011.

[42] E. Seyrek, P. L. Dubin, C. Tribet, and E. A. Gamble, “Ionic strength dependence of protein-polyelectrolyte interactions,” *Biomacromolecules*, vol. 4, no. 2, pp. 273–282, 2003.

[43] M. Asal, Ö. Özen, M. Şahinler, H. T. Baysal, and İ. Polatoğlu, “An overview of biomolecules, immobilization methods and support materials of biosensors,” *Sens. Rev.*, vol. 39, no. 3, pp. 377–386, 2019.

[44] G. Cottone *et al.*, “Entrapment Modulates Biological Catalyst Function,” pp. 1–29, 2019.

[45] P. Reis, T. Witula, and K. Holmberg, “Mesoporous materials as host for an entrapped enzyme,” *Microporous Mesoporous Mater.*, vol. 110, no. 2–3, pp. 355–362, 2008.

[46] D. Pirozzi, E. Fanelli, A. Aronne, P. Pernice, and A. Mingione, “Lipase entrapment in a zirconia matrix: Sol-gel synthesis and catalytic properties,” *J. Mol. Catal. B Enzym.*, vol. 59, no. 1–3, pp. 116–120, 2009.

[47] Y. Jiang *et al.*, “The improved stability of enzyme encapsulated in biomimetic titania particles,” *Mater. Sci. Eng. C*, vol. 29, no. 1, pp. 328–334, 2009.

[48] S. S. Nadar and V. K. Rathod, “Immobilization of proline activated lipase within metal organic framework (MOF),” *Int. J. Biol. Macromol.*, vol. 152, pp. 1108–1112, 2020.

[49] S. R. Saptarshi, A. Duschl, and A. L. Lopata, “Interaction of nanoparticles with proteins: Relation to bio-reactivity of the nanoparticle,” *J. Nanobiotechnology*, vol. 11, no. 1, pp. 1–12, 2013.

[50] P. L. Sóti, D. Weiser, T. Vigh, Z. K. Nagy, L. Poppe, and G. Marosi, “Electrospun polylactic acid and polyvinyl alcohol fibers as efficient and stable nanomaterials for immobilization of lipases,” *Bioprocess Biosyst. Eng.*, vol. 39, no. 3, pp. 449–459, 2016.

[51] J. R. Fernandez Caresani, A. Dallegrave, and J. H. Z. dos Santos, “Amylases immobilization by sol–gel entrapment: application for starch hydrolysis,” *J. Sol-Gel Sci. Technol.*, vol. 94, no. 1, pp. 229–240, 2020.

[52] M. Yan, J. Ge, Z. Liu, and P. Ouyang, “Encapsulation of single enzyme in nanogel with enhanced biocatalytic activity and stability,” *J. Am. Chem. Soc.*, vol. 128, no. 34, pp. 11008–11009, 2006.

[53] D. Dinelli, W. Marconi, and F. Morisi, “Fiber-entraped Enzymes,” *Methods*

Enzymol., vol. 44, pp. 227–243, 1976.

[54] D. Dai and L. Xia, "Effect of lipase immobilization on resolution of (R, S)-2-octanol in nonaqueous media using modified ultrastable-Y molecular sieve as support," *Appl. Biochem. Biotechnol.*, vol. 134, no. 1, pp. 39–50, 2006.

[55] D. Avnir, S. Braun, O. Lev, and M. Ottolenghi, "Enzymes and Other Proteins Entrapped in Sol-Gel Materials," *Chem. Mater.*, vol. 6, no. 10, pp. 1605–1614, 1994.

[56] S. Braun, S. Rappoport, R. Zusman, D. Avnir, and M. Ottolenghi, "Biochemically active sol-gel glasses: The trapping of enzymes," *Mater. Lett.*, vol. 61, no. 14–15, pp. 2843–2846, 2007.

[57] A. C. Pierre and G. M. Pajonk, "Chemistry of aerogels and their applications," *Chem. Rev.*, vol. 102, no. 11, pp. 4243–4265, 2002.

[58] M. T. Reetz, A. Zonta, and J. Simpelkamp, "Efficient Heterogeneous Biocatalysts by Entrapment of Lipases in Hydrophobic Sol–Gel Materials," *Angew. Chemie Int. Ed. English*, vol. 34, no. 3, pp. 301–303, 1995.

[59] M. T. Reetz, "Entrapment of biocatalysts in hydrophobic sol-gel materials for use in organic chemistry," *Adv. Mater.*, vol. 9, no. 12, pp. 943–954, 1997.

[60] C. M. F. Soares, O. A. Dos Santos, H. F. De Castro, F. F. De Moraes, and G. M. Zanin, "Studies on immobilized lipase in hydrophobic sol-gel," *Appl. Biochem. Biotechnol. - Part A Enzym. Eng. Biotechnol.*, vol. 113, no. 1–3, pp. 307–319, 2004.

[61] N. Ganonyan, N. Benmelech, G. Bar, R. Gvishi, and D. Avnir, "Entrapment of enzymes in silica aerogels," *Mater. Today*, vol. 33, no. March, pp. 24–35, 2020.

[62] S. S. Betigeri and S. H. Neau, "Immobilization of lipase using hydrophilic polymers in the form of hydrogel beads," *Biomaterials*, vol. 23, no. 17, pp. 3627–3636, 2002.

[63] X. Wu, J. Ge, C. Yang, M. Hou, and Z. Liu, "Facile synthesis of multiple enzyme-containing metal-organic frameworks in a biomolecule-friendly environment," *Chem. Commun.*, vol. 51, no. 69, pp. 13408–13411, 2015.

[64] B. S. Heater, Z. Yang, M. M. Lee, and M. K. Chan, "In Vivo Enzyme Entrapment in a Protein Crystal," *J. Am. Chem. Soc.*, vol. 142, no. 22, pp. 9879–9883, 2020.

[65] E. P. Schoch, W. A. Felsing, G. W. Watt, and F. L. Okell, *General chemistry*, vol. 72, no. 854. 1947.

[66] F. A. Carey and R. J. Sundberg, *Advanced Organic Chemistry Part A: Structure and Mechanisms*. 2007.

[67] S. W. Lu, J. Thirlway, and J. Micklefield, "Direct site-selective covalent protein immobilization catalyzed by a phosphopantetheinyl transferase," *J. Am. Chem.*

Soc., vol. 130, no. 37, pp. 12456–12464, 2008.

[68] S. Nisha, S. A. Karthick, and N. Gobi, "A Review on Methods, Application and Properties of Immobilized Enzyme," *Che Sci Rev Lett*, vol. 1, no. 3, pp. 148–155, 2012.

[69] B. Hall, a Room, and K. Mosbach, "Proceedings of the Twenty-Ninth Symposium on Biotechnology for Fuels and Chemicals," *Appl. Biochem. Biotechnol.*, vol. 50, p. 775, 2008.

[70] K. Szymańska, J. Bryjak, and A. B. Jarzębski, "Immobilization of invertase on mesoporous silicas to obtain hyper active biocatalysts," *Top. Catal.*, vol. 52, no. 8, pp. 1030–1036, 2009.

[71] T. Iype *et al.*, "A novel method for immobilization of proteins via entrapment of magnetic nanoparticles through epoxy cross-linking," *Anal. Biochem.*, vol. 519, pp. 42–50, 2017.

[72] M. Ashjari, M. Garmroodi, F. Ahrari, M. Yousefi, and M. Mohammadi, "Soluble enzyme cross-linking: Via multi-component reactions: A new generation of cross-linked enzymes," *Chem. Commun.*, vol. 56, no. 67, pp. 9683–9686, 2020.

[73] E. Górecka and M. Jastrzębska, "Review article: Immobilization techniques and biopolymer carriers," *Biotechnol. Food Sci.*, vol. 75, no. 1, pp. 65–86, 2011.

[74] N. Guajardo, K. Ahumada, P. Domínguez de María, and R. A. Schrebler, "Remarkable stability of Candida antarctica lipase B immobilized via cross-linking aggregates (CLEA) in deep eutectic solvents," *Biocatal. Biotransformation*, vol. 37, no. 2, pp. 106–114, 2019.

[75] S. Velasco-Lozano, F. López-Gallego, J. C. Mateos-Díaz, and E. Favela-Torres, "Cross-linked enzyme aggregates (CLEA) in enzyme improvement – a review," *Biocatalysis*, vol. 1, no. 1, pp. 166–177, 2016.

[76] J. Mansfeld and H. Dautzenberg, "Immobilization of Enzymes and Cells," in *Immobilization of Enzymes and Cells*, no. 2, New Jersey: Humana Press, 2020, pp. 319–326.

[77] K. A. Johnson, "A century of enzyme kinetic analysis, 1913 to 2013," *FEBS Lett.*, vol. 587, no. 17, pp. 2753–2766, 2013.

[78] B. Choi, G. A. Rempala, and J. K. Kim, "Beyond the Michaelis-Menten equation: Accurate and efficient estimation of enzyme kinetic parameters," *Sci. Rep.*, vol. 7, no. 1, pp. 1–11, 2017.

[79] D. L. Nelson and M. M. Cox, "Lehninger Principles of Biochemistry 7th," *W.H. Free. Co.*, vol. 2, pp. 721–722, 2017.

[80] K. A. Johnson and R. S. Goody, "The original Michaelis constant: Translation of the 1913 Michaelis-Menten Paper," *Biochemistry*, vol. 50, no. 39, pp. 8264–8269, 2011.

[81] K. J. Laidler and P. S. Bunting, “The Kinetics of Immobilized Enzyme Systems,” vol. 1, 1980.

[82] M. Carrazco-Escalante *et al.*, “A new approach for describing and solving the reversible Briggs-Haldane mechanism using immobilized enzyme,” *Can. J. Chem. Eng.*, vol. 98, no. 1, pp. 316–329, 2020.

[83] I. Hinberg, R. Korus, and K. F. O’Driscoll, “Gel entrapped enzymes: Kinetic studies of immobilized β-galactosidase,” *Biotechnol. Bioeng.*, vol. 16, no. 7, pp. 943–963, 1974.

[84] Z. Dong, M.-Y. Jiang, J. Shi, M.-M. Zheng, and F.-H. Huang, “Preparation of Immobilized Lipase Based on Hollow Mesoporous Silica Spheres and Its Application in Ester Synthesis,” *Molecules*, vol. 24, no. 3, p. 395, 2019.

[85] R. C. Rodrigues, C. Ortiz, Á. Berenguer-Murcia, R. Torres, and R. Fernández-Lafuente, “Modifying enzyme activity and selectivity by immobilization,” *Chem. Soc. Rev.*, vol. 42, no. 15, pp. 6290–6307, 2013.

[86] C. Garcia-Galan, Á. Berenguer-Murcia, R. Fernandez-Lafuente, and R. C. Rodrigues, “Potential of different enzyme immobilization strategies to improve enzyme performance,” *Adv. Synth. Catal.*, vol. 353, no. 16, pp. 2885–2904, 2011.

[87] S. Sotiropoulou and N. A. Chaniotakis, “Lowering the detection limit of the acetylcholinesterase biosensor using a nanoporous carbon matrix,” *Anal. Chim. Acta*, vol. 530, no. 2, pp. 199–204, 2005.

[88] M. Deon *et al.*, “Designing a Support for Lipase Immobilization Based on Magnetic, Hydrophobic, and Mesoporous Silica,” *Langmuir*, vol. 36, no. 34, pp. 10147–10155, 2020.

[89] J. Boudrant, J. M. Woodley, and R. Fernandez-Lafuente, “Parameters necessary to define an immobilized enzyme preparation,” *Process Biochem.*, vol. 90, no. November 2019, pp. 66–80, 2020.

[90] Y. Zhang, J. Ge, and Z. Liu, “Enhanced Activity of Immobilized or Chemically Modified Enzymes,” *ACS Catal.*, vol. 5, no. 8, pp. 4503–4513, 2015.

[91] J. Zdarta, A. Meyer, T. Jesionowski, and M. Pinelo, “A General Overview of Support Materials for Enzyme Immobilization: Characteristics, Properties, Practical Utility,” *Catalysts*, vol. 8, no. 3, p. 92, 2018.

[92] “Sol-Gel Science,” *Sol-Gel Science*. 1990.

[93] H. Schmidt, H. Scholze, and A. Kaiser, “Principles of hydrolysis and condensation reaction of alkoxysilanes,” *J. Non. Cryst. Solids*, vol. 63, no. 1–2, pp. 1–11, 1984.

[94] C. J. BRINKER, “HYDROLYSIS AND CONDENSATION OF SILICATES: EFFECTS ON STRUCTURE,” *J. Non. Cryst. Solids*, vol. 47, no. 10, pp. 31–50, 1988.

[95] G. Zaikov, “Chemistry and technology of silicone polymers,” *Elem. Monomers*,

1968.

[96] A. F. W. Stöber, “Controlled Growth of Monodisperse Silica Spheres in the Micron Size Range,” *J. Colloid Interface Sci.*, vol. 26, pp. 62–69, 1968.

[97] Y. Han *et al.*, “Unraveling the growth mechanism of silica particles in the stöber method: In situ seeded growth model,” *Langmuir*, vol. 33, no. 23, pp. 5879–5890, 2017.

[98] H. Nakabayashi, A. Yamada, M. Noba, Y. Kobayashi, M. Konno, and D. Nagao, “Electrolyte-added one-pot synthesis for producing monodisperse, micrometer-sized silica particles up to 7 μm,” *Langmuir*, vol. 26, no. 10, pp. 7512–7515, 2010.

[99] X. Lei *et al.*, “Synthesis of monodisperse silica microspheres by a modified stöber method,” *Integr. Ferroelectr.*, vol. 154, no. 1, pp. 142–146, 2014.

[100] Y. Chen, *Design, Synthesis, Multifunctionalization and Biomedical Applications of Multifunctional Mesoporous Silica-Based Drug Delivery Nanosystems*. 2016.

[101] W. Li and D. Zhao, “An overview of the synthesis of ordered mesoporous materials,” *Chem. Commun.*, vol. 49, no. 10, pp. 943–946, 2013.

[102] R. Schmidt, M. Stöcker, E. Hansen, D. Akporiaye, and O. H. Ellestad, “MCM-41: a model system for adsorption studies on mesoporous materials,” *Microporous Mater.*, vol. 3, no. 4–5, pp. 443–448, 1995.

[103] H. Yang, Y. Deng, and C. Du, “Synthesis and optical properties of mesoporous MCM-41 containing doped TiO2 nanoparticles,” *Colloids Surfaces A Physicochem. Eng. Asp.*, vol. 339, no. 1–3, pp. 111–117, 2009.

[104] N. Rahmat, A. Z. Abdullah, and A. R. Mohamed, “A review: Mesoporous Santa Barbara amorphous-15, types, synthesis and its applications towards biorefinery production,” *Am. J. Appl. Sci.*, vol. 7, no. 12, pp. 1579–1586, 2010.

[105] J. Fan *et al.*, “Cubic mesoporous silica with large controllable entrance sizes and advanced adsorption properties,” *Angew. Chemie - Int. Ed.*, vol. 42, no. 27, pp. 3146–3150, 2003.

[106] É. Prouzet and C. Boissiére, “A review on the synthesis, structure and applications in separation processes of mesoporous MSU-X silica obtained with the two-step process,” *Comptes Rendus Chim.*, vol. 8, no. 3–4, pp. 579–596, 2005.

[107] S. A. El-Safty, “Review on the key controls of designer copolymer-silica mesophase monoliths (HOM-type) with large particle morphology, ordered geometry and uniform pore dimension,” *J. Porous Mater.*, vol. 15, no. 4, pp. 369–387, 2008.

[108] F. Kleitz, S. H. Choi, and R. Ryoo, “Cubic Ia3d large mesoporous silica: Synthesis and replication to platinum nanowires, carbon nanorods and carbon nanotubes,” *Chem. Commun.*, vol. 9, no. 17, pp. 2136–2137, 2003.

[109] Z. Li, J. C. Barnes, A. Bosoy, J. F. Stoddart, and J. I. Zink, “Mesoporous silica nanoparticles in biomedical applications,” *Chem. Soc. Rev.*, vol. 41, no. 7, pp. 2590–2605, 2012.

[110] G. Xue *et al.*, “Phosphoryl functionalized mesoporous silica for uranium adsorption,” *Appl. Surf. Sci.*, vol. 402, no. January, pp. 53–60, 2017.

[111] D. Carmona, F. Balas, and J. Santamaria, “Pore ordering and surface properties of FDU-12 and SBA-15 mesoporous materials and their relation to drug loading and release in aqueous environments,” *Mater. Res. Bull.*, vol. 59, pp. 311–322, 2014.

[112] D. Díaz-García *et al.*, “Role of folic acid in the therapeutic action of nanostructured porous silica functionalized with organotin(IV) compounds against different cancer cell lines,” *Pharmaceutics*, vol. 12, no. 6, pp. 1–23, 2020.

[113] J. Fan *et al.*, “Nanocasting synthesis of mesoporous SnO2 with a tunable ferromagnetic response through Ni loading,” *RSC Adv.*, vol. 6, no. 106, pp. 104799–104807, 2016.

[114] Z. Ali *et al.*, “Immobilization of lipase on mesoporous silica nanoparticles with hierarchical fibrous pore,” *J. Mol. Catal. B Enzym.*, vol. 134, pp. 129–135, 2016.

[115] A. S. L. Thankamony *et al.*, “Insights into the catalytic activity of nitridated fibrous silica (KCC-1) Nanocatalysts from 15 N and 29 Si NMR Spectroscopy Enhanced by Dynamic Nuclear Polarization,” *Angew. Chemie - Int. Ed.*, vol. 54, no. 7, pp. 2190–2193, 2015.

[116] J. R. H. Manning, T. W. S. Yip, A. Centi, M. Jorge, and S. V. Patwardhan, “An Eco-Friendly, Tunable and Scalable Method for Producing Porous Functional Nanomaterials Designed Using Molecular Interactions,” *ChemSusChem*, vol. 10, no. 8, pp. 1683–1691, 2017.

[117] S. V. Patwardhan, J. R. H. Manning, and M. Chiacchia, “Bioinspired synthesis as a potential green method for the preparation of nanomaterials: Opportunities and challenges,” *Curr. Opin. Green Sustain. Chem.*, vol. 12, pp. 110–116, 2018.

[118] S. V. Patwardhan, “Biomimetic and bioinspired silica: Recent developments and applications,” *Chem. Commun.*, vol. 47, no. 27, pp. 7567–7582, 2011.

[119] M. Fairhead *et al.*, “Crystal structure and silica condensing activities of silicatein α-cathepsin L chimeras,” *Chem. Commun.*, no. 15, pp. 1765–1767, 2008.

[120] S. V. Patwardhan, “Biomimetic and bioinspired silica: Recent developments and applications,” *Chem. Commun.*, vol. 47, no. 27, pp. 7567–7582, 2011.

[121] S. V. Patwardhan, N. Mukherjee, M. Steinitz-Kannan, and S. J. Clarson, “Bioinspired synthesis of new silica structures,” *Chem. Commun.*, vol. 3, no. 10, pp. 1122–1123, 2003.

[122] D. Otzen, “The Role of Proteins in Biosilicification,” *Hindawi Publ. Corp. Sci.*, vol. 2012, p. 22, 2012.

[123] M. Sumper and N. Kröger, “Silica formation in diatoms: The function of long-chain polyamines and silaffins,” *J. Mater. Chem.*, vol. 14, no. 14, pp. 2059–2065, 2004.

[124] C. Forsyth and S. V. Patwardhan, “Controlling performance of lipase immobilised on bioinspired silica,” *J. Mater. Chem. B*, vol. 1, no. 8, pp. 1164–1174, 2013.

[125] D. Cazaban, A. Illanes, L. Wilson, and L. Betancor, “Bio-inspired silica lipase nanobiocatalysts for the synthesis of fatty acid methyl esters,” *Process Biochem.*, vol. 74, no. July, pp. 86–93, 2018.

[126] J. S. Edwards, A. Roberts, A. C. Hemmert, C. C. Edwards, P. M. Potter, and M. R. Redinbo, “Immobilization of Active Human Carboxylesterase 1 in Biomimetic Silica Nanoparticles,” pp. 863–869, 2011.

[127] P. Zamora, A. Narváez, and E. Domínguez, “Enzyme-modified nanoparticles using biomimetically synthesized silica,” *Bioelectrochemistry*, vol. 76, no. 1–2, pp. 100–106, 2009.

[128] J. Matisons, *Bio-Inspired Silicon-Based Materials*. 2014.

[129] A. M. Putz, L. Almásy, A. Len, and C. Ianăşi, “Functionalized silica materials synthesized via co-condensation and post-grafting methods,” *Fullerenes Nanotub. Carbon Nanostructures*, vol. 27, no. 4, pp. 323–332, 2019.

[130] M. Manzano *et al.*, “Studies on MCM-41 mesoporous silica for drug delivery: Effect of particle morphology and amine functionalization,” *Chem. Eng. J.*, vol. 137, no. 1, pp. 30–37, 2008.

[131] M. Bilal, M. Asgher, H. Cheng, Y. Yan, and H. M. N. Iqbal, “Multi-point enzyme immobilization, surface chemistry, and novel platforms: a paradigm shift in biocatalyst design,” *Crit. Rev. Biotechnol.*, vol. 39, no. 2, pp. 202–219, 2019.

[132] Y. Wu, Y. Zhang, J. Zhou, and D. Gu, “Recent progress on functional mesoporous materials as catalysts in organic synthesis,” *Emergent Mater.*, 2020.

[133] D. B. Wilson, “Cellulases and biofuels,” *Curr. Opin. Biotechnol.*, vol. 20, no. 3, pp. 295–299, 2009.

[134] R. Lamed, E. A. Bayer, Y. Shoham, and H. Chanzy, “Cellulose, cellulases and cellulosomes,” *Curr. Opin. Struct. Biol.*, vol. 8, no. 5, pp. 548–557, 1998.

[135] G. Okada, “Cellulase of Aspergillus niger,” *Methods Enzymol.*, vol. 160, no. C, pp. 259–264, 1988.

[136] V. Arantes and J. N. Saddler, “Access to cellulose limits the efficiency of enzymatic hydrolysis: The role of amorphogenesis,” *Biotechnol. Biofuels*, vol. 3, pp. 1–11, 2010.

[137] J. Yan *et al.*, “Functional and structural analysis of Pichia pastoris-expressed Aspergillus Niger 1,4-β-endoglucanase,” *Biochem. Biophys. Res. Commun.*, vol.

475, no. 1, pp. 8–12, 2016.

[138] S. Khademi, D. Zhang, S. M. Swanson, A. Wartenberg, K. Witte, and E. F. Meyer, “Determination of the structure of an endoglucanase from Aspergillus niger and its mode of inhibition by palladium chloride,” *Acta Crystallogr. Sect. D Biol. Crystallogr.*, vol. 58, no. 4, pp. 660–667, 2002.

[139] G. J. Davies, L. Mackenzie, A. Varrot, M. Dauter, and A. M. Brzozowski, “Accelerated Publications Snapshots along an Enzymatic Reaction Coordinate : Analysis of a Retaining,” *Biochem*, vol. 37, no. 34, pp. 11707–11713, 1998.

[140] A. R. Esteghlalian, V. Srivastava, N. Gilkes, D. J. Gregg, and J. N. Saddler, “An overview of factors influencing the enzymatic hydrolysis of lignocellulosic feedstocks,” *ACS Symp. Ser.*, vol. 769, pp. 100–111, 2001.

[141] R. H. Y. Chang, J. Jang, and K. C. W. Wu, “Cellulase immobilized mesoporous silica nanocatalysts for efficient cellulose-to-glucose conversion,” *Green Chem.*, vol. 13, no. 10, pp. 2844–2850, Oct. 2011.

[142] A. Chan, “the Future of Bacteria Cleaning Our Plastic Waste Reviewing Progress in Cleaning Plastic - Filled Oceans Using Novel Biological Methods,” *Berkeley Sci. J.*, vol. 21, no. 1, 2016.

[143] F. Kawai, T. Kawabata, and M. Oda, “Current knowledge on enzymatic PET degradation and its possible application to waste stream management and other fields,” *Appl. Microbiol. Biotechnol.*, vol. 103, no. 11, pp. 4253–4268, 2019.

[144] S. Yoshida *et al.*, “A bacterium that degrades and assimilatespoly(ethyleneterephthalate),” *Research*, vol. 351, no. 6278, p. 5, 2016.

[145] C. C. Chen, X. Han, T. P. Ko, W. Liu, and R. T. Guo, “Structural studies reveal the molecular mechanism of PETase,” *FEBS J.*, vol. 285, no. 20, pp. 3717–3723, 2018.

[146] M. Furukawa, N. Kawakami, K. Oda, and K. Miyamoto, “Acceleration of Enzymatic Degradation of Poly(ethylene terephthalate) by Surface Coating with Anionic Surfactants,” *ChemSusChem*, 2018.

[147] Y. Yang *et al.*, “Characterization and engineering of a plastic-degrading aromatic polyesterase,” *Science (80-.).*, vol. 353, no. 6301, p. 759, 2017.

[148] T. Fecker *et al.*, “Active Site Flexibility as a Hallmark for Efficient PET Degradation by I. sakaiensis PETase,” *Biophys. J.*, vol. 114, no. 6, pp. 1302–1312, 2018.

[149] X. Han *et al.*, “Structural insight into catalytic mechanism of PET hydrolase,” *Nat. Commun.*, vol. 8, no. 1, p. 41467, 2017.

[150] B. Yu *et al.*, “Synthesis and modification of monodisperse silica microspheres for UPLC separation of C60 and C70,” *Anal. Methods*, vol. 8, no. 4, pp. 919–924, 2016.

[151] E. Febriyanti *et al.*, “Further Insight into the Definite Morphology and Formation

Mechanism of Mesoporous Silica KCC-1," *Langmuir*, vol. 32, no. 23, pp. 5802–5811, 2016.

[152] H. S. Mader, "Surface Modification of Silica Particles and Upconverting Particles Using Click Chemistry Surface Modification of Silica Particles and Upconverting Particles Using Click Chemistry," no. April, p. 10, 2010.

[153] A. Szegedi, M. Popova, I. Goshev, S. Klébert, and J. Mihály, "Controlled drug release on amine functionalized spherical MCM-41," *J. Solid State Chem.*, vol. 194, pp. 257–263, 2012.

[154] H. P. Austin *et al.*, "Characterization and engineering of a plastic-degrading aromatic polyesterase," *Proc. Natl. Acad. Sci.*, p. 201718804, 2018.

[155] Laboratories Bio-Rad, "A Guide to Polyacrylamide Gel Electrophoresis and Detection," *Bio-Rad*, p. 47, 2012.

[156] X. Liu, X. Lu, P. Wen, X. Shu, and F. Chi, "Synthesis of ultrasmall silica nanoparticles for application as deep-ultraviolet antireflection coatings," *Appl. Surf. Sci.*, vol. 420, pp. 180–185, 2017.

[157] V. M. Masalov, N. S. Sukhinina, E. A. Kudrenko, and G. A. Emelchenko, "Mechanism of formation and nanostructure of Stöber silica particles.," *Nanotechnology*, vol. 22, no. 27, p. 275718, Jul. 2011.

[158] Y. Lv, Q. Deng, K. H. Row, and T. Zhu, "Silane Coupling Agents Modified Silica and Graphene Oxide Materials for Determination of Sulfamerazine and Sulfameter in Milk by HPLC," *Food Anal. Methods*, vol. 12, no. 3, pp. 687–696, 2019.

[159] M. Meldal and C. W. Tomøe, "Cu-catalyzed azide - Alkyne cycloaddition," *Chem. Rev.*, vol. 108, no. 8, pp. 2952–3015, 2008.

[160] M. Biology, *Cellulases*. .

[161] S. M. Taipakova, I. T. Smekenov, M. K. Saparbaev, and A. K. Bissenbaev, "Characterization of Aspergillus niger endo-1,4-β-glucanase ENG1 secreted from Saccharomyces cerevisiae using different expression vectors," *Genet. Mol. Res.*, vol. 14, no. 2, pp. 6439–6452, 2015.

[162] S. S. Wong and D. M. Jameson, *Chemistry of protein and nucleic acid cross-linking and conjugation, second edition*. 2011.

[163] I. Migneault, C. Dartiguenave, M. J. Bertrand, and K. C. Waldron, "Glutaraldehyde: behavior in aqueous solution, reaction with proteins, and application to enzyme crosslinking," *Biotechniques*, vol. 37, no. 5, pp. 790–802, 2004.

[164] A. P. Minton, "Effects of excluded surface area and adsorbate clustering on surface adsorption of proteins. II. Kinetic models," *Biophys. J.*, vol. 80, no. 4, pp. 1641–1648, 2001.

[165] M. Rabe, D. Verdes, M. Rankl, G. R. J. Artus, and S. Seeger, “A comprehensive study of concepts and phenomena of the nonspecific adsorption of β-lactoglobulin,” *ChemPhysChem*, vol. 8, no. 6, pp. 862–872, 2007.

[166] J. R. H. Manning, B. Walkley, J. L. Provis, and S. V. Patwardhan, “Mimicking Biosintering: The Identification of Highly Condensed Surfaces in Bioinspired Silica Materials,” *Langmuir*, vol. 37, no. 1, pp. 561–568, 2021.

[167] M. S. Rahman, S. Fernando, B. Ross, J. Wu, and W. Qin, “Endoglucanase (eg) activity assays,” *Methods Mol. Biol.*, vol. 1796, pp. 169–183, 2018.